QUANTUM CHEMICAL SIMULATION OF NO REDUCTION BY AMMONIA (SCR REACTION) ON V2O5 CATALYST SURFACE

A THESIS SUBMITTED TO
THE GRADUATE SCHOOL OF NATURAL AND APPLIED SCIENCES
OF
THE MIDDLE EAST TECHNICAL UNIVERSITY

BY

ALPER UZUN

IN PARTIAL FULFILLMENT OF THE REQUIREMENTS FOR THE DEGREE OF
MASTER OF SCIENCE
IN
THE DEPARTMENT OF CHEMICAL ENGINEERING

AUGUST 2003

Approval of the Graduate School of Natural and Applied Sciences

Prof. Dr. Canan Özgen
Director

I certify that this thesis satisfies all the requirements as a thesis for the degree of Master of Science.

Prof. Dr. Timur Dogu
Head of Department

This is to certify that we have read this thesis and that in our opinion it is fully adequate, in scope and quality, as a thesis and for the degree of Master of Science.

Prof. Dr. Isik ÖNAL
Supervisor

Examining Committee Members

Prof. Dr. Inci Eroglu

Prof. Dr. Suzan Kincal

Prof. Dr. Sinasi Ellialtioglu

Assoc. Prof. Dr. Deniz Üner

Prof. Dr. Isik Önal

ABSTRACT

QUANTUM CHEMICAL SIMULATION OF NO REDUCTION BY AMMONIA (SCR REACTION) ON V_2O_5 CATALYST SURFACE

Uzun, Alper
M.S., Department of Chemical Engineering
Supervisor: Prof. Dr. Isik Önal

August 2003, 142 pages

The reaction mechanism for the Selective Catalytic Reduction (SCR) of NO by NH_3 on V_2O_5 surface was simulated by means of density functional theory (DFT) calculations performed at B3LYP/6-31G** level.

As the initiation reaction, ammonia activation on V_2O_5 was investigated. Coordinate driving calculations showed that ammonia is adsorbed on Brønsted acidic V-OH site as NH_4^+ species by a nonactivated process with a relative energy of -23.6kcal/mol. Vibration frequencies were calculated as 1421, 1650, 2857 and 2900cm^{-1} for the optimized geometry, in agreement with the experimental literature. Transition state with a relative energy of -17.1kcal/mol was also obtained. At the end of the Lewis acidic ammonia interaction calculations, it was observed that ammonia is hardly adsorbed on the surface. Therefore, it is

concluded that the SCR reaction is initiated more favorably by the Brønsted acidic ammonia adsorption.

As the second step of the SCR reaction, NO interaction with the preadsorbed NH_4^+ species was investigated. Accordingly, NO interaction results in the formation of gas phase NH_2NO molecule with a relative energy difference of 6.4kcal/mol.

For the rest of the reaction sequence, gas phase decomposition of NH_2NO was considered. Firstly, one of the hydrogen atoms of NH_2NO migrates to oxygen. It then isomerizes in the second step. After that, the reaction proceeds with the isomerization of the other hydrogen. Finally, a second hydrogen atom migration to the oxygen leads to the formation of N_2 and H_2O. Total relative energy for this reaction series was obtained as -60.12kcal/mol, in agreement with the literature.

Keywords: Selective Catalytic Reduction (SCR), NOx Reduction, NH_3, Quantum Chemical Calculations, Density Functional Theory (DFT), V_2O_5

ÖZ

NO'UN AMONYAK ILE V_2O_5 KATALIST YÜZEYI ÜZERINDE INDIRGENMESININ KUANTUM KIMYASAL SIMÜLASYONU

Uzun, Alper
Yüksek Lisans, Kimya Mühendisligi Bölümü
Danisman: Prof. Dr. Isik Önal

Agustos 2003, 142 sayfa

NO'nun amonyak ile V_2O_5 yüzeyi üzerindeki seçici katalitik indirgenme (SCR) reaksiyonu B3LYP/6-31G** düzeyinde uygulanan elektron yogunluk teorisi (DFT) hesaplamalari ile simüle edilmistir.

Baslangiç reaksiyonu olarak amonyagin V_2O_5 üzerindeki etkilesimi incelenmistir. Koordinat yürütme hesaplamalari yardimiyla amonyagin bronsted asidik V-OH sitesi üzerine NH_4^+ olarak adsorbe oldugu gözlenmistir. Aktivasyon enerjisine gerek duymayan bu reaksiyon için relatif enerji -23.6kcal/mol olarak hesaplanmistir. Optimize edilmis son geometrideki titresim frekanslari deneysel literatüre çok yakin olarak 1421, 1650, 2857 ve 2900 cm^{-1} bulunmustur. Bronsted asidik NH_3 adsorpsiyonu için -17.1kcal/mol relatif enerjisine sahip bir geçis durumu da elde edilmistir. Lewis asidik amonyak adsorpsiyonu için yapilan

hesaplamalar sonucunda amonyagin bu site üzerine zorlukla adsorbe oldugu ortaya çikmistir. Bu yüzden SCR reaksiyonunu baslatan reaksiyonun daha yüksek ihtimalle amonyagin Bronsted asidik V-OH sitesi üzerindeki adsorpsiyonunun olduguna karar verilmistir.

SCR'nin ikinci adimi olarak NO'nun önceki adimda yüzeye adsorbe olmus NH_4^+ iyonu ile etkilesimi incelenmistir. Bu etkilesim sonucunda NH_2NO'nun 6.4kcal/mol'luk bir enerji farki ile ortaya çiktigi saptanmistir.

Reaksiyonun geri kalani için NH_2NO'nun gaz fazindaki parçalanma reaksiyonu incelenmistir. Bu reaksiyonun ilk iki adiminda hidrojen atomalarindan biri oksijen atomuna baglanarak O-N bagina göre cis yapisindan trans yapisina isomerize olmaktadir. Sonraki adimlarda ise diger hidrojen atomu N-N bagina göre isomerlesme reaksiyonu geçirerek trans yapisindan cis yapisina geçmektedir. Bu reaksiyonlar serisinin son adiminda da önceki adimda isomerize olan hidrojen atomu oksijen atomuna baglanarak N_2 ve H_2O'yu olusturmaktadir. NH_2NO'nun parçalanmasindaki bütün bu reaksiyonlarin toplam relatif enerjisi literatür ile uyumlu olarak -60.12kcal/mol olarak hesaplanmistir.

Anahtar Kelimeler: Seçici Katalitik Indirgenme (SCR), NOx Indirgenmesi, Quantum Kimyasal Hesaplamalar, Elektron Yogunluk Teorisi (DFT), V_2O_5

To My Family,

ACKNOWLEDGEMENTS

First of all, I would like to express my deepest appreciation to my supervisor Prof. Dr. Isik Önal for his valuable guidance, suggestions, and his humanity and for his kindly attitude toward me throughout this study.

I would also like to thank Prof. Dr. Canan Özgen for always being supportive, understanding and ready to help.

My greatest thanks to my family for their continuous support, encouragement, trust and sacrifices for me that made the accomplishment of this work.

I wish to thank the DFT team, Mustafa Onur Diri, Sezen Soyer and Asli Sayar, for their help, friendship and motivation during the hard course of this study. Special thanks to Basak Açan and Berker Fiçicilar for never let me alone till late nights. Last but not least, I would like to thank my dear friends; Necati Günaydin, Nezih Ural Yagsi, Evren Güner, Isik Asar, Yalçin Yildiz, Sinan Ok, Umut Baris Ayhan, Özge Oguzer, Basak Kurbanoglu, Almila Bahar, Ismail Dogan, Murat Üner, Mustafa Esen Marti, Ugur Yildiz and many others that I could not mention here.

TABLE OF CONTENTS

LIST OF TABLES

Table

LIST OF FIGURES

Figure

CHAPTER 1

INTRODUCTION

1.1. NOx

Nitrous oxide (NOx), one of the most important atmospheric pollutants, typically consists of 95% NO and 5% NO_2. A major source of nitric oxide emissions is fuel combustion in engines and power plants. NOx emissions also can be significant in chemical operations such as nitric acid plants. More recently, the emissions of nitrous oxides from fiber production plants has received attention because of its global warming effects. The nitric oxide and SOx emissions are components of acid rain since when mixed with water vapor in the clouds; they form nitric oxide and sulfuric acid, respectively. Furthermore, NOx participates in photochemical ozone (smog) generation by reaction with hydrocarbons.

NOx is formed in combustion processes by combining the N_2 and O_2 present in the air. At temperatures greater than 1500°C, this reaction proceeds at appreciable rates through a well characterized mechanism called the Zeldovich Equation (Zeldovich et al., 1947). The formation of NO by oxidation of atmospheric nitrogen can be expressed in terms of the overall reaction:

$$\tfrac{1}{2} N_2 + \tfrac{1}{2} O_2 \;?\; NO \qquad (1.1)$$

which is highly endothermic [i.e., $?H_R^o$ (298K) = 90.4 kJ/mol)]. As a result, the equilibrium concentration of NO is high at very high temperatures encountered near stoichiometric combustion and decreases rapidly away from that point (Heck et al. 1995).

Actually, the direct reaction of N_2 with O_2 is too slow to account for significant NO formation. Free oxygen atoms, produced in flames by dissociation of O_2 or by radical attack on O_2, attack nitrogen molecules and begin a simple chain mechanism that was first postulated by Zeldovich et al. (1947), that is,

$$N_2 + O \;?\; NO + N \qquad (1.2)$$

$$N + O_2 \;?\; NO + O \qquad (1.3)$$

The concentration of O_2 is low in fuel rich combustion, so reaction 1.2 is less important than in fuel-lean combustion. Reaction with hydroxyl radical eventually becomes the major sink for N:

$$N + OH \;?\; NO + H \qquad (1.4)$$

The rate constants for the so-called extended Zeldovich mechanism are (Flagan et al., 1988):

$k_{2f} = 1.8 \times 10^8\ e^{-38370/T}\ m^3\ mol^{-1}\ s^{-1}$

$k_{2b} = 3.8 \times 10^7\ e^{-425/T}\ m^3\ mol^{-1}\ s^{-1}$

$k_{3f} = 1.8 \times 10^4\ T\ e^{-4680/T}\ m^3\ mol^{-1}\ s^{-1}$

$k_{3b} = 3.8 \times 10^3\ T\ e^{-20820/T}\ m^3\ mol^{-1}\ s^{-1}$

$k_{4f} = 7.1 \times 10^7\ e^{-450/T}\ m^3\ mol^{-1}\ s^{-1}$

$k_{4b} = 1.7 \times 10^8\ e^{-24560/T}\ m^3\ mol^{-1}\ s^{-1}$

The high activation energy of reaction 1.2, resulting from its essential function of breaking the strong N_2 triple bond, makes this the rate-limiting step of Zeldovich mechanism.

Due to the high activation energy, NO production by this mechanism proceeds at a slower rate than the oxidation of the fuel constituents and its extremely temperature sensitive. The production of atomic oxygen required for the first reaction is also highly temperature sensitive (Flagan et al., 1988).

The quantity of NOx formed depends primarily on the "three t's": temperature, time, and turbulence. In other words, flame temperature and the residence time of the fuel/air mixture, along with the nitrogen content of the coal and the quantity of excess air used for combustion, determine NOx levels in the flue gas. Combustion modifications delay the mixing of fuel and air, thereby reducing temperature and initial turbulence, which minimizes NOx formation.

1.2. NOx Removal Technologies

Many efforts have being made to minimize NOx emission (DeNoxing) either by combustion or post-combustion abatement technologies. Combustion control is achieved by the use of low NOx burners, flue gas recirculation, fuel reburning, staged combustion and water or steam injection. Post-combustion

DeNOxing includes wet methods, as sorption and dry methods, such as catalytic (heterogeneous) or homogeneous reduction (Busca et al. 1998). Although wet methods are insensitive to particulate levels, they are very expensive processes due to their complexity and NO insolubility, also, they require extensive equipments and usually result in the formation of NO_3^- and other potential water pollutants with only moderate NOx removal levels, moreover, wet methods are very sensitive to the flue gas composition of SOx, NOx and O_2. On the other hand, the dry methods are simple and low capital processes with high NOx removal efficiency (<90%). Therefore dry methods are more attractive than wet methods for the reduction of NOx emission. Among the flue gas treatment methods the selective catalytic reduction (SCR) is best developed and used world-wide for the control of stationary sources due to its efficiency, selectivity and economics (Forzatti, 2001).

1.3. Selective Catalytic Reduction Process

Selective Catalytic Reduction (SCR) refers to the process wherein NOx is reduced by NH_3 over a heterogeneous catalyst in the presence of O_2. The process is termed selective because the NH_3 preferentially reacts with NOx rather than with O_2. Oxygen, however, enhances the reaction and is a necessary component of the process.

SCR is the most technically advanced post-combustion technology capable of reducing NO_x emissions to the extremely low levels mandated in many areas of the world. Compared to other post-combustion NO_x reduction processes, SCR clearly is the most mature process. The technology has been

employed throughout the world to reduce emissions generated by gas-, oil-, and low-sulfur-coal-fired utility power plants.

Selective Catalytic Reduction Technology has the following advantages:

- It is one of the few NO_x technologies capable of removing high levels (80% or more) from high-sulfur coals.
- It is applicable to all types of boilers, including cyclone-fired boilers that cannot be retrofitted easily with other types of NO_x control technologies.
- It can be used by new and existing power plants.
- It potentially can create thousand of jobs in various industries (raw material supply, catalyst manufacturing, construction and operation of facilities) while helping save jobs associated with high-sulfur coal mining.
- No chemical by-products that require marketing or off-gases that require regeneration or disposal are produced. (Only nitrogen and water are formed)
- No significant re-engineering of the boiler heat exchange cycle is required.
- No solid adsorbents are required. This eliminates the need for energy-consuming handling and transfer processes.
- Relatively little capital and operating costs are incurred.
- The process relies on a simple chemical reaction. This simplicity improves the overall reliability of the technology.
- SCR is a dry process with few moving parts. The system requires only a few boiler alterations.
- All catalysts perform well at the targeted NO_x removal rates with slip less than 2 ppm under baseline conditions (i.e., 80% NO_x removal) and in many cases the measured slip was below the 1ppm detection limit.

The SCR processes are relatively simple, requiring only a reactor, a catalyst, and an ammonia storage and injection system. An illustration of a simple SCR reactor is given in Figure 1.1. The optimum temperature for the noncatalytic reaction is about 1300K. The catalyst effectively reduces the reaction temperature to the range 570 to 720K. In order to avoid the need to reheat the flue gas, the reactor is usually located just after the boiler, either before or after the particulate control device (Flagan et al. 1988).

Performance criteria for SCR are analogous to those for other catalytic oxidation systems: NO_x conversion, pressure drop, catalyst/system life, cost, and minimum SO_2 oxidations to SO_3. An optimum SCR catalyst is one that meets both the pressure drop and NO_x conversion targets with the minimum catalyst volume. Because of the interrelationship between cell density, pressure drop, and catalyst volume, a wide range of optional catalyst cell densities are needed for optimizing SCR system performance.

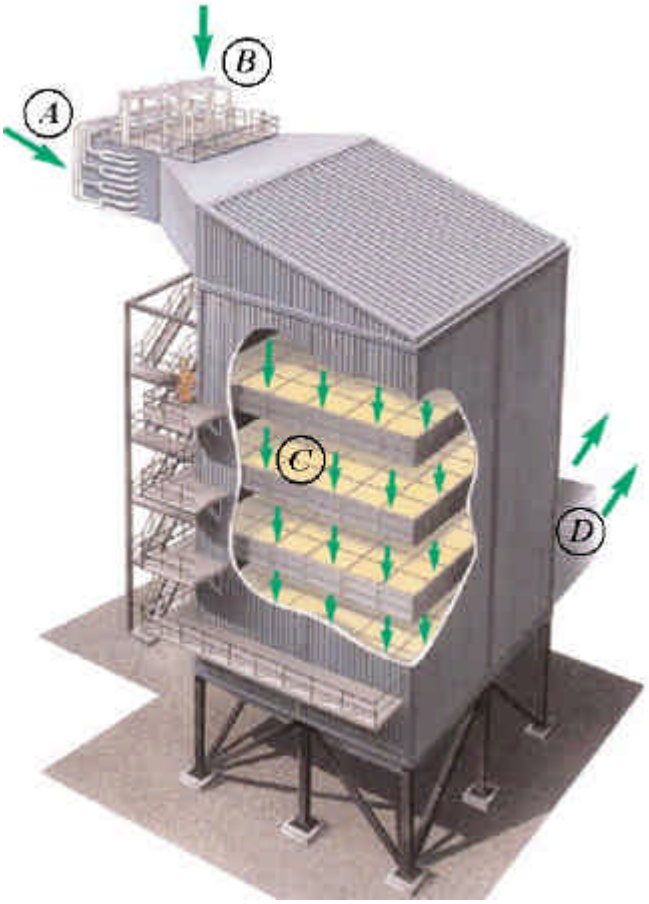

Figure 1.1. A Simple SCR Reactor, **A)** Flue gas containing NOx is admitted from the boiler to the SCR reactor, **B)** Ammonia is added to the flue gas, **C)** The gas mixture flows over catalyst elements, which cause nitrogen oxides and ammonia to react, **D)** The reaction converts the nitrogen oxide to pure nitrogen and water. Figure is taken from the ABB Alstom Power Environmental Systems Brochure.

SCR catalysts are made of a ceramic material that is a mixture of carrier and active components. The two leading shapes of SCR catalyst used today are honeycomb and plate. The honeycomb form usually is an extruded ceramic with the catalyst either incorporated throughout the structure (homogeneous) or coated on the substrate. In the plate geometry, the support material is generally coated with catalyst. When processing flue gas containing dust, the reactors are typically vertical, with down flow of flue gas. The catalyst is typically arranged in a series of two to four beds, or layers. For better catalyst utilization, it is common to use three or four layers, with provisions for an additional layer which is not initially installed.

Although many different types of catalyst compositions and configurations have been developed for SCR process, there is no SCR catalyst that can operate economically over the whole temperature range possible for combustion systems. Therefore, catalyst selection depends largely on the temperature of the flue gas being treated. A given catalyst exhibits optimum performance within a temperature range of about 30 to 50°C. Below this optimum temperature range, the catalyst activity is greatly reduced, allowing unreacted ammonia to slip through. Above this range, ammonia begins to be oxidized to form additional NO_x. Operations having adequate temperature controls are important, as are uniform flue gas temperatures (Campbell et al, 1991). The active catalytic component and temperature ranges may be classified as:

Low temperature (175-250°C) : Platinum

Medium temperature (260-450°C) : Vanadium

High temperature (350-600°C) : Zeolite

The precious-metal platinum catalysts were primarily developed in the 1960s for operation at temperatures between about 175 and 250°C. However, because of sensitivity to poisons, these catalysts are unsuitable for many combustion applications. Variations in sulfur levels of as little as 0.4 ppm can shift the catalyst required temperature window completely out of a system's operating temperature range. Additionally, operation with liquid fuels is further complicated by the potential for deposition of ammonium sulfate salts within the pores of the catalyst (Speronello et al., 1992). These low temperature catalysts exhibit NO_x conversion that rises with increasing temperature, then rapidly drops off, as oxidation of ammonia to nitrogen oxides begins to dominate the reaction.

The most popular SCR catalyst formulations are those that were developed in Japan in the late 1970s comprised of base metal oxides such as vanadium pentoxide, V_2O_5, supported on titanium dioxide TiO_2 (Farrauto et al. 1992). As for low temperature catalysts, NO_x conversion rises with increasing temperatures to a plateau and then falls as ammonia oxidation begins to dominate the SCR reaction. However, peak conversion occurs in the temperature range between 300 and 450°C, and the fall-off in NO_x conversion is more gradual than for low temperature catalysis (Speronello et al., 1992). Moreover Vanadium/Titanium catalysts have higher resistance to poisoning by SOx.

A family of zeolite catalysts has been developed, and is being increasingly used in SCR applications. Zeolites which can function at higher temperatures than the conventional catalysts are claimed to be effective over the range of 350 to 600°C, having an optimum temperature range from 360 to 580°C (Campbell et al., 1991, Shareef et al., 1992). However, ammonia oxidation to NOx begins around 450°C and is predominant at temperatures in excess of 500°C. Zeolites suffer the same performance and potential damage problems as conventional catalysts when used outside the optimum temperature range. In particular, at around 550°C the zeolite structure may be irreversibly degraded because of loss of pore density. Zeolite catalysts have not been continuously operated commercially at temperatures above 500°C (Campbell et al., 1991).

1.4. Reactions of SCR of NO by NH_3

The reaction stoichiometry in typical SCR reaction condition is the following:

$$4NH_3 + 4NO + O_2 \;?\; 4N_2 + 6\,H_2O \qquad (1.5)$$

Using isotopically labeled reactants, it has been demonstrated that both vanadia and nobel metal-based catalysts, the two nitrogen atoms of N_2 arise, one from NO and the other from ammonia.

V_2O_5-based catalysts also catalyze the reduction of NO_2 in the presence of oxygen.

$$4NH_3 + 2NO_2 + O_2 \; ? \; 3N_2 + 6\,H_2O \qquad (1.6)$$

In general, authors agree that under typical SCR conditions, with NH_3/NO near 1, few percent oxygen and $T<400^oC$, reaction 1.5 stands for the overall stoichiometry on vanadia based catalysts. Accordingly, the SCR process occurs when N_2 is produced with selectivity close to 100% and the ratio of converted moles of NO and NH_3 is 1 (Busca et al. 1998).

For the SCR process one undesirable reaction is the formation of N_2O which is considered to be a powerful greenhouse gas:

$$2NH_3 + 2O_2 \; ? \; N_2O + 3H_2O \qquad (1.7)$$

During the SCR process, the injected ammonia can be wasted by catalytic partial oxidation to elemental nitrogen. This is a nonselective reaction.

$$4NH_3 + 3O_2 \; ? \; N_2 + 6H_2O \qquad (1.8)$$

It can also be completely oxidized to NO. This is another nonselective reaction.

$$4NH_3 + 5O_2 \;?\; 4NO + 6H_2O \qquad (1.9)$$

At temperatures below about 100-200°C, the ammonia can also react with the NO_2 present in the process gas producing explosive NH_4NO_3.

$$2NH_3 + 2NO_2 + H_2O \;?\; NH_4NO_3 + NH_4NO_2 \qquad (1.10)$$

This reaction can be avoided by never allowing the temperature to fall below about 200°C. The tendency for the formation of NH_4NO_3 can also be minimized by metering into the gas stream less than the precise amount of NH_3 necessary to react stoichiometrically with the NOx (Heck et al., 1995).

1.5 Objective of This Study

The objective of this study is to investigate the catalytic pathways for the selective catalytic reduction (SCR) reaction of NO by NH_3 on vanadium pentoxide catalytic surface by means of density functional theory (DFT) calculations. From the experiments, it has been mostly concluded in the literature that the SCR reaction follows an Eley-Rideal mechanism, where NO attacks adsorbed NH_3, however there is a disagreement on the activation mode of the ammonia on the V_2O_5 surface. Therefore before continuing with the reaction mechanism, it is desired to determine the activation mode of the ammonia over the catalytic surface. Then, it is aimed to complete the catalytic cycle by introducing NO to the system.

Moreover, it is also aimed to develop a computational methodology in the field of catalysis in order to use this powerful and newly developing tool more efficiently.

CHAPTER 2

LITERATURE SURVEY

2.1. Experimental Studies

Although there are several studies carried out on the selective catalytic reduction (SCR) reaction of NO by NH_3 over the V_2O_5 catalytic surface, the complete elucidation of the reaction mechanism has not been achieved. Accordingly, there are two different possible mechanism suggested by different researchers for the SCR reaction of NO by NH_3 over vanadium oxide catalyst surface that are:

1- SCR reaction takes place via a Langmuir-Hinshelwood type mechanism.
2- SCR reaction occurs by an Eley-Rideal type mechanism.

The Langmuir-Hinshelwood type mechanism was first suggested by Takagi et al. (1979). In their work, they separately studied the elementary steps of the reaction for the elucidation of the reaction mechanism by using volumetric, infrared, x-ray photoelectron spectroscopy, and mass spectroscopy techniques. Accordingly, no adsorption of NO was observed on the V_2O_5 catalyst surface, even when the surface was oxidized by oxygen or reduced by hydrogen.

However, when a gas mixture of NO and O_2 was introduced onto the V_2O_5 surface, the adsorption took place and NO_2 is adsorbed onto the surface. Also, NH_3 was adsorbed as NH_4^+ over the catalyst surface. Therefore, as the first step of the SCR reaction, NO oxidized by ambient O_2 was adsorbed as NO_2 on V_2O_5, and NH_3 as NH_4, respectively. Then both adsorbate reacts to form the product via a Langmuir-Hinshelwood type mechanism.

On the other hand, Eley-Rideal type mechanism for the SCR reaction of NO by NH_3 is the other possible mechanism type suggested by several researchers. Inomata et al. (1980) were the first group that suggested this kind of a mechanism. By means of the temperature programmed desorption (TPD) experiments they observed a single desorption peak of NH_3, but for NO they did not. Furthermore, from the pulse chromatographic measurements of the adsorptions of NO and NH_3 they found out that NH_3 is strongly adsorbed whereas NO is hardly adsorbed on V_2O_5 at 150°C. When NH_3 gas was introduced onto the catalyst treated with NO gas in the absence or in the presence of O_2 at 250°C, N_2 was not obtained at all as a reaction product, while in the reverse case a considerable amount of N_2 was produced. Also, in the IR spectra, they did not observe any adsorption bonds corresponding to NO, such as NO^+ (ad), NO^- (ad), and NO_2 (ad) species, when NO gas was introduced onto V_2O_5 at temperature higher than room temperature. Nevertheless, when NH_3 gas was introduced onto V_2O_5 surface, they observed peaks contributed to NH_4^+ species. From these results they concluded that the strongly adsorbed NH_3 species on V_2O_5, i.e. NH_4^+ (ad), can react readily with a gaseous NO to form N_2 and H_2O, suggesting an Eley-Rideal mechanism.

Another suggestion for the Eley-Rideal type mechanism was made by Janssen et al. (1987). By means of the isotopic transient studies with oxygen-18 and nitrogen-15, they found out that ammonia did not react with O_2 or O from any source during the reaction and NO did not oxidize to NO_2. For the reaction mechanism it was suggested that both chemisorbed ammonia species and the physisorbed ammonia species were able to react with nitric oxide via an Eley-Rideal mechanism. Chemisorbed ammonia species were defined as being nitrogen-hydrogen-containing species present on the surface during the reaction at 400°C and physisorbed ammonia species were defined as the result of the reaction of OH groups present on the surface with NH_3. They also suggested that two types of water molecule were formed during the reaction: one was originated from the reaction of gaseous NO with the chemisorbed ammonia species and the other was formed as a result of the dehydration of OH groups present on the surface of the catalyst. Thus, it was concluded that lattice oxygen shared with adjacent sites was involved in the reaction.

Gasior et al. (1988) investigated the mechanism of the SCR reaction over unsupported vanadium pentoxide catalyst by pulse reaction technique and suggested that ammonia was strongly adsorbed onto the catalytic surface as NH_4^+ ion, whereas, NO was either weakly adsorbed or not adsorbed at all. Therefore, the reaction was believed to be proceeding by an Eley-Rideal type reaction mechanism.

In 1990, Nan-Yu Topsøe suggested the same type of mechanism by conducting FTIR studies on V_2O_5 surface structures and on the adsorption properties. In order to simulate the different states of the catalyst which may be present during a catalytic cycle, the catalyst had been investigated both in

oxygen and after exposure to the reactants NO and NH_3 alone or together. The catalyst had also been studied after more extensive prereduction in hydrogen. Accordingly, no adsorption of NO was evidenced on the oxidized or the NH_3-reduced surface of V_2O_5 and adsorption occurred only on the H_2-reduced samples. On a partially reduced catalyst with preadsorbed NH_3, NO was observed to oxidize the surface at room temperature. This suggested that NO reduction by NH_3 occurs by an Eley-Rideal type mechanism and V_2O_5 catalyst has an acid-redox function. Their findings did not give any support for the reaction between NO_2 and surface NH_4^+ as postulated by Takagi et al. (1979).

In order to probe the catalytic chemistry of nitric oxide reduction by ammonia on V_2O_5 surface, temperature programmed desorption (TPD) and temperature programmed reaction (TPR) studies were conducted by Srnak et al. in 1992. Accordingly, TPR studies of the reaction between nitric oxide and ammonia probed a Langmuir-Hinshelwood step between adsorbed nitric oxide and ammonia under vacuum conditions, whereas powder TPR studies involve an Eley-Rideal step between adsorbed ammonia and gaseous (or weakly adsorbed) nitric oxide. From their results they concluded that both the Langmuir-Hinshelwood and the Eley-Rideal mechanisms may be effective for selective catalytic reduction of nitric oxide, depending on the reaction conditions. Furthermore, the reactivities appear to be comparable for the strongly and weakly adsorbed nitric oxide species in these two mechanisms, respectively, since the reaction is controlled by the activation of ammonia. Under typical SCR reaction conditions the amount of strongly adsorbed nitric oxide is negligible, and the Eley-Rideal mechanism would seem to dominate.

In 1996, Ramis et al. performed FT-IR studies for the selective catalytic reduction of NOx by NH_3 reaction over the V_2O_5 based catalysts including pure V_2O_5. In their spectra they detected NH_2 vibrations while no adsorbed NO species vibration was observed. They suggested that the main mechanism that leads to reaction products water and N_2 was the reaction between preadsorbed ammonia, i.e. NH_2 species, and gaseous NO, via an Eley-Rideal type mechanism.

As in the case of the reaction mechanism, there is also no general agreement on the nature of the surface sites that involve in the selective catalytic reduction of NO by NH_3 over V_2O_5 catalytic surface. This is due to the surface characteristics of the vanadium pentoxide catalyst. The oxide surface is highly dynamic in nature under reaction conditions consisting of double-bonded oxygen sites, Brønsted acidic V-OH sites, and oxygen vacancies being created, used, or interconverted to one another in the presence of water and the gas phase oxygen. So, for the reaction, there are three different types of adsorbed ammonia species that have been suggested by different researchers: a) V-ONH_2, b) V-ONH_3, c) V-ONH_4. Therefore, it can be concluded that ammonia adsorption over the V_2O_5 catalytic surface may occur either through a Lewis acidic adsorption (as coordinatively bonded NH_3 or NH_2 by abstracting one hydrogen) or by a Brønsted acidic adsorption (as adsorbed NH_4^+ ion) reaction.

Inomata et al. (1980) suggested from the TPD and IR studies that the active site for the ammonia activation is the Brønsted acidic V_s-OH site adjacent to V^{5+}=O site. Ammonia is strongly adsorbed on this site as NH_4^+(ad). Then, gas phase NO reacts with this species to form N_2 and H_2O by reducing the surface to V-OH. The V-OH species are then reoxidized to V^{5+}=O by either gaseous O_2, or bulk V=O species. This suggests that V^{5+}=O sites also play an essential role in

the reaction. The mechanism suggested by Inomata et al. (1980) is summarized in Figure 2.1.

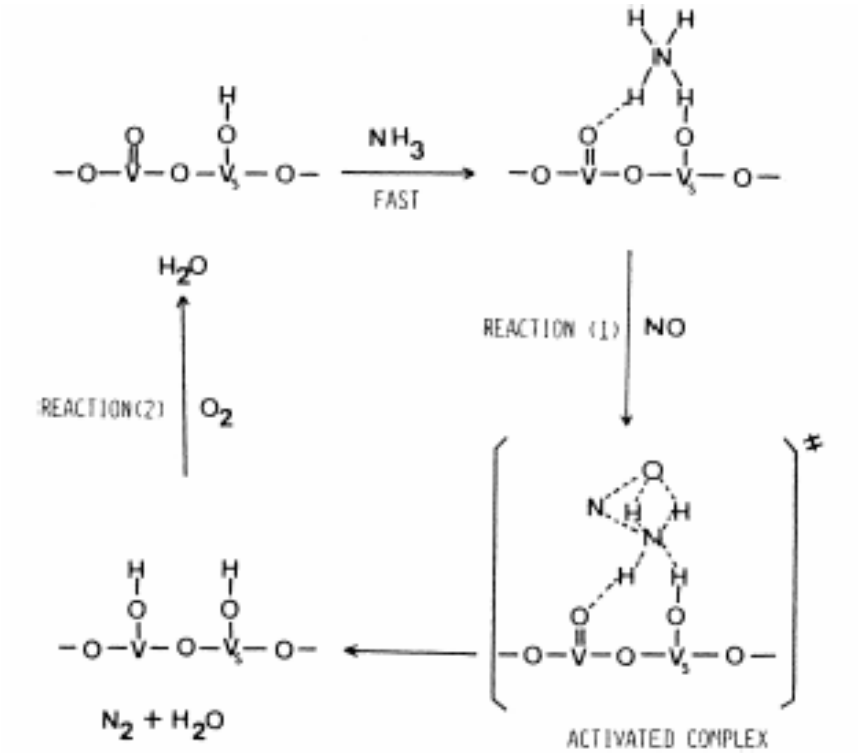

Figure 2.1. Mechanism of the NO-NH_3 reaction on vanadium oxide catalysts proposed by Inomata et al. (1980) in the presence of oxygen.

For the selective catalytic reduction reaction of NO by NH_3 over V_2O_5 catalytic surface, Janssen et al. (1987) found that at least two types of active site were present on the surface of the catalyst and that these sites were probably due to the presence of vanadium species with valances of both +4 and +5. Two different reactions occur on these different sites: the oxidized sites could be reduced by ammonia while reoxidation can be brought about by ambient oxygen, by lattice oxygen from underlying layers, or by the oxygen of NO, depending on the reaction conditions. Therefore the V=O species was considered to be the active sites that were easily reduced. Accordingly, ammonia was adsorbed on this site as V-ONH_2 that is proposed as the key intermediate in

the SCR reaction by reducing the adjacent V=O site to V-OH. The proposed reaction mechanism is given in Figure 2.2.

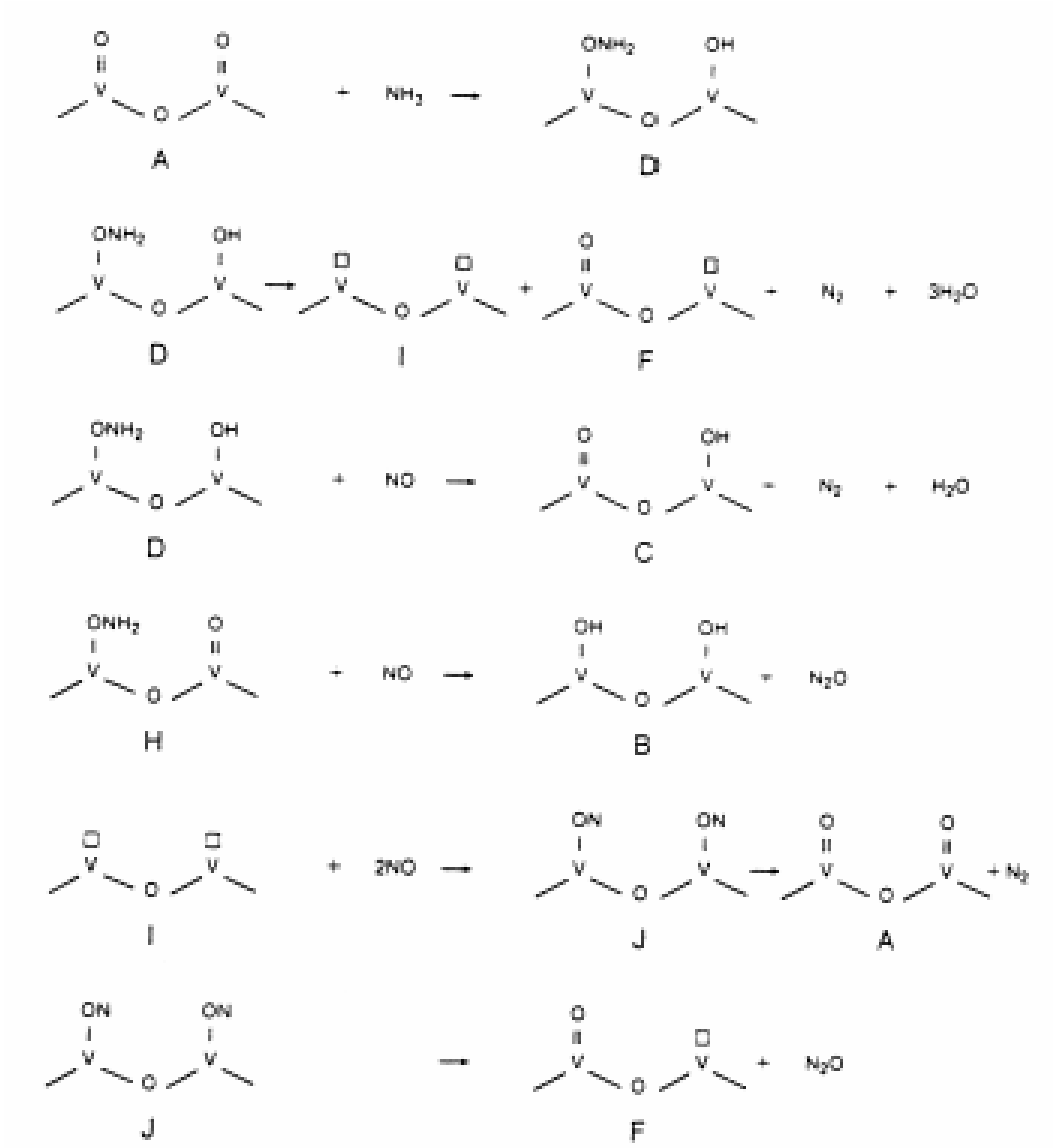

Figure 2.2. Reaction mechanism of the NO-NH_3 reaction on V_2O_5 surface proposed by Janssen et al. (1980)

Nan-Yu Topsøe (1990) observed a slight intensity increase of the V=O band in the FTIR spectra when the catalyst was reduced by NH_3. This was considered as associated with a decrease in V-OH concentration on the surface. And also the IR spectra of ammonia adsorbed on V_2O_5 in its oxidized and reduced states showed distinct bands attributed to NH_4^+ species and weak bands

due to the coordinated NH_3 species, which in turn suggested that predominantly Brønsted acid sites (V-OH) were present on the surface of oxidized V_2O_5. Therefore, ammonia was preferentially adsorbed on Brønsted acidic V-OH sites as NH_4^+ ion. Moreover, when NO was introduced to the system pretreated by NH_3, it was seen that NH_4^+ species were preferentially removed indicating that the reaction is predominantly between NO and surface NH_4^+ species, in agreement with the proposal of Gasior et al.(1988).

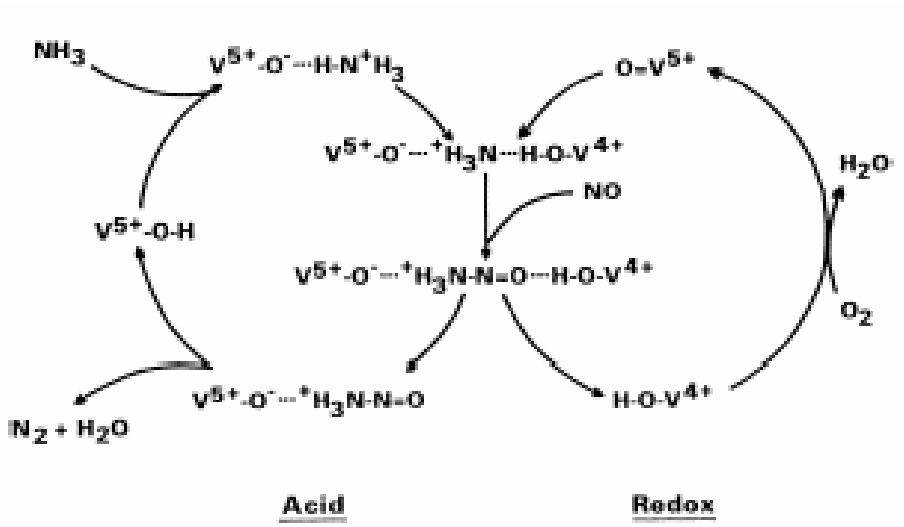

Figure 2.3. Illustration for the reaction mechanism for the SCR over V_2O_5 proposed by Topsøe et al. (1990)

In 1994, by means of the isotopic labeling studies using $^{18}O_2$, $^{15}NH_3$, ^{15}NO, and $^{15}N^{18}O$, Ozkan et al. suggested that ammonia adsorbs on at least three types of sites present on V_2O_5 catalyst surface, which were denoted as types A, B, and C. The type A sites were pairs of V=O centers located on the (010) planes that lead to dissociative adsorption of ammonia to give $V\text{-}ONH_2$ and V-OH species. The ammonia species thus created were believed to be short lived, converting quickly to NO and water with an oxygen vacancy and OH group left behind. The type B sites, which were also located on the (010) planes, were thought to be double-bonded oxygen sites neighboring a V-OH group, leading to the formation

of V-ONH_3 species. These species appeared to have a longer “surface life” and had the ability to couple between themselves to form nitrogen and nitrous oxide or to react with NO to give nitrous oxide. The type C sites were thought to be located mainly on the side planes and to consist of pairs of V-OH groups, leading to the formation of surface ammonium ion species. From the structural specificity studies that link nitrogen selectivity in SCR reaction to the side planes, they concluded that these sites (type C) were the primary sites that reduce NO selectively.

In contrast to these studies, Ramis et al. (1996) observed very intense bonds corresponding to the coordinatively bonded NH_3 mode in the NH stretching region of the adsorbed ammonia on V_2O_5 surface. This was considered to be sensitive to the strength of the Lewis acid-base interaction. Furthermore, they investigated the activity of CuO/TiO_2 catalyst for the SCR reaction and observed only species coordinated on Lewis acid sites. According to the similarity of the catalytic behavior of these materials (CuO/TiO_2 and V_2O_5) in the SCR reaction, they suggested that Brønsted acidity is not a necessary requirement for SCR activity. Ammonia is activated for SCR by coordination over Lewis acidic sites not on the Brønsted acidic V-OH sites and this activated ammonia is easily transformed to amide NH_2 species by the hydrogen abstraction. NH_2 species formed reacts with NO to give rise to reaction products nitrogen and water. The catalytic cycle is closed by re-oxidation of the reduced catalyst by gaseous oxygen. Since amide species is formed during the reaction as an intermediate, they referred to this mechanism as the “amide-nitrosamide” mechanism. The reaction mechanism of the selective catalytic reduction reaction of NO by NH_3 proposed by Ramis et al. (1996) is summarized in Figure 2.4.

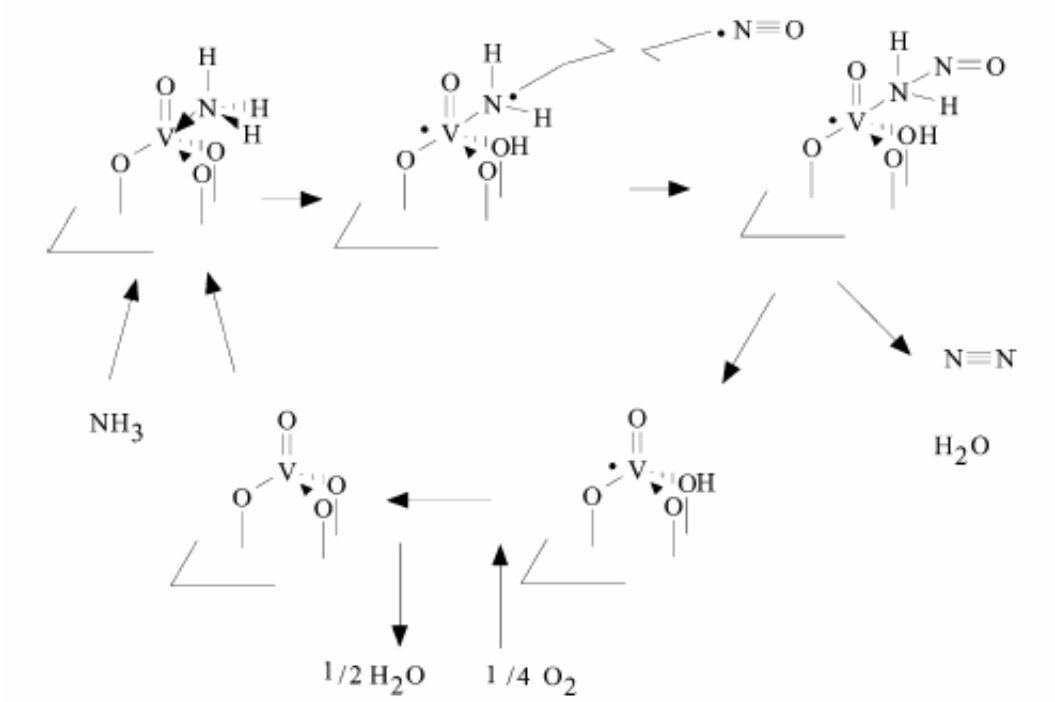

Figure 2.4. The proposed reaction mechanism of Ramis et al. (1996) for the SCR reaction of NO by NH_3

2.2. Theoretical Studies

Although there are several experimental studies performed to elucidate the mechanism of the SCR reaction of NO by NH_3, there is still disagreement concerning the active sites involved in the SCR reaction. There are very few studies that have been carried out to obtain more detailed information about the nature of the active sites theoretically.

The study that was carried out by Gilardoni et al. (1997) is one of them. In this work, Gilardoni et al. performed quantum chemical calculations by using density functional theory (BP86 method) to model the mechanism of selective catalytic reduction of NO by NH_3 on vanadium oxide catalytic surface starting from the ammonia activation over Brønsted acidic V-OH site. For the calculations a cluster with C_s symmetry was constructed as $V_2O_9H_6$-H with a Brønsted acidic

V-OH site. During the study the following computational procedure was followed; the adsorbing molecule was located in the vicinity of the active site of the cluster and then one point equilibrium geometry calculations were performed. At the end of the calculations carried out for the first step of the reaction (Brønsted acidic ammonia adsorption), two different geometries were obtained. By comparing calculated total energies and calculated vibration frequency data, it was concluded that one of the geometries with higher energy and one imaginary frequency is a transition state structure. The other geometry was considered as the global minimum geometry, in other words, equilibrium geometry for the ammonia adsorption over Brønsted acidic V-OH site. The relative energy for this geometry was calculated as -25kcal/mol. As the second step of the SCR reaction, NO molecule was introduced to the equilibrium geometry of the first step and equilibrium geometry calculation was performed by freezing the structural parameters of i) the oxygen atom bridging the two vanadyl groups, ii) the vanadium atoms, and iii) the six O-H groups bonded to the vanadium centers. This led to the release of the adduct H_2NNO (N-nitrosamide) and the formation of two V-OH sites. The heat of this reaction was found to be +18.2kcal/mol, corresponding to an endothermic process. Then the intermediate formed at the end of this step, undergoes a series of H atom migrations and some isomerisation reactions to yield reaction products N_2 and water. At the end of the DFT calculations carried out for the SCR reaction of NO by NH_3 starting from the NH_3 adsorption over Brønsted acidic V-OH site, Gilardoni et al. concluded that the adsorbed NH_3 (as NH_4^+) is activated by transferring an H to the V^{5+}=O site, which becomes partly reduced. Gaseous or weakly adsorbed NO subsequently reacts with this activated NH_3, leading to the formation of V^{4+}-OH and NH_2NO. In order to complete the catalytic cycle, it was suggested that V^{4+}-OH must be oxidized to V^{5+}=O at the end of the reaction. In this study, since only one point

equilibrium geometry calculations were performed (they did not perform coordinate driving calculations, so they could not obtain energy profiles), the information about the transition state structures is not sufficient; the geometries obtained may not be the exact transition state geometries. And also there is a lack of information about the other possible types of ammonia adsorption modes, such as Lewis acidic adsorption; it was assumed that the SCR reaction is started with the ammonia adsorption over Brønsted acidic V-OH site.

In a very similar manner, Dumesic et al. (2002) performed density functional theory (B3LYP method) calculations to probe various adsorption geometries and energies for the interaction of ammonia with hydrogen atoms present on clusters representing vanadium oxide, with the aim of addressing various factors involved in controlling the formation of Brønsted acid sites that interact with ammonia to form NH_4 species. For the calculations, several vanadium pentoxide clusters consisting of one to four vanadium atoms were constructed with different oxidation states of vanadium atoms, +4 and +5. While constructing these clusters, some angles and distances were kept constant. The computational procedure followed by Dumesic et al. was very close to what Gilardoni et al. followed. The adsorbing molecule was located in the vicinity of the active site of the cluster, and geometry optimization calculations were performed to obtain the equilibrium geometries. At the end of the calculations that were performed over the cluster with one vanadium atom (VO_4H_3), it was concluded that ammonia is adsorbed on the vanadia monomers as H-bonded NH_3 species, with an energy change of adsorption equals to -59kJ/mol. The adsorption of ammonia calculations were also performed on the clusters with the formula of $H\text{-}V_2O_7H_4.(H_2O)_2$. As with the VO_4H_3 monomer, the calculations showed that ammonia is adsorbed on these clusters as H-bonded NH_3 species,

with adsorption energy changes near -50kJ/mol. Thus, it was observed that neither of these clusters led to the formation of NH_4^+ ion at the end of the adsorption of NH_3 reaction. In order to address the factors responsible for the adsorption of ammonia to form NH_4 species, they constructed several other clusters containing two to four vanadium atoms with different oxidation states. By means of the DFT calculations performed on these clusters it was concluded that ammonia adsorption as NH_4 is not possible in clusters where the formal oxidation state of the vanadium cations was 4+, over these type of clusters, ammonia is adsorbed as H-bonded NH_3. On the other hand, over the clusters $V_2O_9H_8$ and $V_4O_{16}H_{12}$ in which vanadium has an oxidation state of +5, the adsorbed ammonia forms NH_4 species between two V=O sites, with adsorption energy changes of -112kJ/mol and -110kJ/mol, respectively. Moreover, the total Mulliken charge on the NH_4 species formed was calculated as +0.802e, suggesting that ammonia was adsorbed as NH_4^+ species.

As a continuation of this work, Dumesic et al. published another article in 2003. In this article, the steps involved in the formation of the adsorbed NH_2NO on the $V_4O_{16}H_{12}$ cluster were investigated and the steps involved in the catalytic decomposition of NH_2NO to form reaction products N_2 and H_2O were addressed. Furthermore, ammonia adsorption energies over three different types of Brønsted acidic sites were calculated. To obtain three different types of the Brønsted acidic sites, hydrogen atom was placed either on the doubly bonded Oxygen atom (O1), or on the bridging oxygen atom between two vanadium atoms (O2), or on the bridging Oxygen atom between three vanadium atoms (O3). At the end of the calculations, it was concluded that the Brønsted acidic site located on the doubly bonded oxygen atom (O1-H site) is the most active site for the ammonia adsorption reaction. For the interaction of NO with the

adsorbed ammonia species, Dumesic et al. performed a series of geometry optimization calculations where the N-N bond was constrained at successively shorter distances and all other atoms in the NH_4-NO complex were relaxed fully. Among the optimized geometries in this series, the one with the higher energy was considered as the approximate transition state. By means of the DFT calculations the energy of the approximate transition state was obtained as +4kJ/mol, and that for the equilibrium geometry was calculated as -25kJ/mol with respect to the $V_4O_{16}H_{12}$ cluster and gas phase NO and NH_3. From the adsorbed NH_3NHO species, the reaction was preceded by the transfer of two hydrogen atoms to the $V_4O_{16}H_{12}$ cluster which led to the formation of the NH_2NO intermediate. The energy of the approximate transition state was calculated as +48kJ/mol and that for the adsorbed NH_2NO species on the $V_4O_{16}H_{12}$ cluster was obtained as -87kJ/mol with respect to the $V_4O_{16}H_{12}$ cluster plus gas phase NH_3 and NO species. At the end of the DFT calculations, it was found out that to form the reaction products N_2 and H_2O, the NH_2NO reaction intermediate must undergo a series of hydrogen-transfer steps in a “push-pull” manner on the vanadium cluster. In each of those steps, a hydrogen atom is transferred from a VOH group to an adsorbed species with NH_2NO stoichiometry, and a second hydrogen atom is simultaneously transferred from the NH_2NO-stoichiometric species to an adjacent V=O group. The resulting reaction mechanism and the energy changes of the geometries at each of the geometries with respect to the $V_4O_{16}H_{12}$ cluster and gas phase NH_3 and NO obtained is given in Table 2.1.

Table 2.1. The reaction mechanism suggested by Dumesic et al. (2003) and the energy changes of the geometries at each of the reactions w.r.t. the $V_4O_{16}H_{12}$ cluster and gas phase NH_3 and NO.

Reaction	**Energy, kJ/mol**
$NH_{3(g)}$ + V=O ? (V=O) – NH_4 – (O=V)	-110
(V=O) – NH_4 – (O=V) + NO ? (V=O) – NH_3NHO – (O=V)	-25
(V=O) – NH_3NHO – (O=V) ? (V-OH) – NH_2NO + VOH	-87
(V-OH) – NH_2NO + V=O ? (VOH) – *trans* – HN=NOH + V=O	-82
(VOH) – *trans* – HN=NOH + V=O ? (VOH) – *cis* – HN=NOH + V=O	-53
(VOH) – *cis* – HN=NOH ? (VOH) – *cis* – HN=NO – trans – H	-76
(VOH) – *cis* – HN=NO – trans – H + V=O ? N_2(g) + H_2O (g) + VOH + V=O	-273

Although Dumesic et al. performed a very detailed study for the SCR reaction of NO by NH_3 reaction on different catalyst clusters with different size and oxidation states, there were some missing points in their work. Vibration frequency calculation is one of them. For none of the equilibrium geometries obtained, especially for the adsorbed NH_4^+ species, for which there are many experimental vibration frequency data in literature, vibration frequencies were calculated by means of the DFT methods. And also transition state structures suggested by Dumesic et al. were not the exact structures, since they did not perform any transition state calculations; they only reported the structure with the highest energy in a series of constrained geometry optimization calculations as the approximate transition state geometry.

CHAPTER 3

METHODOLOGY OF THEORETICAL INVESTIGATIONS

3.1. Theory of the Computational Quantum Chemical Methods

3.1.1. Background of the Computational Quantum Chemistry

Classical mechanics is concerned with the trajectories of particles which theoretically can be calculated from knowledge of the initial conditions and the structure of the Hamilton H, or the sum of a kinetic - energy contribution T and potential-energy function V.

$$H = T + V \tag{3.1}$$

However, the existence of the atom can not be explained classically, but rather by the wave properties of the electron bounded to the nucleus. For this reason Schrödinger suggested to replace the classical kinetic and potential energy functions of (3.1) with linear operators $\hat{T}$ and $\hat{V}$ set up a wave equation of the form

$$\hat{H}\Psi = E\Psi \tag{3.2}$$

where the solutions Ψ, the so called wave functions, would describe the behavior of all the particles and the quantum-mechanical Hamilton above is

$$\hat{H} = \hat{T} + \hat{V} \tag{3.3}$$

For one electron system such as the hydrogen atom, with the electron centered on the atomic nucleus, kinetic and potential energy operators are

$$\hat{T} = -\frac{h}{8p^2 m}\tilde{N}^2 \tag{3.4}$$

$$\hat{V} = -\frac{Ze^2}{r} \tag{3.5}$$

where m is the mass of the electron, r is the distance of the electron from the nucleus, Z is the atomic number, and e is the unit of the electronic charge, and in equation (3.3) the Laplacian $\tilde{N}^2$ is in cartesian coordinates.

Born-Oppenheimer approximation states that because the nuclei are so much more massive than the electrons, the electrons adjust essentially instantaneously to any motion of the nuclei, consequently we may consider the nuclei to be fixed at some internuclear separation in order to solve the Schrödinger equation (3.2) for the electronic wave function in other words separation of wave function into

$$\Psi \approx \Psi_N \Psi_{elec} \tag{3.6}$$

where the first term in the product of equation (3.6) accounts for the motion of the nuclei and the second term involves the electron motion. Furthermore, introducing center-of mass and relative coordinates, the nuclear wave function reduces to

$$\Psi_N \approx \Psi_{trans}(C.M.)\Psi_{rot}\Psi_{vib} \tag{3.7}$$

where the center-of mass translation, and rotational and vibrational contributions to the nuclear wave function are now explicitly shown. Thus, the problem of determining the structure of a complex molecule reduces to solving each Schrödinger equation for the electronic motion, the translational motion of the center of mass, and the rotational and vibrational of the nuclei separately. The electronic energy is estimated therefore by the Schrödinger equation for a molecule with n electrons calculation procedure is similar for the other types of motion

$$\hat{H}_{elec}(1,2,\ldots,n)\Psi_{elec}(1,2,\ldots,n) = E_{elec}\Psi_{elec}(1,2,\ldots,n) \tag{3.8}$$

and for a given intermolecular distance the total energy of the system is

$$E_T^0 \approx E_{elec} + \sum_{A<B} e^2 Z_A Z_B r_{AB}^{-1} \tag{3.9}$$

where the second term is the electrostatic internuclear repulsion energy and A, B designate different nucleus.

Molecular orbital theory is concerned with electronic wave functions only, and henceforth the electronic subscripts will be dropped from the electronic Hamiltonian and wave function. The molecular energy given by equation (3.9) is the energy at absolute zero with no contributions from the translational, rotational or vibrational motions. The later forms of energy must be considered to determine thermochemistry under conditions of practical interest as

$$E_T \approx E_{trans} + E_{vib} + E_{rot} + E_{elec} \qquad (3.10)$$

Once the total energy E_T^0 of equation (3.9) is known for a given molecular geometry, a potential energy hypersurface (PES) can be generated as function of geometry, and the minima on the (PES) corresponds to the most stable configuration, or in mathematical terms for molecules or radicals,

$$\partial E_T^0 / \partial g_i = 0$$

$$\partial^2 E_T^0 / \partial (g_i)^2 > 0$$

where g_i is any geometrical variable.

The heat of formation for the molecule can then be obtained from the total energy of equation (3.10) via

$$\Delta H_f = E_T - \sum_{k=1}^{n} E_k^A + \sum_{i=1}^{N} \Delta H_{fi}^A \qquad (3.11)$$

where E_k^A and ΔH_{fi}^A are the electron energies and the heats of formation of individual atoms, respectively. Clearly, this approach requires the accurate knowledge of the atomic heats of formation, which may or may not be available.

The electronic Hamilton (non-relativistic) of a molecule is given by the following expression in atomic units (h/2π = e = m = 1)

$$\hat{H} = -\sum_p \tfrac{1}{2}\nabla_p^2 - \sum_A \sum_P Z_A r_{Ap}^{-1} + \sum_{p<q} r_{pq}^{-1} \qquad (3.12)$$

where A designate the nuclei, p, q electrons, and r is the interparticle distance.

The solutions to the electronic Schrödinger equation (3.8) are infinite but for stationary, bound states only the continuous, single-value eigenfunctions that vanish at infinity need to be considered, and the electronic energies are the eigenvalues E_i or

$$\hat{H}\Psi_i = E_i\Psi_i \qquad (3.13)$$

The eigenfunctions are normalizable and mutually orthogonal (i.e., orthonormal) or mathematically they satisfy the condition

$$\int \Psi_i \Psi_j dt = \langle \Psi_i | \Psi_j \rangle = d_{ij} \qquad \text{all i ,j} \qquad (3.14)$$

In equation 3.14, the interaction is over the volume element for the electron, and it is given with the matrix or Dirac notation for the integral, where

d_{ij} is the Kronecker delta. The electronic energy of the system E_i is the expectation value of the Hamiltonian or the solution for E_i is

$$\int \Psi_i \hat{H} \Psi_j dt = \left\langle \Psi_i \middle| \hat{H} \middle| \Psi_j \right\rangle = E_i \qquad (3.15)$$

The complete treatment of a quantum-mechanical problem involving electronic structure requires the complete solution of the Schrödinger equation (3.8). This is only possible for one-electron systems, and for many-electron systems, where the electron repulsion term in the Hamilton renders an analytical solution impossible, the variation principle is applied. This method in its full form is completely equivalent to the differential equations, and it has many advantages in the ways it can be adapted to approximate solution wave functions (Pople, 1970). The variation principle states that if ψ is a solution to equation (3.8) then for any small change $\delta\psi$

$$d\,E = d\langle \Psi | \hat{H} | \Psi \rangle = 0 \qquad (3.16)$$

If this criterion is applied to an electronic wave function ψ, in the appropriate number of dimensions, all the eigenfunctions ψ_i for the Hamilton will be obtained. If only an approximation to the wave function ψ is used, and then the eigenfunctions ψ_i and eigenvalues E_i are only approximations to the correct values, with the accuracy of the estimates improving as better approximations for the total wave function ψ is used.

The orbital approximation suggests that the total electron wave function ψ can be written as the Hartree product of one-electron wave functions, $\psi_i\eta(\zeta)$,

called spin orbitals (Gasiorowicz 1974) consisting of the product of spatial and spin functions, where $\eta(\zeta)$ is the spin function that can take values α or β, or

$$\Psi(1,2,\ldots,n) = O(s)A\left[y_1(1)a(1)y_2(2)b(2)y_3(3)a(3)\ldots y_n(n)b(n)\right] \tag{3.17}$$

In equation (3.17) A is the antisymmetrizer, ensuring that the wave function changes sign on interchange of any two electrons in accordance with the Pauli exclusion principle, and O(S) is a spin projector operator that ensures that the wave function remains an eigenfunction of the spin-squared operator S^2

$$S^2\Psi = S(S+1)\Psi \tag{3.18}$$

O(S) can become quite complex but for a closed shell molecule, with all electrons paired in the spin orbitals O(S)=1. Thus, for a closed-shell system with 2n electrons, and two electrons paired in each spatial orbital, the many-electron wave function becomes

$$\Psi(1,2,\ldots,n) = A\left[y_1(1)a(1)y_1(2)b(2)y_2(3)a(3)\ldots y_n(2n-1)a(2n-1)y_n(n)b(n)\right] \tag{3.19}$$

Equation (3.19) is known as *Slater determinant* which is the proper form for the many electron wave function for closed shells as a single determinant of spin orbitals. The discussion now proceeds to the details of the actual determination of the electron spatial orbitals ψ_i for a closed-shell system. This involves the application of the variational principle or equation (3.16) for the solution of (3.19). The best molecular orbitals, therefore, are obtained by

varying all the contributing one-electron functions $\psi_1, \psi_2, \psi_3, \ldots \psi_n$, in the Slater determinant equation (3.19) until the electronic energy achieves its minimum value. This will give the best approximation to the many-electron wave function, ψ and the electron orbital or molecular orbitals ψ_i so obtained are referred to as *self consistent* or *Hartree-Fock* molecular orbitals.

Mathematically, the problem involves the minimization of the total electron energy with the orthonormality constraint for the electron orbitals as

Minimize $G = E - 2 \sum_i \sum_j e_{ij} S_{ij}$ (3.20)

where, Orthonormality $S_{ij} = \int \psi_i^* \psi_j \, dt = \delta_{ij}$ (3.21)

and $E = \langle \Psi(1,2,\ldots,n) | \hat{H} | \Psi(1,2,\ldots,n) \rangle$ (3.22)

where $\psi(1,2,3,\ldots,n)$ is given by equation (3.19).

The minimization consists of setting $\delta G = 0$ and leads to the following differential equations (see Pople, 1970 for derivations).

$$\left[\hat{H}^{core} + \sum_j 2 J_j - \hat{K}_j \right] \psi_i = e_i \psi_i \qquad i = 1,2,\ldots,n \qquad (3.23)$$

or, $\hat{F} \psi_i = e_i \psi_i$ $\qquad i = 1,2,\ldots,n$ (3.24)

In equation (3.24) F is the one-electron Hartree-Fock Hamiltonian operator consisting of the terms defined in equation (3.23) within the square brackets. Equation (3.24) is known as the *Hartree-Fock* equation and states that the best molecular orbitals are eigenfunctions of the Hartree-Fock equation Hamiltonian operator. The first operator of the Hartree-Fock Hamiltonian in

equation (3.23) is the one-electron Hamiltonian for an electron moving in the field of the bare nuclei, which is defined as

$$\hat{H}(p)^{core} = -\tfrac{1}{2}\nabla_p^2 - \sum Z_A r_{pA}^{-1} \qquad (3.25)$$

The second operator accounts for the average effective potential of all other electrons affecting the electron in the molecular orbital ψ_i , can be defined by

$$\hat{J}_j(1) = \int \psi_j^*(2)\frac{1}{r_{12}}\psi_j(2)dt_2 \qquad (3.26)$$

The final operator in the square bracket of equation (3.23) is the exchange potential and it arises from the effect of the antisymmetry of the total wave function on the correlation between electrons of parallel spin and it can be defined by

$$K_j(1)\psi_i(1) = \left[\int \psi_j^*(2)\frac{1}{r_{12}}\psi_i(2)dt_2\right]\psi_j(1) \qquad (3.27)$$

To account for the correlation of electrons of different spin, the term missing in equation (3.23), Configuration Interaction (CI) method can be applied. This method incorporates virtual orbitals or nonbonding orbitals into the total wave function. This is beyond the scope of this discussion. For more information see Pople (1970)

The eigenvalues of equation (3.23) or (3.24) are the energies of electrons occupying the orbitals ψ_i are thus known as orbital energies, defined as

$$e_i = H_{ij}^{core} + \sum_i \left(2J_{ij} - K_{ij}\right) \tag{3.28}$$

where the one-electron core energy for an electron moving in the field of bare nuclei is

$$H_{ij}^{core} = \int \psi_i^*(1)\, \hat{H}^{core}\, \psi_i\, d\tau_j \tag{3.29}$$

the coulomb interaction energy is given by

$$J_{ij} = \iint \psi_i^*(1)\psi_j^*(2)\frac{1}{r_{12}}\psi_i(1)\psi_j(2)\, d\tau_1 d\tau_2 \tag{3.30}$$

and the exchange energy is

$$K_{ij} = \iint \psi_i^*(1)\psi_j^*(2)\frac{1}{r_{12}}\psi_j(1)\psi_i(2)\, d\tau_1 d\tau_2 \tag{3.31}$$

The general procedure for solving the Hartree-Fock equations is iterative. A first solution for the molecular orbitals ψ_i is assumed for generating the Hartree-Fock operator F. The set of molecular orbitals generated by this estimate of the Hartree-Fock operator is then used to repeat the calculations and so on until the orbital no longer changes, within a certain tolerance, on further interaction. These orbitals are said to be *self consistent with the potential field*

they generate. In addition to the n occupied orbitals, there will be unoccupied orbitals called virtual orbitals of higher energy.

The method outlined above for solving the Hartree-Fock equation is impractical or molecular systems of any size and other approaches must be found (Pople, 1970). The most rewarding approach consists of approximating the molecular orbitals by a *linear combination of atomic orbitals* or LCAO in the form

$$y_i = \sum_m c_{mi} f_m \qquad (3.32)$$

where the ϕ_μ are the atomic orbitals constituting the molecular orbital or basis set.

In carrying out numerical calculations of molecular orbitals, it is necessary to have convenient analytical forms for the atomic orbitals of equation (3.32) for each type of atom in the molecule. The solutions of the Schrödinger equation for one-electron systems (H-atom) can be written in the form by separation of variables

$$\Phi(r, q, f) = R_{n,l}(r) Y_{lm}(q, f) \qquad (3.33)$$

where r, θ, and ϕ are the spherical coordinates centered on the atom. The angular part of the above equation or $Y_{lm}(\theta,\phi)$ are the spherical harmonics defined as

$$Y_{lm}(q, j) = \Theta_{lm}(q) \phi_m(j) \qquad (3.34)$$

where l is the azimutal quantum number, and m is the magnetic quantum number. For the radical part of the atomic function, the so called *Slater Type Orbitals* (STO) are used with the form

$$R_{n,l}(r) = (2V)^{n+1/2}\left[(2n)!\right]^{-1/2} r^{n-1} \exp(-Vr) \qquad (3.35)$$

where n is the principle quantum number, and l is the orbital exponent, a function of the atomic number.

The variational principle is then applied as previously outlined except the total electron wave function consists of the product of molecular orbitals such as given in equation (3.32) above and the orthonormality of the electron wave function leads to

$$\sum_{mn} c_{mi}^{*} c_{nj} S_{mn} = d_{ij} \qquad (3.36)$$

where $S_{\mu\nu}$ is the overlap integral for the atomic orbitals, defined as

$$S_{mn} = \int f_m(1) f_n(1) dt_1 \qquad (3.37)$$

This leads to the so called *Roothan equations* given by

$$\sum_{n} \left(F_{mn} - e_i S_{mn}\right) C_{ni} = 0 \qquad i = 1,2,\ldots,n \qquad (3.38)$$

where the elements of the matrix representation of the Hartree-Fock hamiltonian are

$$F_{mn} = H_{mn} + \sum_{ls} P_{ls}\left[(mn|ls) - \tfrac{1}{2}(ml|ns)\right] \tag{3.39}$$

and

$$H_{mn} = \int f(1)\hat{H}^{core} f_{v}(1)dt_1 \tag{3.40}$$

$$P_{mn} = 2\sum_{i}^{occ} c_{mi}^{*} c_{vi} \tag{3.41}$$

$$(mn|ls) = \iint f_m^{*}(1) f_n^{*}(1) \frac{1}{r_{12}} f_l(2) f_s(2) dt_1 dt_2 \tag{3.42}$$

The matrix of elements $P_{\mu\nu}$ is the electron density matrix, $H_{\mu\nu}$ are the elements of the core Hamiltonian with respect to atomic orbitals, and equation (3.42) is the general two-electron interaction integral over atomic orbitals. Equations (3.38) are algebraic equations in contrast with the differential equations (3.23) or (3.24) previously derived.

The Roothan equation (3.38) can be written in matrix from as

$$FC = SCE \tag{3.43}$$

where E is the diagonal matrix of the ε_i. The matrix elements of the Hartree-Fock Hamiltonian operator are dependent on the orbitals through the elements $P_{\mu\nu}$, and the Roothan equations are solved by first assuming an initial set of linear expansion coefficients $c_{\mu i}$, generating the corresponding density matrix $P_{\mu\nu}$ and computing a first guess to $F_{\mu\nu}$. The diagonalization procedure is effected by standard matrix eigenvalue techniques, and new expansion coefficients are calculated. The whole process is repeated until the coefficients no longer change within a given tolerance on repeated iteration (Pople, 1970).

3.1.2. Basis Sets

Ab initio methods try to derive information by solving the Schrödinger equation without fitting parameters to experimental data. Actually, *ab initio* methods also make use of experimental data, but in a somewhat more subtle fashion. Many different approximate methods exist for solving the Schrödinger equation, and the one to use for a specific problem is usually chosen by comparing the performance against known experimental data. Experimental data thus guides the selection of the computational model, rather than directly entering the computational procedure.

One of the approximations inherent in essentially all *ab initio* methods is the introduction of a basis set. Expanding an unknown function, such as a molecular orbital, in a set of known functions is not an approximation, if the basis is complete. However, a complete basis means that an infinite number of functions must be used, which is impossible in actual calculations. An unknown molecular orbital (MO) can be thought of as a function in the infinite coordinate system spanned by the complete basis set. When a finite basis is used, only the components of the MO along those coordinate axes corresponding to the selected basis can be represented. The smaller the basis, the poorer the representation. The type of basis functions used also influence the accuracy. The better a single basis function is able to reproduce the unknown function, the fewer are basis functions necessary for achieving a given level of accuracy. Knowing that the computational effort of *ab initio* methods scales formally as at least M^4, it is of course of prime importance to make the basis set as small as possible without compromising the accuracy.

3.1.2.1. Slater and Gaussian Type Basis Sets

There are two types of basis functions (also called *Atomic Orbitals,* AO, although in general they are not solutions to an atomic Schrödinger equation) commonly used in electronic structure calculations: *Slater Type Orbitals* (STO) and *Gaussian Type Orbitals* (GTO). Although STO provides more accurate results, GTO is more favored due to the ease of the calculation process. Slater type orbitals have the functional form

$$X_{x,n,l,m}(r,q,j) = NY_{l,m}(q,j)r^{n-1}e^{-zr} \qquad (3.44)$$

N is a normalization constant and $Y_{l,m}$ are the usual spherical harmonic functions. The exponential dependence on the distance between the nucleus and the electron mirrors the exact orbitals for the hydrogen atom. However, STOs do not have any radial nodes.

Nodes in the radial part are introduced by making linear combinations of STOs. The exponential dependence ensures a fairly rapid convergence with increasing number of functions. However, the calculation of three- and four-centre two-electron integrals cannot be performed analytically. STOs are primarily used for atomic and diatomic systems where high accuracy is required and in semi-empirical methods where all three- and four-centre integrals are neglected.

Gaussian type orbitals can be written in terms of polar or cartesian coordinates:

$$X_{x,n,l,m}(r,q,j) = NY_{l,m}(q,j)r^{(2n-2-l)}e^{-zr^2}r$$
$$X_{x,l_x,l_y,l_z}(x,y,z) = Nx^{l_x}y^{l_y}z^{l_z}e^{-zr^2} \qquad (3.45)$$

where the sum of l_x, l_y and l_z determines the type of orbital (for example $l_x + l_y + l_z = 1$ is a p-orbital). Although a GTO appears similar in the two sets of coordinates, there is a subtle difference. A d-type GTO written in terms of the spherical functions has five components *($Y_{2.2}$, $Y_{2.1}$, $Y_{2.0}$, $Y_{2.-1}$, $Y_{2.-2}$)*, but there appear to be six components in the Cartesian coordinates *(x^2, y^2, z^2, xy, xz. yz).* The latter six functions, however, may be transformed to the five spherical d-functions and one additional s-function *($x^2 + y^2 + z^2$).* Similarly, there are 1O cartesian "f-functions" which may be transformed into seven spherical f-functions and one set of spherical p-functions. Modem programs for evaluating two-electron integrals are geared to Cartesian coordinates, and they generate pure spherical d-functions by transforming the six Cartesian components to the five spherical functions. When only one d-function is present per atom the saving by removing the extra s-function is small, but if many d-functions and or higher angular moment functions (f-, g-, h- etc. functions) are present, the saving can be substantial. Furthermore, the use of only the spherical components reduces the problems of linear dependence for large basis sets.

The r^2 dependence in the exponential makes the GTO inferior to the STOs in two aspects. At the nucleus the GTO has zero slope, in contrast to the STO which has a "cusp" (discontinuous derivative), and GTOs have problems representing the proper behavior near the nucleus. The other problem is that the GTO falls off too rapidly far from the nucleus compared with an STO, and the "tail" of the wave function is consequently represented poorly. Both STOs and GTOs can be chosen to form a complete basis, but the above considerations

indicate that more GTOs are necessary for achieving a certain accuracy compared with STOs. A rough guideline says that three times as many GTOs as STOs are required for reaching a given level of accuracy. The increase in number of basis functions, however, is more than compensated for by the ease by which the required integrals can be calculated. In terms of computational efficiency, GTOs are therefore preferred, and used almost universally as basis functions in electronic structure calculations. Furthermore, essentially all applications take the GTOs to be centered at the nuclei. For certain types of calculation the centre of a basis function may be taken not to coincide with a nucleus, for example being placed at the centre of a bond.

There are many different basis sets available in the literature or built into programs, and the average user usually only needs to select a suitable quality basis for the calculation. Below is a short description of some basis sets which often used in routine calculations (generally called Pople Style Basis Sets).

a) STO-nG basis sets: Slater Type Orbital consisting of n PGTOs. This is a minimum type basis where the exponents of the PGTO are determined by fitting to the STO, rather than optimizing them by a variational procedure. Although basis sets with n = 2-6 have been derived, It has been found that using more than three PGTOs to represent the STOs gives little Improvement, and the STO-3G basis is a widely used minimum basis. This type of basis set has been determined for many elements of the periodic table. The designation of the carbon/hydrogen STO-3G basis is (6s3p/3s) ? [2s1p/1s].

b) k-nlmG basis sets These basis sets have been designed by Pople and co-workers. And are of the split valence type, with the *k* in front of the dash indicating how many PGTOs are used for representing the core orbitals. The *n/m*

after the dash indicates both how many functions the valence orbitals are split into, and how many PGTOs are used for their representation. Two value s (e.g. *nl)* indicate a split valence, while three values (e.g. *nlm)* indicate a triple split valence. The values before the G (for Gaussian) indicate the s- and p-functions in the basis; the polarization functions are placed after the G. This type of basis sets has the further restriction that the same exponent is used for both the sand p-functions in the valence. This increases the computational efficiency, but of course decreases the flexibility of the basis set. The exponents in the PGTO have been optimized by variational procedures.

c) 3-21G This is a split va1ence basis, where the core orbitals are a contraction of three PGTOs, the inner part of the valence orbitals is a contraction of two PGTOs and the outer part of the valence is represented by one PGTO. The designation of the carbon/hydrogen 3-21G basis is (6s3p/3s) ? [3s2p/2s]. Note that the 3-21G basis contains the same number of primitive GTOs as the STO-3G, however, it is much more flexible as there are twice as many valence functions which can combine freely to make MOs.

d) 6-31G This is also a split valence basis, where the core orbitals are a contraction of six PGTOs, the inner part of the valence orbitals is a contraction of three PGTOs and the outer part of the valence represented by one PGTO. The designation of the carbon/hydrogen 6-31G basis is (10s4p/4s) ? [3s2p/2s]. In terms of contracted basis functions it contains the same number as 3-2IG, but the representation of each functions is better since more PGTOs are used.

e) 6-311G This is a triple split valence basis, where the core orbitals are a contraction of six PGTOs and the valence split into three functions, represented by three, one and one PGTOs, respectively.

To each of these basis sets can be added diffuse and/or polarization functions. Diffuse functions are normally s- and p-functions and consequently go before the G. They are denoted by + or ++, with the first + indicating one set of diffuse s- and p-functions on heavy atoms, and the second + indicating that a diffuse s-function is also added to hydrogens. The arguments for adding only diffuse functions on non-hydrogen atoms is the same as that for adding only polarization functions on non-hydrogens. Polarization functions are indicated after the G, with a separate designation for heavy atoms and hydrogens. The 6-31+G(d) is a split valence basis with one set of diffuse sp-functions on heavy atoms only and a single d-type polarization function on heavy atoms. A 6-311++G(2df,2pd) is similarly a triple split valence with additional diffuse sp-functions, and two d- and one f-functions on heavy atoms and diffuse s- and two p- and one d-functions on hydrogens. The largest standard Pople style basis set is 6-311++G(3df, 3pd). These types of basis sets have been derived for hydrogen and the first row elements, and some of the basis sets have also been derived for second and higher row elements.

If only one set of polarization functions is used, an alternative notation in terms of * is also widely used. The 6-31G* basis is identical to 6-31G(d), and 6-31G** is identical to 6-31G(d,p). A special note should be made for the 3-21G* basis. The 3-21G basis is basically too small to support polarization functions (it becomes unbalanced). However, the 3-21G basis by itself performs poorly for hypervalent molecules, such as sulfoxides and sulfones. This can be substantially

improved by adding a set of d-functions. The 3-21G* basis has only d-functions on second row elements (it is sometimes denoted 3-21G(*) to indicate this), and should not be considered a polarized basis. Rather, the addition of a set of d-functions should be considered an *ad hoc* repair of a known flaw.

3.1.3. Density Functional Theory

Shortly after the formulation of quantum mechanics in the mid 1920's, Thomas (1926) and Fermi (1928) introduced the idea of expressing the total energy of a system as a functional of the total electron density. Because of the crude treatment of the kinetic energy term, i.e. the absence of molecular orbitals, the accuracy of these early attempts was far from satisfactory. It was not until the 1960's that an exact theoretical framework called density functional theory (DFT) was formulated by Hohenberg and Kohn (1964) and Kohn and Sham (1965) that provided the foundation for accurate calculations. Earlier, motivated by the search for practical electronic structure calculations, Slater (1951) had developed an approach, later to become the Xa method (Slater, 1974) which was originally intended as an approximation to Hartree-Fock theory. Today, the Xa method is generally viewed as a simplified form or precursor of density functional theory.

DFT offers a powerful and elegant method for calculating the ground-state total energy and electron density of a system of interacting electrons. The system may range in complexity from a single atom to a complex system together with the atoms of the solid surface on which they are about to be adsorbed and where they will react with one another, guided by the total energy. The whole theory is based on *functional* (which means a function of a function)

of the electron density, which therefore plays the central role. However, the key functional, which describes the total energy of the electrons as a functional of their density, is not known exactly: the part of it which describes electronic *exchange and correlation* has to be approximated in practical calculations.

The existence of correlations between the particles, the main formal difficulty encountered in treating a materials problem in quantum mechanics, is a familiar one in many contexts. The positions and motions of the particles that make up a molecule or material are correlated because the particles interact with each other and exert forces upon each other as they move. In quantum mechanics, the situation is further compounded by the mysterious forces that devolve from the Pauli Exclusion Principle governing electrons. This causes correlations to appear even between (fictitious) noninteracting particles that have no direct interaction with each other. Such forces are referred to as *exchange forces* because they have to do with the set of rules in quantum mechanics that govern what happens when the labels characterizing indistinguishable particles are exchanged.

Whether due to interactions (e.g., the Coulomb force) or exchange, correlations can be characterized as either long- or short-range. The former can be dealt with by averaging techniques and a mean-field or a self-consistent field (meaning that the field experienced by an atom depends on the global distribution of atoms). Short-range correlations involve the local environment around a particular atom, i.e., deviations of the local environment from average behavior, and are much more difficult to treat. In large part, the central problem of quantum methods in chemistry and condensed matter physics has been the search for more and more accurate ways of incorporating short-range

correlations into mean-field theory. The massive CPU requirement of codes that employ modern methods such as coupled clusters or Quantum Monte Carlo bear witness to the degree of difficulty of the problem. These methods are applicable only to relatively small molecules or very simple crystalline solids and their scaling properties as the system size increases are very unfavorable.

Fortunately, the fine details of short range correlations are often of only minor importance so that a theory based on the concept of a mean or self-consistent field is sufficiently accurate for many purposes. Where this is not the case, as in the high temperature ceramic superconductors, or valence-mixed solids, one refers to strongly correlated systems, implying that the short-range correlations between electrons due to exchange and their mutual Coulomb repulsions must be accounted for very accurately if even the qualitative features of observed behavior are to be reproduced.

Several promising methods of dealing with the problem of strong correlations have been developed in recent years but this is still at the cutting edge of research in condensed matter physics and none of these methods is quite ripe for inclusion in a suite a general software tools. An important advance in the calculation of the energy of collections of atoms and the forces on each atom was made by Kohn and Sham (1965), who showed how a mean-field theory could be applied to this problem. In their method, the electron density plays a crucial role so that, although the term has more general applicability, the Kohn-Sham method is commonly referred to as density functional theory (DFT). This has since advanced to become a very important method for determining the energy of many-electron, and therefore many-atom systems. In addition, Kohn-Sham density functional theory is equally applicable to molecules (bounded

collections of atoms) and crystalline materials (where a specific unit cell is repeated throughout space).

In the density functional theory, the energy is not written in terms of the many-electron wavefunction as is conventional in quantum chemistry, but as a functional of the electron density. Kohn and Sham proposed that the total energy of an n-electron system can be written without approximations as:

$$E_{el} = -\tfrac{1}{2}\sum_i \int f_i(\vec{r}_1)\nabla^2 f_i(\vec{r}_i)d\vec{r}_1 + \sum_A \int \frac{Z_A}{\left|\vec{R}_A - \vec{r}_1\right|} r(\vec{r}_i)d\vec{r}_1 + \tfrac{1}{2}\int \frac{r(\vec{r}_1)r(\vec{r}_2)}{\left|\vec{r}_1 - \vec{r}_2\right|} d\vec{r}_1 d\vec{r}_2 + E_{xc} \tag{3.46}$$

the first term in equation 3.46 represents the kinetic energy of n noninteracting electrons with the same density $r(\vec{r}_1) = \sum_i f_i(\vec{r}_1)f_i(\vec{r}_2)$ as the actual system of interacting electrons. The second term accounts for the electron-nucleus attraction and the third term for the Coulomb interaction between the two charge distributions $r(\vec{r}_1)$ and $r(\vec{r}_2)$. The last term contains the exchange-correlation energy can be expressed in terms of the spherically averaged exchange-correlation hole functions $\overrightarrow{r_x}^{gg'}(\vec{r}_1, s)$ as:

$$E_{xc} = \sum_g \sum_{g'} -4p/2 \int \frac{\vec{r}_1^{\,g}(\vec{r}_1)\vec{r}_1^{\,gg'}(\vec{r}_1, s)}{s} d\vec{r}_1 s^2 ds \tag{3.47}$$

where the spin indices γ and γ` both run over a α-spin as well β-spin and $s = \left|\vec{r}_1 - \vec{r}_2\right|$ the one electron orbitals, $\left\{f_i(\vec{r}_1); i = 1,..., n\right\}$ of equation 3.46 are solutions to the set of one-electron Kohn-Sham equations:

$$\left[-1/2\nabla^2 + \sum_A \frac{Z_A}{\left|\vec{R}_A - \vec{r}_1\right|} + \int r(\vec{r}_2) + V_{xc}\right] f_i(\vec{r}_1) = h_{KS} f_i(\vec{r}_1) = e_i f_i(\vec{r}_1) \tag{3.48}$$

where the exchange-correlation potential V_{xc} is given as the functional derivative of E_{xc} with respect to the density:

$$V_{xc}[r] = dE_{xc}[r]/dr \tag{3.49}$$

the hole function $\overrightarrow{r_x}^{gg'}(\vec{r}_1, s)$ contains all information about exchange and correlation between the interacting electrons as well as the influence of correlation on the kinetic energy. The interpretation of $\overrightarrow{r_x}^{gg'}(\vec{r}_1, s)$ is that an electron at $\vec{r}_1$ to a larger or smaller extend will exclude the other electrons from approaching within a distance s. the extend of exclusion or screening increases with the magnitude of $\overrightarrow{r_x}^{gg'}(\vec{r}_1, s)$. Examples of the hole function are shown in Figure 3.1 for γ = γ`, part a, as well as γ ? γ`, part b. The intricate function $\overrightarrow{r_x}^{gg'}(\vec{r}_1, s)$, can in practice only be obtained from an exact solution to the Schrödinger equation of our n-electron system. The set of one electron Kohn-Sham equations is a consequence of limited value for exact solutions to many-electron systems. They form, however, the starting point for an approximate

treatment in which $\overrightarrow{r}_x^{gg'}(\vec{r}_1, s)$ is replaced by model hole functions. The form of the exact hole function $\overrightarrow{r}_x^{gg'}(\vec{r}_1, s)$ is not known in detail. Nevertheless, a number of properties of $\overrightarrow{r}_x^{gg'}(\vec{r}_1, s)$ can be deduced from general considerations. It can readily be shown that the spherically averaged (Coulomb) hole-correlation functions $\overrightarrow{r}_x^{gg'}(\vec{r}_1, s)$, with γ ? γ`, have the following properties:

$$4p \int \dot{r}_x^{gg`}(\dot{r}_1, s)_1 s^2 ds = 0 \qquad (3.50a)$$

whereas the corresponding (Fermi) functions $\overrightarrow{r}_x^{gg'}(\vec{r}_1, s)$, with γ = γ`, satisfy the normalization condition:

$$4p \int \dot{r}_x^{gg`}(\dot{r}_1, s)_1 s^2 ds = 1 \qquad (3.50b)$$

Further, the Fermi contributions:

$$\vec{r}_x^{gg`}(\vec{r}_1, 0) = \vec{r}_1^{\,g}(\vec{r}_1) \qquad (3.50c)$$

The two Coulomb functions $\vec{r}_x^{ab}(\vec{r}_1, 0)$ and $\vec{r}_x^{ba}(\vec{r}_1, 0)$ are in general considered to be smaller than $\vec{r}_x^{gg`}(\vec{r}_1, 0)$ although different from zero. They cannot be related to $\vec{r}_1^{\,g}(\vec{r}_1)$ in a simpler way.

The model hole function are in general constructed in such a way that the constraints given in equations 3. 50a-c are satisfied. Thus, the Fermi function of Figure 3.1a with $\gamma = \gamma`$, is seen to satisfy the constraints of equations 3.50b & 3.50c, whereas the Coulomb Function of Figure3.1b with $\gamma$ ? $\gamma`$satisfies equation 3.50a.

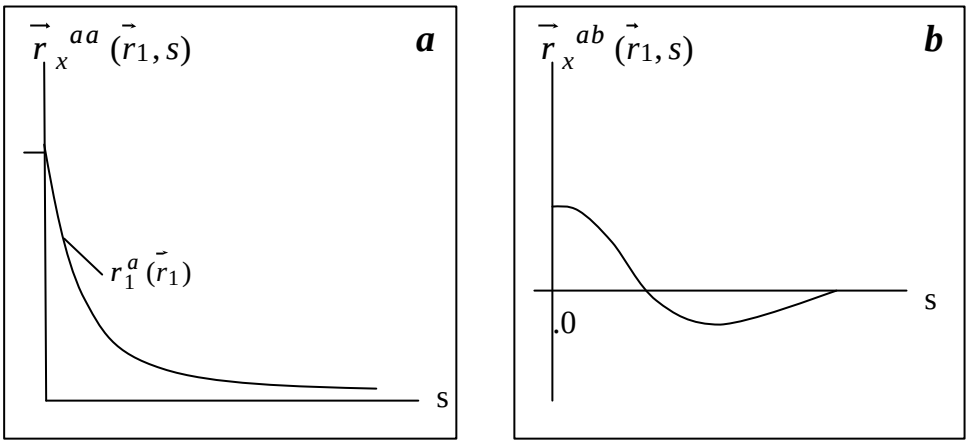

Figure 3.1. (a) Fermi hole function as a function of the interelectronic distance. (b) The Coulomb hole function as a function of the interelectronic distance.

3.1.3.1. Local Density Methods

In the Local Density Approximation (LDA) it is assumed that the density locally can be treated as a uniform electron gas, or equivalently that the density is a slowly varying function. The exchange-correlation energy for the homogeneous electron gas can be written as:

$$E_{xc}^{LDA} = E_x^{LDA} + E_c^{LDA} \tag{3.51}$$

the first term, representing the exchange energy, has the form:

$$E_x^{LDA} = -9/4a_{ex}[3/4p]^{1/3}\sum_g \int \left[r_1^g(\vec{r}_1)\right]^{4/3} d\vec{r}_1 \qquad (3.52)$$

where the electron gas value for the exchange scale factor α_{ex} is 2/3. The exact exchange energy in the Kohn-Sham theory is simply E_{xc} corresponding to single determinantal wave function constructed from the exact Kohn-Sham orbitals. The second term, representing the correlation energy, has the form:

$$E_c^{LDA} = \int r_1(\vec{r}_1) e_c \left[r_1^a(\vec{r}_1)\, r_1^b(\vec{r}_1)\right] d\vec{r}_1 \qquad (3.53)$$

where $e_c\left[r_1^a, r_1^b\right]$ represents the correlation energy per electron in a gas with the spin densities r_1^a and r_1^b. The specific correlation energy, $e_c\left[r_1^a, r_1^b\right]$, is not known analytically. However, approximations of increasing accuracy have been developed.

Simplified versions of LDA were known long before the formal development of DFT. Of particular importance is Hartree-Fock-Slater, or Xα. This method is retains only the exchange part (see equation 3.52) of the total expression for the exchange-correlation energy given in equation 3.51 and adopts in many cases values for the exchange scaling factor that differs somewhat from 2/3.

The exchange-correlation hole functions for the homogeneous electron gas satisfy the general constraints given in equation 3.50 and can thus be used as models for calculations on atoms and molecules by substituting the

corresponding (in homogeneous) electron densities into the expression for the exchange-correlation energy in equation 3.51.

The LSDA approximation in general underestimates the exchange energy by ~10%, thereby creating errors which are larger than the whole correlation energy. Electron correlation is furthermore overestimated. Despite the simplicity of the fundamental assumptions, LSDA methods are often found to provide results with accuracy similar to that obtained by wave mechanics HF methods.

3.1.3.2. Gradient Corrected Methods

Improvements over the LSDA approach have to consider a non-uniform electron gas. A step in this direction is to make the exchange and correlation energies dependent not on the electron density, but also on derivatives of the density. Such methods are known as Gradient Corrected or Generalized Approximation (GGA) methods (a straightforward Taylor expansion does not lead to an improvement over LSDA, it actually makes things worse, thus the name generalized gradient approximation). GGA methods are also sometimes referred to as non-local methods, although this somewhat misleading since the functionals since the functionals depend only on the density (and derivatives) at a given point, not on a space volume as for example the Hartree-Fock exchange energy.

Perdew and Wang (PW86) proposed modifying the LSDA exchange expression to that shown in equation 3.54, where x is a dimensionless gradient variable, and a, b, c being suitable constants (summation over equivalent expressions for the α and β densities is implicitly assumed).

$$e_x^{PW86} = e_x^{LDA}(1 + ax^2 + bx^4 + cx^6)^{1/15}$$
$$x = \frac{|\nabla r|}{r^{4/3}} \tag{3.54}$$

Becke proposed a widely used correction (B or B88) to the LSDA exchange energy, which has the correct $-r^{-1}$ asymptotic behavior for the energy density (but not for the exchange potential).

$$e_x^{B88} = e_x^{LDA} + De_x^{B88}$$
$$D_x^{B88} = -b\,r^{1/3}\frac{x^2}{1 + 6\,bx\sinh^{-1}x} \tag{3.55}$$

The β parameter is determined by fitting to known atomic data and x is defined in equation 3.55. Another functional form (not a correction) proposed by Becke and Roussel (BR) has the form:

$$e_x^{BR} = -\frac{2 - 2e^{-ab} - abe^{-ab}}{4b}$$
$$a^3 e^{-ab} = 8p\,r$$
$$a(ab - 2) = b\frac{\nabla^2 r - 2D^2}{r} \tag{3.56}$$
$$D = \sum_i^N |\nabla f_i|^2 - \frac{(\nabla r)^2}{4r}$$

This functional contains derivatives of the orbitals, not just the gradient of the total density, and is computationally slightly more expensive. Despite the apparent difference in functional form, exchange expressions 3.55 & 3.56 have been found to provide results of similar quality.

Perdew and Wang have proposed an exchange functional similar to B88 to be used in connection with the PW91 correlation functional given below.

$$e_x^{PW91} = e_x^{LDA}\left(\frac{1 + xa_1 \sinh^{-1}(xa_2) + (a_3 + a_4 e - bx^2)x^2}{1 + xa_1 \sinh^{-1}(xa_2) + a_5 x^2}\right) \tag{3.57}$$

where $a_{1\text{-}5}$ and b again are suitable constants and x is defined in equation 3.54.

There have been various gradient corrected functional forms proposed for the correlation energy. One popular functional (not a correction) is due to Lee, Yang and Parr (LYP) and has the form:

$$\begin{aligned} e_c^{LYP} &= -a\frac{g}{(1+dr^{-1/3})} - ab\frac{ge^{-cr^{-1/3}}}{9(1+dr^{-1/3})r^{8/3}} \\ &\times\begin{bmatrix} 18(2^{2/3})C_F(r_a^{8/3} + r_b^{8/3}) - 18rt_w \\ + r_a(2t_w^a + \nabla^2 r_a) + r_b(2t_w^b + \nabla^2 r_b) \end{bmatrix} \\ g &= 2\left[1 - \frac{r_a^2 + r_b^2}{r^2}\right] \\ t_W^s &= \frac{1}{8}\left(\frac{|\nabla r_s|^2}{r_s} - \nabla^2 r_s\right) \end{aligned} \tag{3.58}$$

where the a, b, c and d parameters are determined by fitting to data for the helium atom. The t_w functional is known as the local Weizsacker kinetic energy density. Note that the γ-factor becomes zero when all the spins are aligned ($\rho=\rho_\alpha$, $\rho_\beta=0$), i.e., the LYP functional does not predict any parallel spin correlation in such a case (e. g. the LYP correlation energy in triplet He is zero).

Perdew proposed a gradient correction to the LSDA result. It appeared in 1986 and is known as by the acronym P86. Then the formalism proposed by Perdew was modified by Perdew and Wang in 1991, this modified form of the formalism is known as PW91 or P91.

It should be noted that several of the proposed functionals violate fundamental restrictions, such as predicting correlation energies for one-electron systems (for example P86 and PW91) or failing to have the exchange energy cancel the coulomb self-repulsion.

3.1.3.3. Hybrid Methods

Since the GGA methods give a substantial improvement over LDA, a generalized version of the Half-and-Half method may be defined by writing the exchange energy as a suitable combination of LSDA, exact exchange and a gradient correction term. The correlation energy may similarly be taken as the LSDA formula plus a gradient correction term.

$$E_{xc}^{B3} = (1-a)E_x^{LSDA} + aE_x^{exact} + bDE_x^{B88} + E_c^{LSDA} + cDE_x^{GGA} \qquad (3.59)$$

Models which include exact exchange are often called hybrid methods, the names Adiabatic Connection Model (ACM) and Becke 3 parameter functional (B3) are examples of such hybrid models defined by equation 3.59. The a, b, c parameters are determined by fitting to experimental data and depend on the form chosen for E_c^{GGA}, typical values are a~0.2, b~0.7 and c~0.8. Owing to the substantially better performance of such parameterized functionals the Half-and-

Half model is rarely used anymore. The B3 procedure has been generalized to include more fitting parameters; however, the improvement is rather small.

3.1.3.4. Applications of DFT

There are two general approaches for modeling surface chemistry with quantum mechanics: the cluster approach and the extended band surface (or slab) approach. In the cluster approach, the local molecular fragment orbitals are explicit, thus making the local chemical interaction, chemical bonding, and charge transfer mechanism between the adsorbate and the metal surface orbitals very easy to elucidate. This detailed level of focus, however, makes is difficult to treat the bulk electronic structure. The extended band surface approach provides a more accurate representation of the materials electronic structure. The cluster approach, instead of a continuous conduction and valance bands, is based on discrete orbitals which have specific energy gaps.

Both cluster, as well as the slab approaches, will likely to play invaluable roles in the future toward the quantitative prediction of transition metal surface chemistry.

3.1.3.5. Assessment of DFT methods

The status of density functional calculations for solids, surfaces, and molecules can be characterized as follows.

3.1.3.5.1. Capability

Like Hartree-Fock methods, density functional calculations provide structural, energetic, and vibration properties. More than Hartree-Fock calculations, density functional calculations enable also the prediction of electronic, optical, and magnetic properties of condensed phases.

3.1.3.5.2. Generality

The density functional approach is applicable to all atoms of the periodic table, provided relativistic effects are taken into account for heavier elements such as third-row transition metals, rare-earths, and actinides. The approach can be used for metallic, covalent, and ionic bonds. Its greatest strength is metallic condensed systems, yet its range also includes organic molecules. With the inclusion of gradient corrections for the exchange-correlation term, even weaker interactions such as hydrogen bonds can be reasonably well described. Furthermore, so-called "difficult" molecules such as ozone seem to be treated by density functional methods with the same level of accuracy as other molecules. Within molecular applications, the approach is particularly useful for organometallic systems. Thus, in terms of generality and robustness, density functional theory seems to be superior to the Hartree-Fock approach. Local density functional calculations do encounter problems for narrow-gap insulators and certain oxides. The LDA tends to overemphasize the metallic character and one needs to be careful in the interpretation of the density functional one-electron energies. Furthermore, weaker bonds such as hydrogen bonds are significantly overestimated in the LDA. The primary results of density functional calculations are the electron density, the spin density, the total energy, and the one-particle energies and wave functions. From these quantities, one can derive

important electronic, optic and magnetic properties including dipole (and higher) moments, polarizabilities and hyper-polarizabilities, and magnetic moments. LDA calculations for systems in their electronic ground state can be used to estimate electronic excitation energies including work functions, optical and UV spectra, and core level spectra for solids, surfaces, and molecules.

3.1.3.5.3. Accuracy

Quite consistently, for a great number of strong bonds in solids, molecules, and surfaces, interatomic equilibrium distances are predicted by precise density functional calculations to within about 0.02°A of experiment; bond angles and dihedral angles are found within a few degrees of their experimental values. Within the local density approximation, binding energies are typically overestimated, sometimes by as much as a factor of two. Inclusion of non-local gradient corrections improves the values of binding energies and brings them to within about 10 kJ/mol of experiment. The results obtained at this level of theory are comparable with sophisticated correlated quantum mechanical methods such as coupled cluster theory. Vibration frequencies are predicted to within 10-50 cm^{-1}. At present, there is no clear theoretical path that would allow the systematic improvement of the accuracy of density functional methods. This is a major conceptual difference to Hartree-Fock based methods, where at least in principle there is a way for systematic improvements. Practical density functional calculations involve numerical integrations in addition to the evaluation of analytical expressions. These numerical integrations introduce a numerical noise that can be noticed, for example, in geometry optimizations of highly flexible molecules. By increasing the size of the numerical grid, this numerical noise can be controlled, though at the expense of computational

effort. This is in contrast to Hartree-Fock methods, which are usually implemented in a completely analytical way. Thus, the numerical precision of Hartree-Fock calculations is limited by the machine precision (typically 14 decimal figures) whereas the precision of density functional calculations is governed by the grid resolution. One could argue that if a theory has a certain inherent error compared with experiment, any computational approach that gives results within that error range is acceptable and any improvement in numerical precision has no physical meaning. On the other hand, it can be desirable, for example in the investigation of subtle trends, to have a high numerical precision.

3.1.3.5.4. System Size

Density functional calculations are possible for systems of the order of 100 atoms. By exploring point-group symmetry, calculations for clusters of over 1000 atoms have been demonstrated for fixed geometries. While the self-consistent-field procedure converges typically in 10-20 iterations for organic materials and semiconductors, metallic systems and especially magnetic transition metals such as Fe and Ni are very difficult to converge. In practice, this limits the size of systems that can be treated to perhaps less than 60 atoms per unit cell or cluster.

3.1.3.5.5. Tractable Time Scale

Recently, Density functional calculations have become possible for studying dynamic phenomena. However, for a system with about 100 atoms, accurate density functional calculations are about 1000 times slower than force

field calculations, thus reducing the accessible time scales to the range of picoseconds. In practice, the Car-Parrinello method is presently used for structure optimizations by simulated annealing rather than for dynamic simulations, which has been done so far only for a few cases.

3.1.3.5.6. Computational Efficiency

Depending on the system under investigation, for example a metallic alloy or a molecular crystal, density functional theory can be implemented in quite different ways thus leading to efficient methods for particular materials. On the other hand, practical Hartree-Fock methods require the use of Gaussian basis functions, which can be fairly inefficient, for example for close-packed systems. Thus, in general, density functional theory tends to be computationally more efficient than Hartree-Fock calculations. Without doubt, compared with correlated post-Hartree-Fock methods, density functional calculations are by far more efficient computationally, scaling at worst with a third power in the number of basis functions. In fact, significant effort is dedicated to the development of so-called order-N methods, i.e. methods for which the computational effort increases linearly with system size. Such methods have been successfully demonstrated, yet the pre-factor is rather large so that these methods are competitive with conventional density functional implementations only for systems with several hundred atoms. In molecular calculations it can be important to calculate vibration frequencies in order to determine ground state structures, transition states, and to predict infrared spectra. In Hartree-Fock theory, this approach is well established, whereas the evaluation of vibration frequencies (i.e. the calculation of the second derivatives of the total energy with respect to nuclear displacements) for molecular density functional is been done

by a finite difference technique using analytic first derivatives. This is computationally not very efficient compared with analytical methods. While this type of calculation has been used for density functional methods within the pseudopotential plane wave approach for some time, the implementation of analytic second derivatives in localized orbital density functional calculations is a fairly recent development. However, this type of calculation is quite time consuming and may require supercomputer resources for larger molecules.

3.2. Computational Procedure:

All of the quantum chemical calculations performed in this study were carried out by means of the software called "SPARTAN'02 for Windows Edition". For the DFT calculation the Becke's three-parameter hybrid method using the Lee, Yang, and Parr correlation functional (B3LYP) formalism was utilized. The basis sets employed in the DFT calculations was 6-31G**.

There are four types of quantum chemical calculations that were performed during the study. The first type is the "Single Point Energy" calculations; these types of calculations are convenient for property calculations such as vibration frequency and charge calculations, since the total energy of a given geometry is calculated without any geometry changes. The second type is the "Equilibrium Geometry" calculations. At the end of these calculations, an optimized geometry with the minimum energy is obtained for a given geometry. At the equilibrium geometry, the gradient (first derivative) of the energy with respect to the coordinates is zero, and the force constant (second derivative) is positive where the force constants are represented as the eigenvalues of the Hessian Matrix. The third type is "Transition State Geometry" calculations. In this

type of calculation, the molecular structure at the maximum of the potential energy connecting two minima of reactants and products can be obtained. This geometry is also described mathematically as a first order saddle point, being maximum in one direction and minimum in the others. The gradient for a saddle point is zero. However, the second derivative of the energy with respect to the coordinates has a negative value. Therefore, at a transition state geometry, there is only one negative eigenvalue in the Hessian Matrix. For the activated adsorption reactions (reactions that need activation energy to proceed), transition state geometry has always the maximum energy and so gives the activation energy. The last type of the calculations used in the study is "Coordinate Driving" calculations. Coordinate Driving calculations are the series of constrained equilibrium geometry calculations. One can obtain an energy profile for a specific reaction by selecting a reaction coordinate by means of these calculations.

During the study, the following procedure was followed: first of all, all of the molecules, both the cluster and the adsorbing molecules, are fully optimized geometrically by means of the equilibrium geometry calculations. Then, the adsorbing molecule is located over the active site of the cluster and then coordinate driving calculation is performed by selecting a reaction coordinate in order to obtain the variation of the relative energy with decreasing reaction coordinate, which is called energy profile.

The relative energy is defined as the following formula:

$$?E = E_{System} - (E_{Cluster} + E_{Adsorbate}) \qquad (3.60)$$

where E_{System} is the calculated energy of the given geometry containing cluster and the adsorbing molecule at any distance, $E_{Cluster}$ is the energy of the cluster and $E_{Adsorbate}$ is that of the adsorbing molecule. In other words, the relative energy is defined to be the difference between the total enthalpy of formation of the reactant molecule plus vanadium oxide cluster at any interatomic distance and the sum of the enthalpies of formation of the free catalyst cluster and the approaching reactant molecule at infinite separation.

After having obtained the energy profile for the desired reaction, the geometry with the minimum energy on the energy profile is reoptimized by means of the equilibrium geometry calculations to obtain the final geometry for the reaction. For the calculated final geometry, vibration frequency and atomic charges are computed by Single Point Energy calculations. Furthermore, from the energy profile, the geometry with the highest energy was taken as the input geometry for the transition state geometry calculations. Starting from these geometries, the transition state structures with only one negative eigenvalue in Hessian Matrix were obtained.

Throughout the study, for all of the calculations, atoms in the vanadium oxide clusters were frozen totally, except for the active sites (O of the V=O site and OH of the V-OH site) and adsorbing molecules.

Moreover, all of the calculations except for the single point energy calculations the following parameters were used: SCF density convergence, optimization energy convergence, gradient tolerance and distance tolerance equal to 0.0001, 0.0000001, 0.001 and 0.01 respectively. For the single point

energy calculations default values of the SPARTAN were used in order to obtain more accurate results especially for the vibration frequency data.

For the vibration frequencies calculated by means of the B3LYP methods a scaling factor of 0.9613 was used. This value was recommended by Ming et al. (1996) for the B3LYP formalisms. Ming et al. performed vibration frequency calculations for a set of 122 molecules (a total of 1066 frequencies) and compared them with the experimental frequencies. At the end of their calculations, Ming et al. concluded that all the DFT methods perform well for the calculation of vibration frequencies with overall root mean square errors (34-48cm^{-1}) significantly less than that reported for *ab-initio* Moller Plesset MP2 methods (61cm^{-1}) and the hybrid functionals represent a significant improvement over the local and non-local density functionals and recommended the following scaling factors for reproducing experimental fundamentals: 0.9833, 0.9940, 0.9820, 0.9613 and 0.9561, for s-VWN, B-LYP, B-VWN, B3-LYP, B3-P86, respectively.

3.3. Methodology of Creating Vanadium Oxide (V_2O_5) Structure

The finite cluster approximation to an infinite surface of a substrate is widely used in model studies of chemisorption/desorption processes in heterogeneous catalysis. This approach is valid when the adsorbate creates rather short-range perturbation of a substrate, localized mainly on the active site responsible for substrate-adsorbate bonding (Gilardoni et al., 1997). During the study this assumption was assumed to be valid and two different clusters were constructed, one with Lewis acidic (V=O) site as $V_2O_9H_6$ and one with Bronsted acidic (V-OH) site as $V_2O_9H_6$-H.

For the construction of these vanadium oxide clusters, the procedure derived by Nazli Uzman as a part of her MSc. Thesis studies (2000) and ChE511 lecture notes was followed. The experimental parameters of bulk vanadium oxide, such as bimolecular unit edge lengths and Wyckoff positions of atoms and parameters, has been obtained from Wyckoff, 1963. Accordingly, the edge lengths are a=11.519 A, b=3.564 A, and c=4.373 A, and the crystallographic structure of vanadium oxide is orthorhombic. It has the Space Group of P*mmn* with International Tables Number 59 (International Tables for X-Ray Crystallography, 1962). Vanadium oxide has a bimolecular unit cell (Cell Formula Unit = 2) and V_4O_{10} is the unit cell formula. The symmetry operators of space group P*mmn* are found directly from Wyckoff, 1963. The experimental parameters are summarized in Table 3.1.

Table 3.1. Experimental Parameters of Vanadium Oxide (V_2O_5), Wyckoff, 1963

Lattice Parameters	a = 11.519 A, b = 3.564 A, c = 4.373 A			
Space Group	P*mmn*			
International Table No	59			
Cell Formula Unit	2			
Atom Positions	(2a) 0 0 u; ½ ½ -u			
	(4f) u 0 v; -u 0 v; ½-u ½ -v; u+½ ½ -v			
Atomic parameters:				
Atom	**Position**	**X**	**Y**	**Z**
V	(4f)	0.1487	0	0.1086
O (1)	(4f)	0.146	0	0.4713
O (2)	(4f)	0.3191	0	-0.0026
O (3)	(2a)	0	0	-0.0031

By means of the atomic position equations given in Table 3.1, the fractional atomic coordinates were obtained. Then, these values were multiplied by the respective lattice parameter in order to obtain the atomic positions of unit cell of vanadium oxide in XYZ coordinates in Angstrom. Calculated values of the fractional atomic coordinates and the atomic positions of vanadium oxide unit cell are given in Table 3.2.

Table 3.2. The calculated Fractional Atomic Coordinates and Atomic Positions for V_2O_5 unit cell (V_4O_{10}) in Angstroms

Atom	Fractional Atomic Coor.			Atomic Positions		
	X	Y	Z	X	Y	Z
V-1 (4f)	0.1487	0.0000	0.1086	1.7129	0.0000	0.4749
V-2 (4f)	-0.1487	0.0000	0.1086	-1.7129	0.0000	0.4749
V-3 (4f)	0.3513	0.5000	-0.1086	4.0466	1.7820	-0.4749
V-4 (4f)	0.6487	0.5000	-0.1086	7.4724	1.7820	-0.4749
O1-1 (4f)	0.1460	0.0000	0.4713	1.6818	0.0000	2.0610
O1-2 (4f)	-0.1460	0.0000	0.4713	-1.6818	0.0000	2.0610
O1-3 (4f)	0.3540	0.5000	-0.4713	4.0777	1.7820	-2.0610
O1-4 (4f)	0.6460	0.5000	-0.4713	7.4413	1.7820	-2.0610
O2-1 (4f)	0.3191	0.0000	-0.0026	3.6757	0.0000	-0.0114
O2-2 (4f)	-0.3191	0.0000	-0.0026	-3.6757	0.0000	-0.0114
O2-3 (4f)	0.1809	0.5000	0.0026	2.0838	1.7820	0.0114
O2-4 (4f)	0.8191	0.5000	0.0026	9.4352	1.7820	0.0114
O3-1 (2a)	0.0000	0.0000	-0.0031	0.0000	0.0000	-0.0136
O3-2 (2a)	0.5000	0.5000	0.0031	5.7595	1.7820	0.0136

The geometry of the V_2O_5 unit cell is given in Figure 3.2. After having obtained the unit cell structure, it was enlarged in x and y directions by several times to obtain the (010) surface. In 1999, Witko et al. performed ZINDO and DFT calculations for the vanadium oxide clusters of different sizes ranging from

$V_2O_9H_8$ to two layer $V_{38}O_{116}H_{42}$ cluster. At the end of these calculations, it was found out that the atomic populations and bond orders in the two layer cluster were very close to that of the one layer clusters. Therefore, it was concluded that the presence of the second layer did not affect the electronic structure of the first layer and can be neglected for the electronic structure of V_2O_5 (010) surface. For this reason, it was not considered to enlarge the surface in z direction, since there was no need to take into account the effect of the second layer. Geometry of (010) surface is given in Figure 3.3.

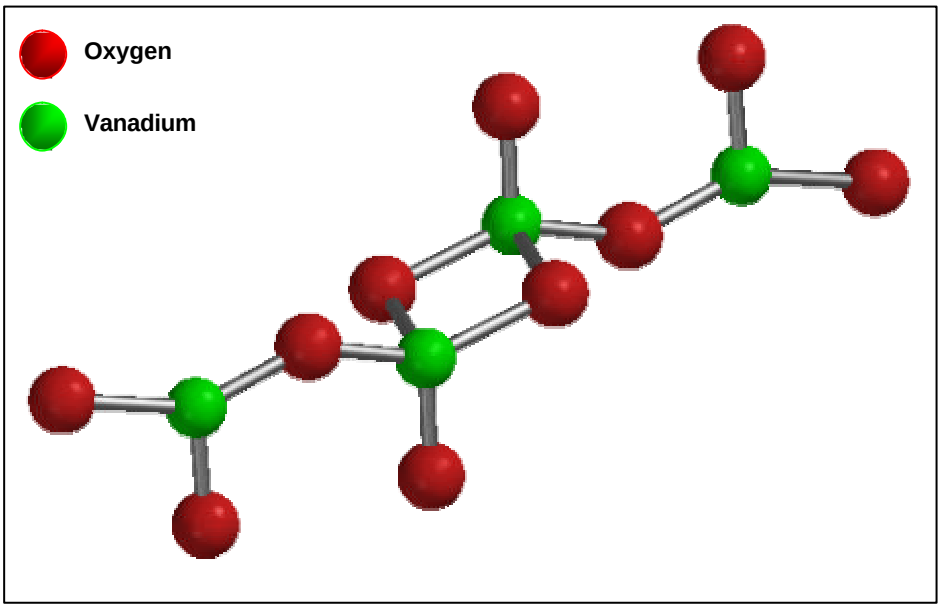

Figure 3.2. The Unit Cell (V_4O_{10}) structure for V_2O_5.

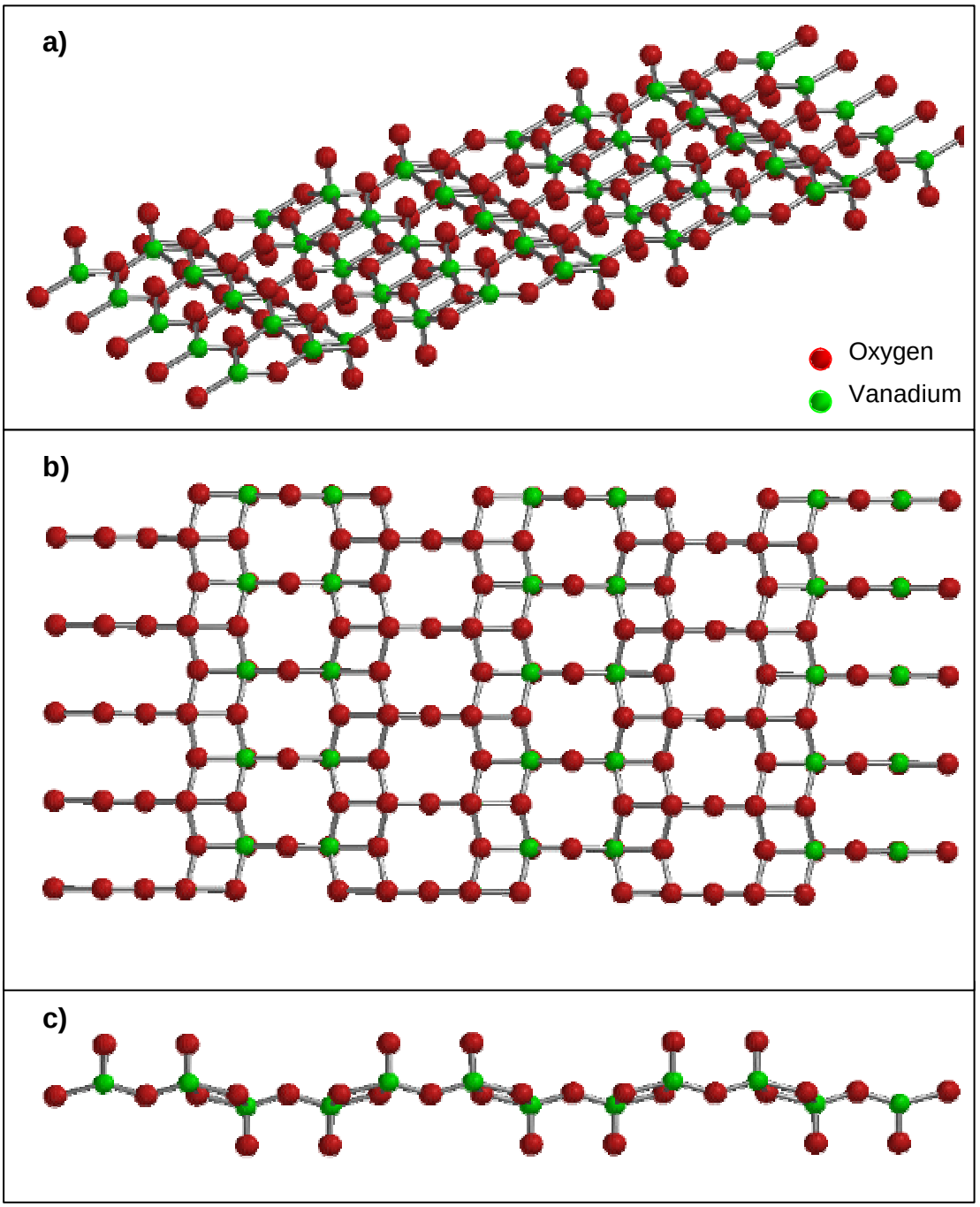

Figure 3.3. (010) surface of V_2O_5, b)Top view, c) Side view

V_2O_5 cluster that was used for the adsorption/desorption calculations was obtained from this (010) surface by cutting out V_2O_9 part and saturating all of the peripheral oxygen atoms by hydrogen atoms. The effect of peripheral bond

saturation was studied by Michalak et al. (1997) by means of the ab initio density functional theory calculations carried out on (saturated) $V_2O_9H_8$ and (unsaturated) V_2O_9 clusters, and it was concluded that the saturation of the peripheral oxygen atoms has a rather small effect on the electronic structure of the clusters. The dihedral angles of the added hydrogen atoms were determined such that the effect of these atoms on the adsorbing molecules should be minimized. A similar approach to this was also applied by Dumesic et al. (2003). The obtained geometry of the $V_2O_9H_6$ cluster is given in Figure 3.4.

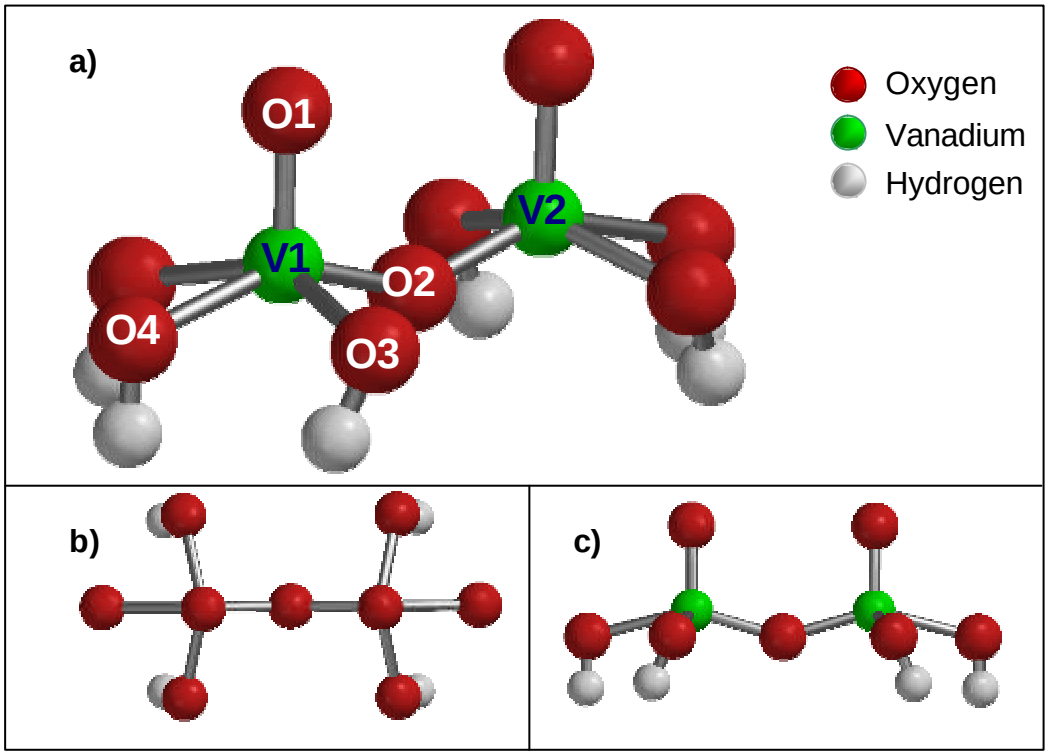

Figure 3.4. The structure of $V_2O_9H_6$ cluster, b) Top view, c) Side View

Michalak et al. (1997) showed that this size of the cluster gives a very reasonable description of the local electronic structure near the V_2O_5 (010) surface. In order to check the reliability of this cluster, the atomic distance and

angle values were compared with the data available in literature, which is given in Table 3.3. Since all the distance and angle values were very close to the literature values, it was decided to use this cluster for the SCR of NO by ammonium reaction mechanism calculations.

Table 3.3. Comparison of Calculated Atomic Distances and Angles with Hermann et al. (1999)

	$V_2O_9H_6$ cluster	**Hermann et al. 1999**
d(V1-O1), A	1.583	1.58
d(V1-O2), A	1.781	1.78
d(V1-O3), A	1.878	1.88
d(V1-O4), A	2.022	2.02
<(O1-V1-O2)	106.46	104.8
<(O1-V1-O3)	104.18	104.5
<(V1-O2-V2)	148.17	148.1

However, for the first step of the reaction there are two possible interaction type of ammonia over the catalytic surface, one is Lewis Acidic, the other one is Brønsted Acidic interaction. Although $V_2O_9H_6$ cluster has a Lewis Acidic V=O site, it does not have a Brønsted acidic site. Therefore, a second cluster with Brønsted acidic V-OH site was constructed by adding one Hydrogen atom to the O1 atom of the $V_2O_9H_6$ cluster and performing equilibrium geometry calculation. The resulting geometry ($V_2O_9H_6$-H) is given in Figure 3.5.

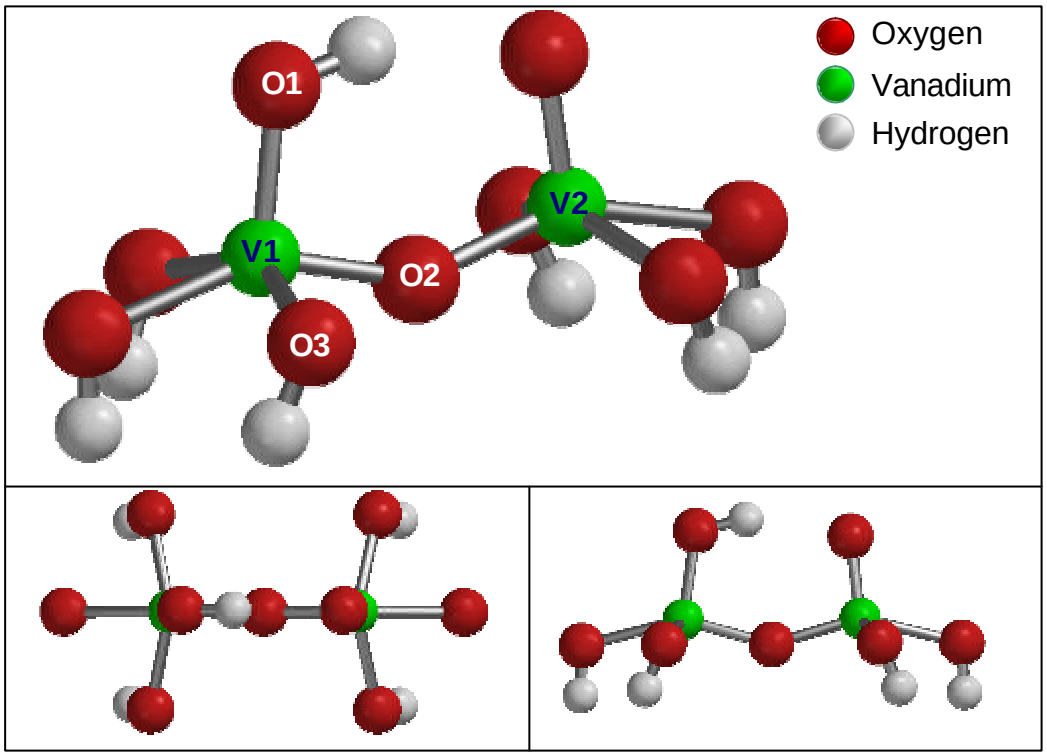

Figure 3.5. The structure of $V_2O_9H_6$ –H Cluster, b) Top view, c) Side View

The location of the Brønsted acidic site was selected as doubly bonded O1 atom since this site was considered as the most active site of the V_2O_5 cluster in literature. Dumesic et al. (2002) performed DFT B3LYP calculations on V_2O_5 clusters by locating hydrogen atom on different oxygen sites and concluded that the interaction of hydrogen with O1 site was the strongest; therefore, they located the Brønsted Acidic Hydrogen atom on the O1 site. Also, Gilardoni et al. (1997) selected O1-H as the Brønsted acidic site. Moreover, Hermann et al. (1999) performed DFT calculations for the hydrogen adsorption reaction over $V_{10}O_{31}H_{12}$ cluster, and showed that the strongest adsorptive binding is for the doubly bonded O1 site among the active oxygen sites of the V_2O_5 cluster. They also found out that the V=O double bond at the O1 site was reduced to a single bond since the bond distance increased 1.58 A to 1.70 A at the end of the H adsorption. A comparison of the bond distance values of Brønsted acidic V-OH site on $V_2O_9H_6$-H cluster with literature is given in Table 3.4.

Table 3.4. Comparison of Calculated Atomic Distances with Literature

	$V_2O_9H_6$-H cluster	Hermann et al. 1999	Gilardoni et al. 1997
d(V1-O1H), A	1.732	1.70	1.78
d(O1-H), A	0.990	1.01	0.996

CHAPTER 4

RESULTS AND DISCUSSION

4.1. SCR of NO by NH_3

The global reaction for the selective catalytic reduction of NO by NH_3 over V_2O_5 catalytic surface is the following:

$$4NH_3 + 4NO + O_2 \; ? \; 4N_2 + 6\,H_2O \qquad (4.1)$$

Before performing mechanism calculations over catalytic surface, the reactants (NH_3 and NO) were optimized by means of the equilibrium geometry calculations. For the calculations, NH_3 was considered as neutral with singlet spin multiplicity and NO was considered as neutral with doublet spin multiplicity since it has one unpaired electron. Optimized geometries for NH_3 and NO are given in Figure 4.1. All the calculated bond distance and bond angle values as well as the vibration frequencies showed excellent agreement with the experimental data. A comparison of the calculated values with their experimental counter parts reported in the literature are given in Tables 4.1 and 4.2 for NO and NH_3, respectively.

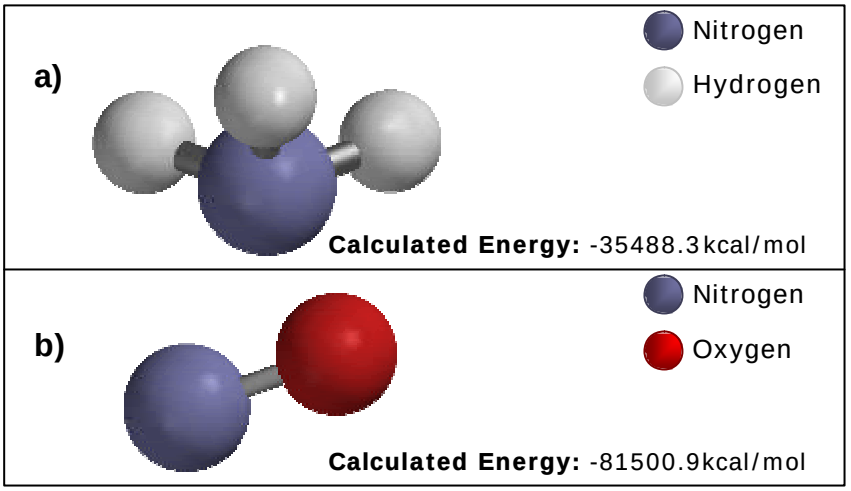

Figure 4.1. Optimized geometries of the reactants. (a) NH_3, (b) NO

Table 4.1. Comparison of the calculated bond distance and vibration frequency data of NO with experimentally obtained ones.

Distance, A	**Calculated**	**Stewart et al. (1990)**
N-O	1.159	1.151
Frequency, cm^{-1}	**Calculated**	**Huber et al. (1979)**
Stretching, N-O	1913	1904

Table 4.2. Comparison of the calculated bond distance and vibration frequency data of NH_3 with experimentally obtained ones.

Geometry	**Calculated**	**Stewart et al. (1990)**
d(N-H), A	1.018	1.012
<(H-N-H)	105.73	106.7
Frequency, cm^{-1}	**Calculated**	**Stephens et al. (1990)**
Bending (sym.), N-H	1048	950
Bending (asym.), N-H	1628	1627
Stretching (sym.), N-H	3326	3337
Stretching (sym.), N-H	3449	3444

4.1.1. Gas Phase Interactions of Reactants

Before conducting the actual mechanism calculations over the catalytic surface, possible gas phase interaction mechanisms of NH_3 and NO were investigated. For this purpose two different reactions were considered, since gas phase interaction of the reactants may occur either between nitrogen of NH_3 and nitrogen of NO or between one of the hydrogen atoms of NH_3 and oxygen of NO. Therefore, two different coordinate driving calculations were performed for these reactions.

4.1.1.1. Gas Phase Reaction with the N-N Reaction Coordinate

The reaction between the nitrogen atoms of the reactants is one of the possible gas phase reactions. In order to investigate this interaction, the distance between two nitrogen atoms (nitrogen of NH_3 and Nitrogen of NO) were chosen as the reaction coordinate and coordinate driving calculation was performed. For the calculation, the spin multiplicity of NO was considered as doublet, while that for NH_3 was considered as singlet. The input geometry for this calculation is given in Figure 4.2. At the end of the calculations the energetic given in Figure 4.3 was obtained. Since the energy profile shows a continuous rise with decreasing reaction coordinate, this reaction is not a favorable reaction.

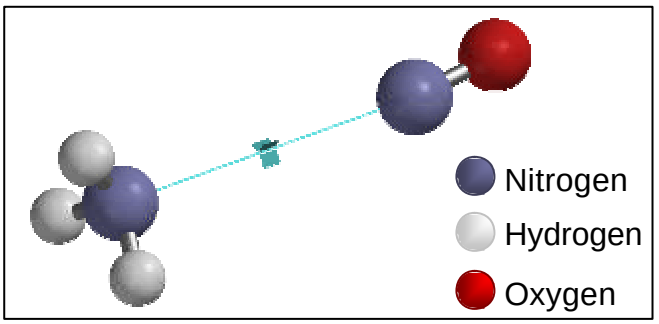

Figure 4.2. Input geometry for the gas phase interaction of the reactants, N-N distance is the reaction coordinate.

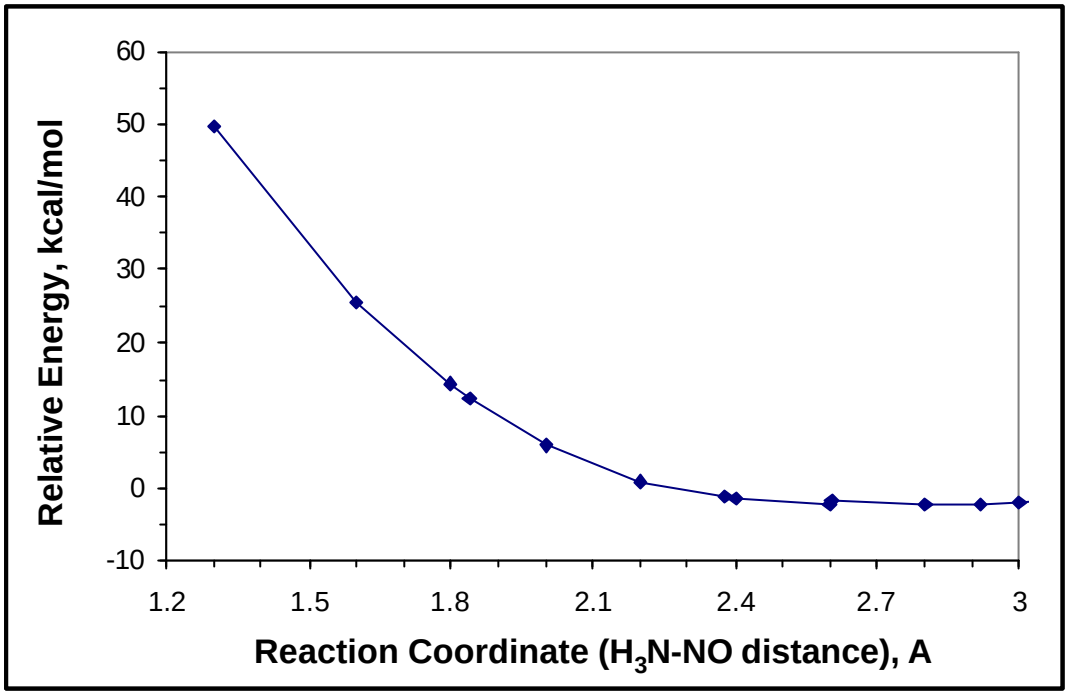

Figure 4.3. Energy profile for the gas phase interaction of the reactants, where the distance between Nitrogen atoms of NH_3 and NO is the reaction coordinate.

4.1.1.2. Gas Phase Reaction with the H-O Reaction Coordinate

Another possible gas phase interaction of the reactants is the reaction for which the distance between one of the Hydrogen atoms of NH_3 and oxygen atom of NO is the reaction coordinate. For this interaction, a coordinate driving calculation with the same spin multiplicity considerations with the previous one was performed. The input geometry for this calculation and the energy profile obtained at the end of this calculation are given in Figure 4.4 and Figure 4.5, respectively. From the energy profile obtained, it was concluded that, similar to previous one, this reaction is an unfavorable reaction.

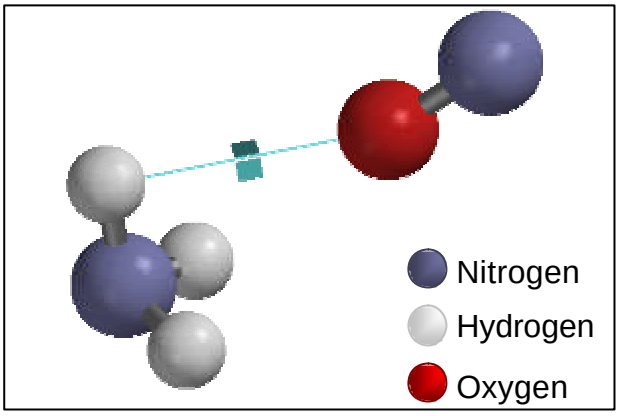

Figure 4.4. Input geometry for the gas phase interaction of the reactants, H-O distance is the reaction coordinate.

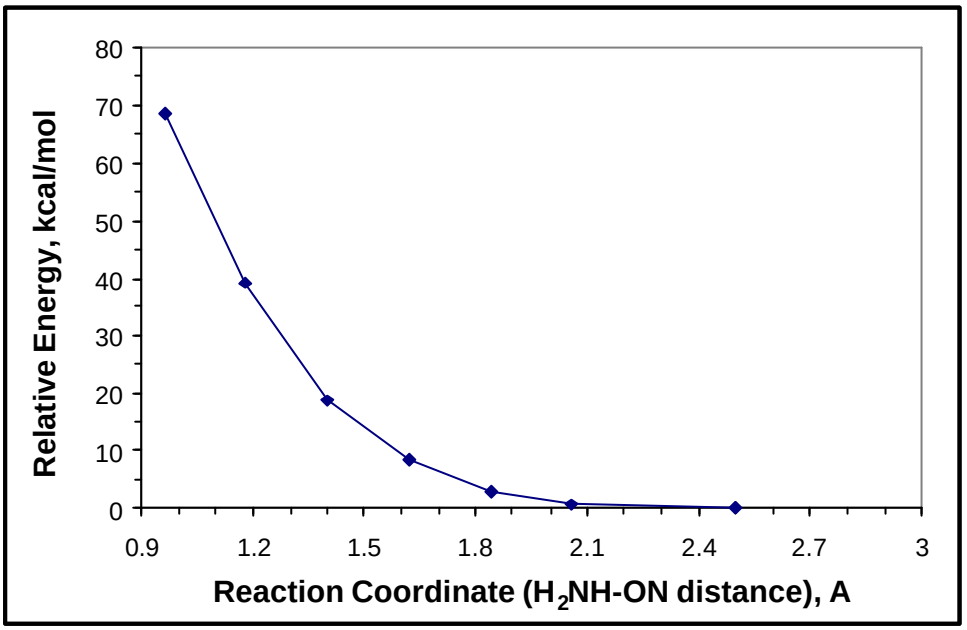

Figure 4.5. Energy profile for the gas phase interaction of the reactants, where the distance between one of the H atoms of NH_3 and O of NO is the reaction coordinate.

4.1.2. SCR of NO by NH_3 in the Presence of V_2O_5

Since both of these gas phase interactions of the reactants are unfavorable, it is obvious that there is a need for catalytic activity for NO to

reduce N_2 and water by NH_3. In the following sections, the catalytic pathway for the SCR of NO by NH_3 over V_2O_5 catalytic surface is simulated by means of the DFT calculations.

4.1.2.1. Initiation Step of SCR of NO by NH_3 over V_2O_5

The mechanism of the SCR reaction has been experimentally investigated over vanadium pentoxide catalyst by several authors. It is generally agreed that the reaction is initiated with the activation of ammonia by strong adsorption over the catalytic surface, and it then proceeds by the interaction of NO with preadsorbed ammonia, suggesting an Eley-Rideal type mechanism.

Therefore, as the initiation reaction of the SCR of NO by NH_3, ammonia activation over the V_2O_5 catalytic surface was considered.

4.1.2.1.1. Ammonia Activation over V_2O_5 Surface

Ammonia activation may occur through two different mechanisms: ammonia can be adsorbed on vanadia catalyst through a Lewis-type interaction as molecularly adsorbed ammonia, or the adsorption of ammonia occurs over Brønsted acidic, -OH surface hydroxyl, groups as ammonium ions. Therefore, in order to determine the activation mode of the ammonia, these two possibilities were considered separately and a comparison among them was made to select the most favorable one.

4.1.2.1.1.1. Lewis Acidic Ammonia Adsorption

Ammonia adsorption through a Lewis acidic interaction is one of the possible activation modes of ammonia over V_2O_5 surface. This interaction type was investigated over a $V_2O_9H_6$ cluster. The methodology for the construction of the $V_2O_9H_6$ cluster is described in Section 3.3, the structure for this cluster is given in Figure 3.4.

In order to investigate the ammonia activation through a Lewis type interaction, the distance between one of the Hydrogen atoms of ammonia and O1 site of the $V_2O_9H_6$ cluster was selected as the reaction coordinate, and then coordinate driving calculation was performed. During the calculation, reaction coordinate was decreased from 3 A to 0.9 A while all the atoms of the cluster were kept frozen except for the active sites (two O1 atoms) and the adsorbing molecule (NH_3). The input geometry for this coordinate driving calculation is given in Figure 4.6, where the line between H and O1 atoms represents the reaction coordinate.

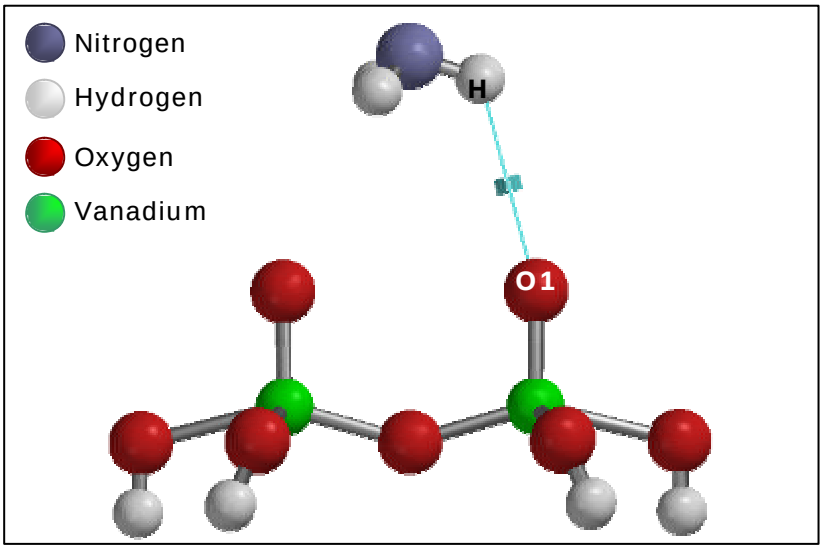

Figure 4.6. Input geometry for the ammonia activation through a Lewis type interaction.

At the end of the coordinate driving calculation, NH_2 is formed through the abstraction of one H atom of ammonia by O1 active site. During the calculation, as ammonia approaches to O1 active site, the bond distance of V=O1 increases form 1.581 A to 1.658 A. This shows that the double bond between V and O1 atoms turns into a single bond as ammonia interacts with O1 site and gives one of its Hydrogen atoms to that site. However, this reaction seems to be an unfavorable reaction, because the total energy of the system shows a continuous rise as ammonia gets close to active site, O1. Energy profile obtained from the coordinate driving calculation is shown in Figure 4.7. As a result, it is concluded that ammonia is hardly adsorbed on the Lewis acidic V=O site of the V_2O_5 surface forming an NH_2 species and ammonia activation on Lewis acidic V=O site should not be considered as the initiation reaction for SCR of NO by NH3 reaction. The final geometry of this calculation is given in Figure 4.8.

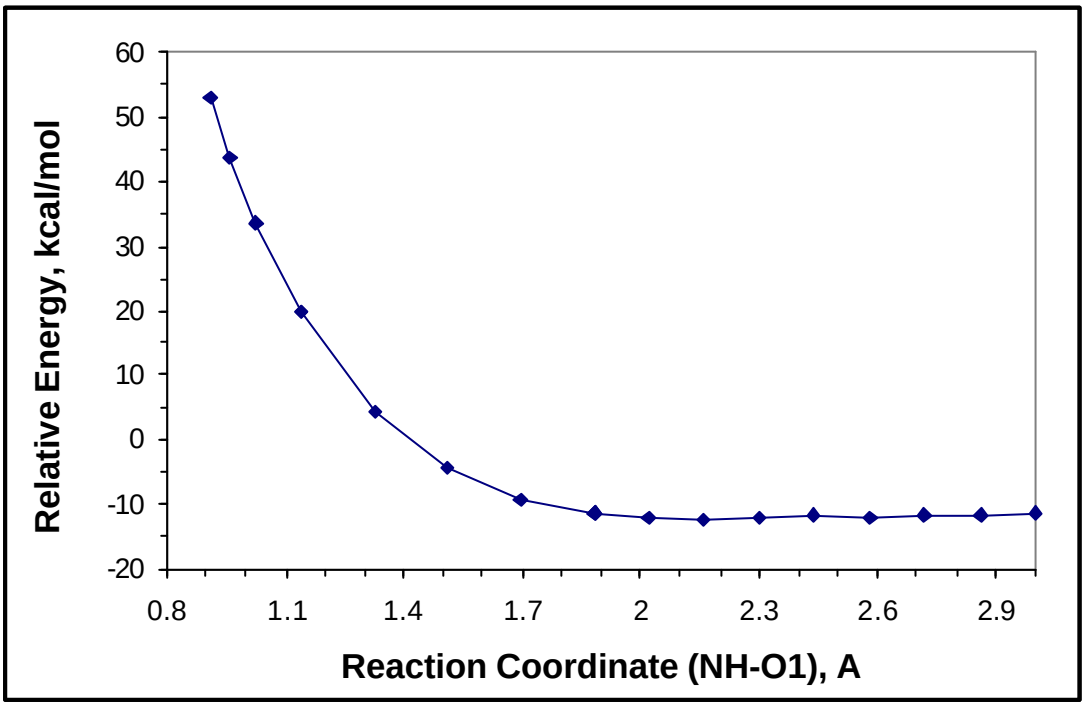

Figure 4.7. Energy profile for the ammonia activation on Lewis acidic V=O1 site.

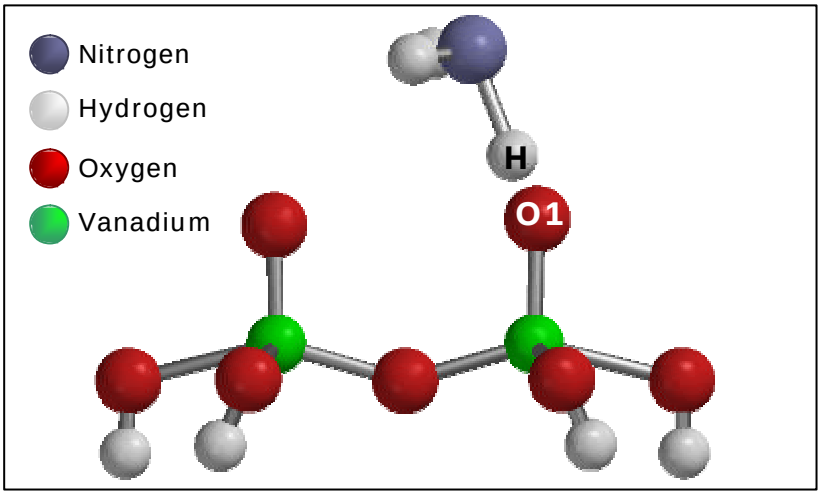

Figure 4.8. The final geometry of the Lewis acidic ammonia adsorption calculation

4.1.2.1.1.2. Brønsted Acidic Ammonia Adsorption

Another possible activation mode of ammonia on V_2O_5 catalytic surface is the adsorption over Brønsted acidic V-OH site of V_2O_5 surface. This interaction type was investigated over a $V_2O_9H_6$-H cluster. The methodology for the construction of the $V_2O_9H_6$-H cluster is described in Section 3.3 and the structure for this cluster is given in Figure 3.5.

In order to investigate the Brønsted acidic ammonia adsorption over $V_2O_9H_6$-H cluster, the distance between Nitrogen atom of ammonia and Brønsted acidic H-O1 site of the $V_2O_9H_6$-H cluster was selected as the reaction coordinate for coordinate driving calculation. During the calculation, reaction coordinate was decreased from 3 A to 1 A while all the atoms of the cluster were kept frozen except for the active sites (O1-H site and adjacent doubly bonded O atom) and the adsorbing molecule (NH_3). The input geometry for this coordinate driving

calculation is given in Figure 4.9, where the line between N and H-O1 atoms represents the reaction coordinate.

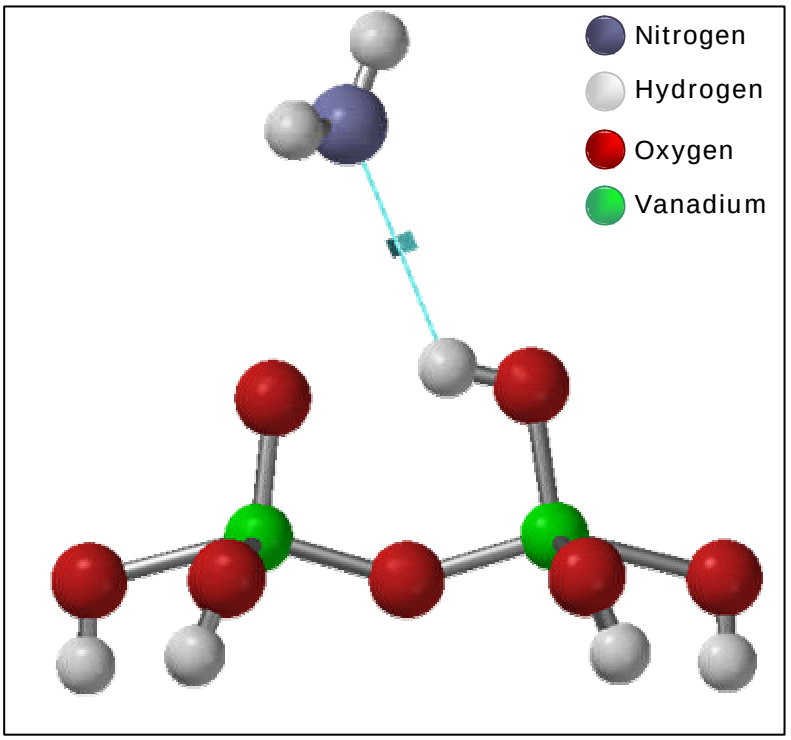

Figure 4.9. Input geometry for the ammonia activation through a Brønsted acidic interaction.

At the end of the coordinate driving calculation, energy profile given in Figure 4.10 was obtained. For this profile, relative energy was calculated with respect to the energies of $V_2O_9H_6$-H cluster plus gas phase ammonia molecule. As it is seen from this profile, ammonia is adsorbed over Brønsted acidic V-OH site through a nonactivated adsorption process which is in agreement with what Srnak et al. (1992) suggested via TPD experiments. They suggested that ammonia activation over Brønsted acidic V-OH site occurs through a nonactivated process.

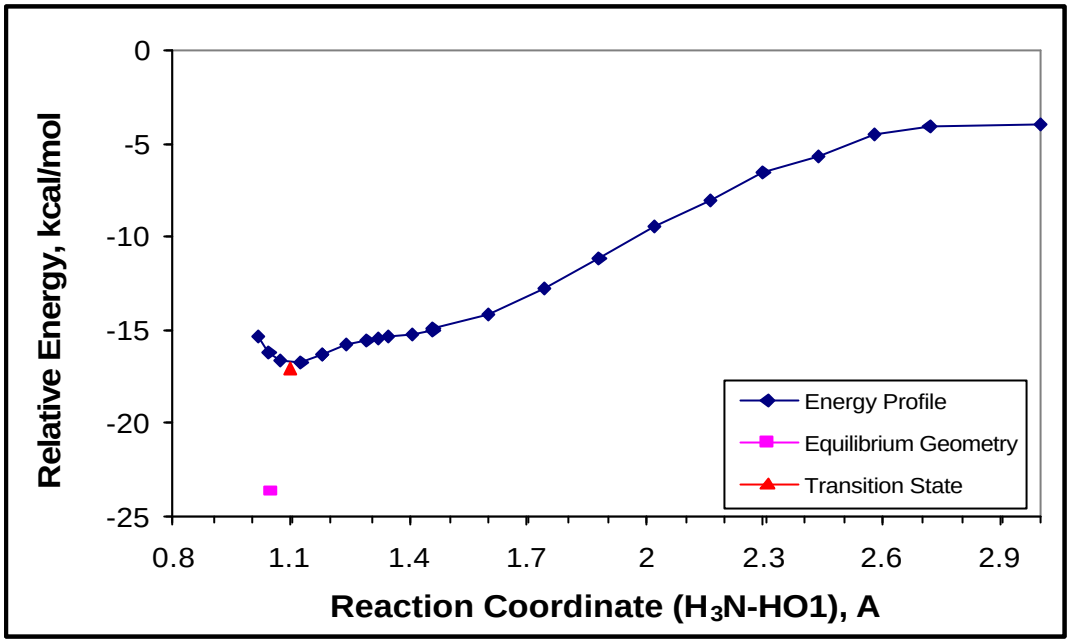

Figure 4.10. Energy Profile for NH_3 adsorption on Brønsted acidic V-OH site

For the nonactivated ammonia adsorption over Brønsted acidic V-OH site reaction, transition state and equilibrium geometry structures were also obtained. For the transition state calculation the geometry with a reaction coordinate of 1.236A and for the equilibrium geometry calculation the resulting geometry of the transition state calculation were given as input geometries, respectively. Geometries obtained from these calculations are illustrated on Figure 4.11 and in Table 4.3. The relative energy difference for the transition state structure was calculated as -17.1kcal/mol, which also proves the nonactivated ammonia adsorption over Brønsted acidic V-OH site, since it is a negative value and transition state energy gives the activation energy.

Calculated equilibrium geometry has a relative energy of -23.6kcal/mol. This is again in agreement with what Srnak et al. (1992) observed via TPD experiments and what Dumesic et al. (2002) and Gilardoni et al. (1997) calculated by DFT calculations. Srnak et al. (1992) observed the desorption

activation energy of nonactivated adsorption of NH_3 over Brønsted acidic V-OH site as 18kcal/mol via TPD experiments. Moreover, Dumesic et al. (2002) and Gilardoni et al. (1997) calculated the relative energy of the adsorbed NH_3 species over Brønsted acidic V-OH site of the V_2O_5 catalyst as -26kcal/mol and -25kcal/mol, respectively.

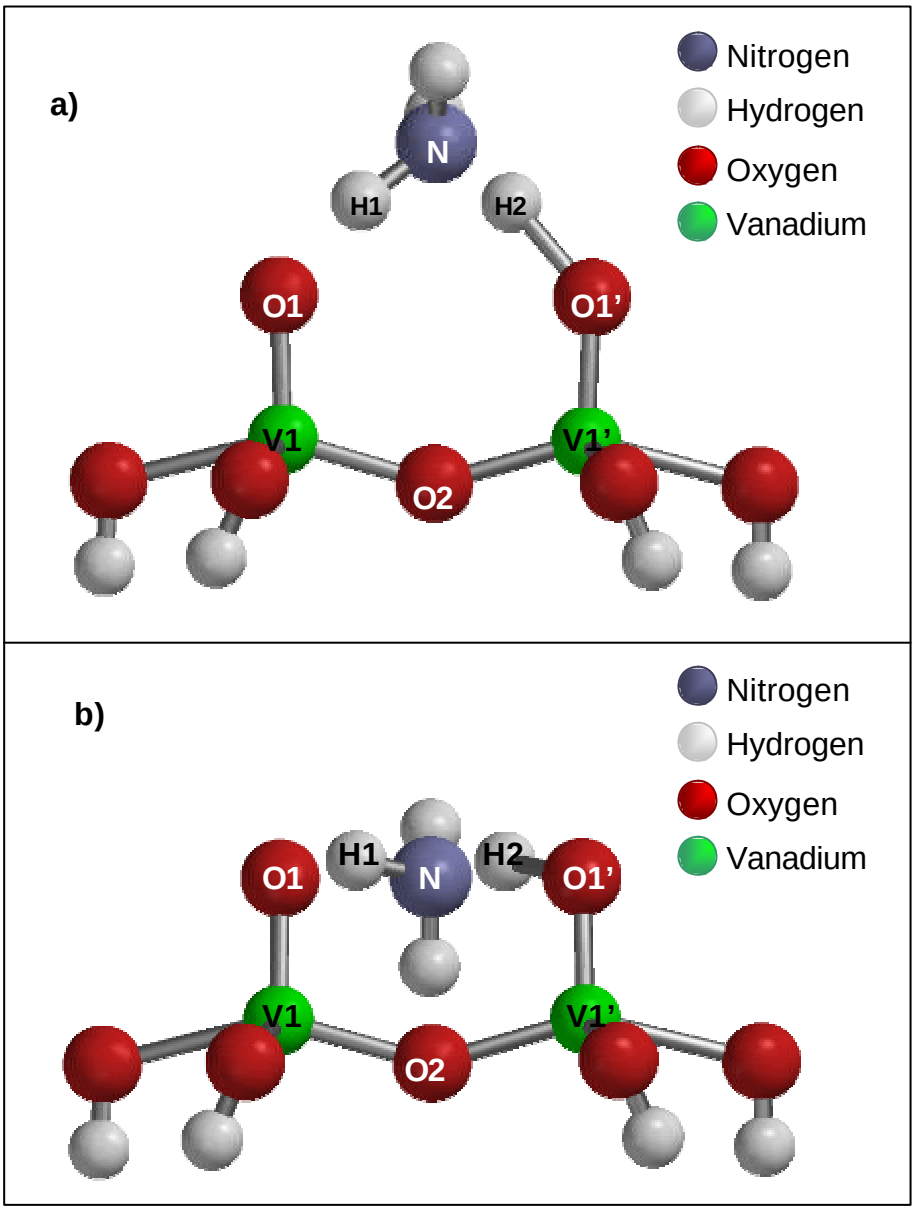

Figure 4.11. Transition state and equilibrium geometry structures for Brønsted acidic NH_3 adsorption reaction; (a) Transition state structure, (b) Equilibrium geometry structure.

Table 4.3. Bond distance and angle values for the transition state and equilibrium geometry structures of Brønsted acidic NH_3 adsorption.

	Transition State Structure	**Equilibrium Geometry Structure**
d(H1-O1), A	1.451	1.728
d(H2-O1'), A	1.450	1.736
d(N-H1), A	1.097	1.051
d(N-H2), A	1.098	1.051
d(O1-V1), A	1.621	1.608
d(O1'-V1'), A	1.622	1.607
<(O1-V1-O2)	107.88	104.93
<(O1'-V1'-O2)	107.82	104.79
<(V1-O2-V1')	148.17	148.17

For the optimized geometry of Brønsted acidic NH_3 adsorption reaction, single point energy calculations were carried out to obtain vibration frequencies and Mulliken charges. Vibration frequencies were calculated as 1421, 1650, 2857 and 2900cm^{-1}, which are contributed by symmetric and asymmetric bending and stretching frequencies of NH_4, respectively. In the experimental literature, the values reported by use of FT-IR studies on the V_2O_5 surface are in the range of 1417-1445cm^{-1}, and 1660-1680cm^{-1} for symmetric and asymmetric bending vibrations of NH_4, respectively, and stretching frequencies of NH_4 were detected in the region between 2600 and 3020cm^{-1}. Table 4.4 shows a comparison of the calculated vibration frequencies with the experimental literature.

Table 4.4. Comparison of the calculated vibration frequency data for the optimized geometry of Brønsted acidic NH_3 adsorption reaction with experimentally obtained ones.

Vibrations	Calculated B3LYP/6-31G**	Ramis et al. (1996), FTIR	Nan-Yu Topsøe (1991), FTIR
NH_4 bend. (asym.)	1421 cm^{-1}	1425 cm^{-1}	1417 cm^{-1}
NH_4 bend. (sym.)	1650 cm^{-1}	1680 cm^{-1}	1670 cm^{-1}
NH_4 stret. (asym.)	2857 cm^{-1}	2850 cm^{-1}	2808 cm^{-1}
NH_4 stret. (sym.)	2900 cm^{-1}	3000 cm^{-1}	3019 cm^{-1}

The Mulliken charge calculated for the equilibrium geometry of the Brønsted acidic NH_3 adsorption reaction is +0.782e. This result is very close to what Dumesic et al. (2003) calculated (+0.808e) and suggests that NH_3 is adsorbed on Brønsted acidic V-OH site as NH_4^+ ion.

Thus, it is concluded that the SCR reaction is initiated more favorably by the strong nonactivated ammonia adsorption reaction on Brønsted acidic V-OH site and the adsorbed ammonia forms NH_4^+ ion over the catalytic surface. Since the activation mode of the ammonia over the catalytic surface was decided as Brønsted acidic adsorption, the second step of the SCR reaction was investigated by introducing NO to the final geometry of the Brønsted acidic NH_3 adsorption reaction.

4.1.2.2. Second Step of SCR of NO by NH_3 over V_2O_5

As the second step of the SCR reaction, NO interaction with the preadsorbed NH_3 species was investigated. For this purpose a coordinate driving calculation was performed. In Figure 4.12, the input geometry for this calculation

is illustrated. For the calculation three different reaction coordinates, were determined and all of these three reaction coordinates were simultaneously decreased step by step during the calculation. The first of these reaction coordinates is between Nitrogen atoms of preadsorbed NH_3 and gas phase NO molecule, which is labeled by “a”, and the other two are between the Hydrogen atoms of the NH_4 species and O1 active sites, which are labeled by “b” and “c”, respectively.

Energy profile obtained at the end of this calculation is illustrated in Figure 4.13, where relative energy is calculated with respect to the sum of the energies of $V_2O_9H_6$-H cluster and gas phase energies of NH_3 and NO at infinite separation.

In order to obtain the optimized geometry for this reaction, an equilibrium geometry calculation was performed starting from the final geometry on the energy profile. At the end of this calculation, the optimized geometry was reached with a relative energy difference of +6.4 kcal/mol corresponding to an endothermic reaction, where NH_2NO (nitrosamide) species is released from the $V_2O_9H_6$-H cluster. The optimized geometry is given Figure 4.14. In experimental literature there is no data for the heat of formation of NH_2NO species over V_2O_5 catalytic surface; however this value was calculated theoretically as +18.2kcal/mol and +5.5kcal/mol by Gilardoni et al. (1997) and Dumesic et al. (2003), respectively. Moreover, nitrosamide species was not observed experimentally under typical SCR conditions. This may be due to very fast decomposition of NH_2NO to the SCR reaction products N_2 and water.

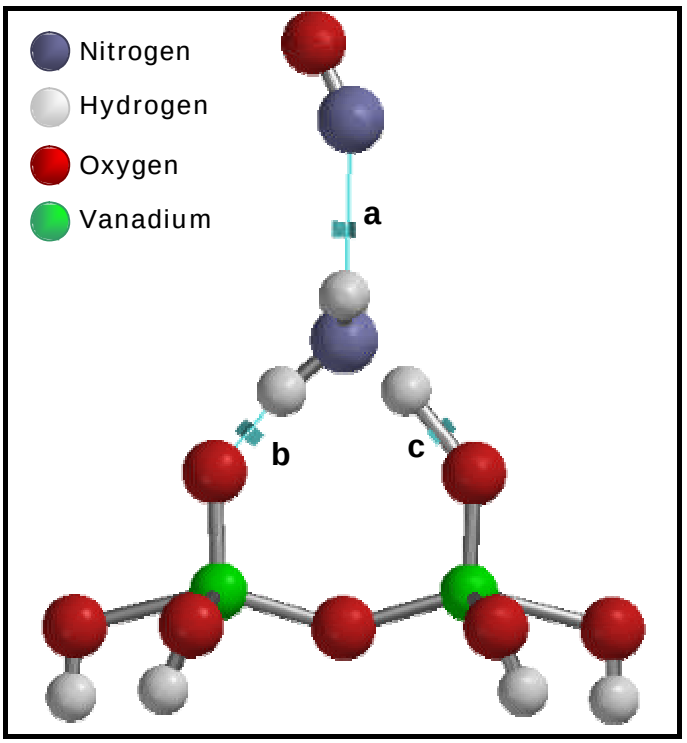

Figure 4.12. The input geometry for the interaction of NO with the preadsorbed NH_3 species as the second step of the SCR reaction. a, b and c are three different reaction coordinates.

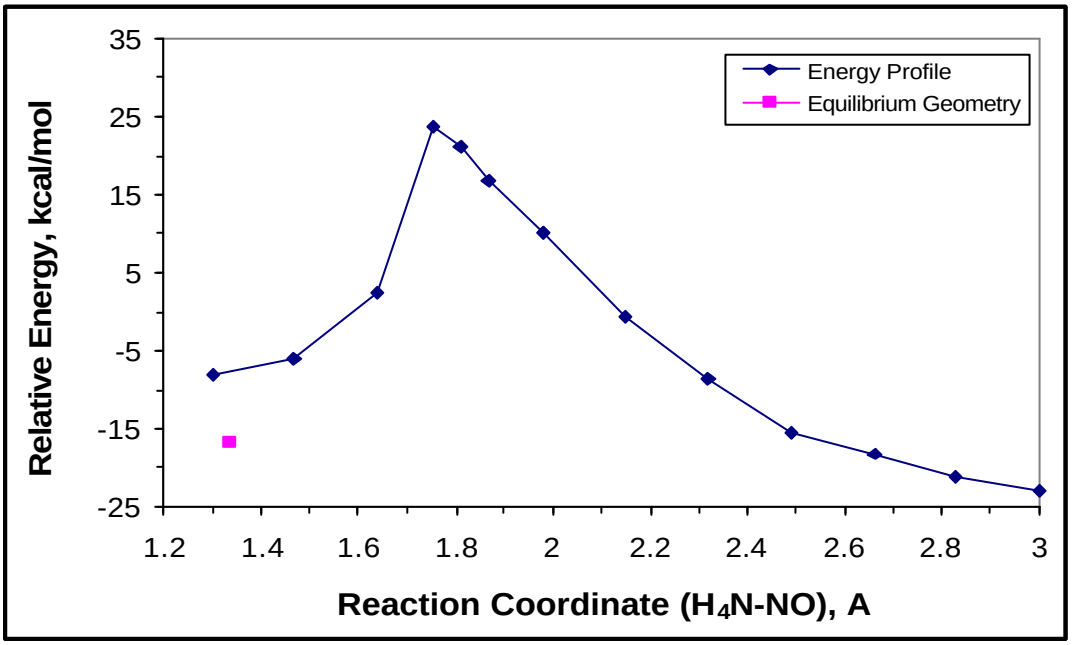

Figure 4.13. Energy profile obtained for the interaction of gas phase NO with the preadsorbed NH_4 species.

Due to the complexity of the reaction, a successful transition state geometry calculation could not be achieved. Therefore, only an approximate transition state geometry is reported. The approximate transition state is the geometry at which the energy profile reaches a maximum value. This geometry which has a relative energy difference of 46.9kcal/mol is also illustrated in Figure 4.14.

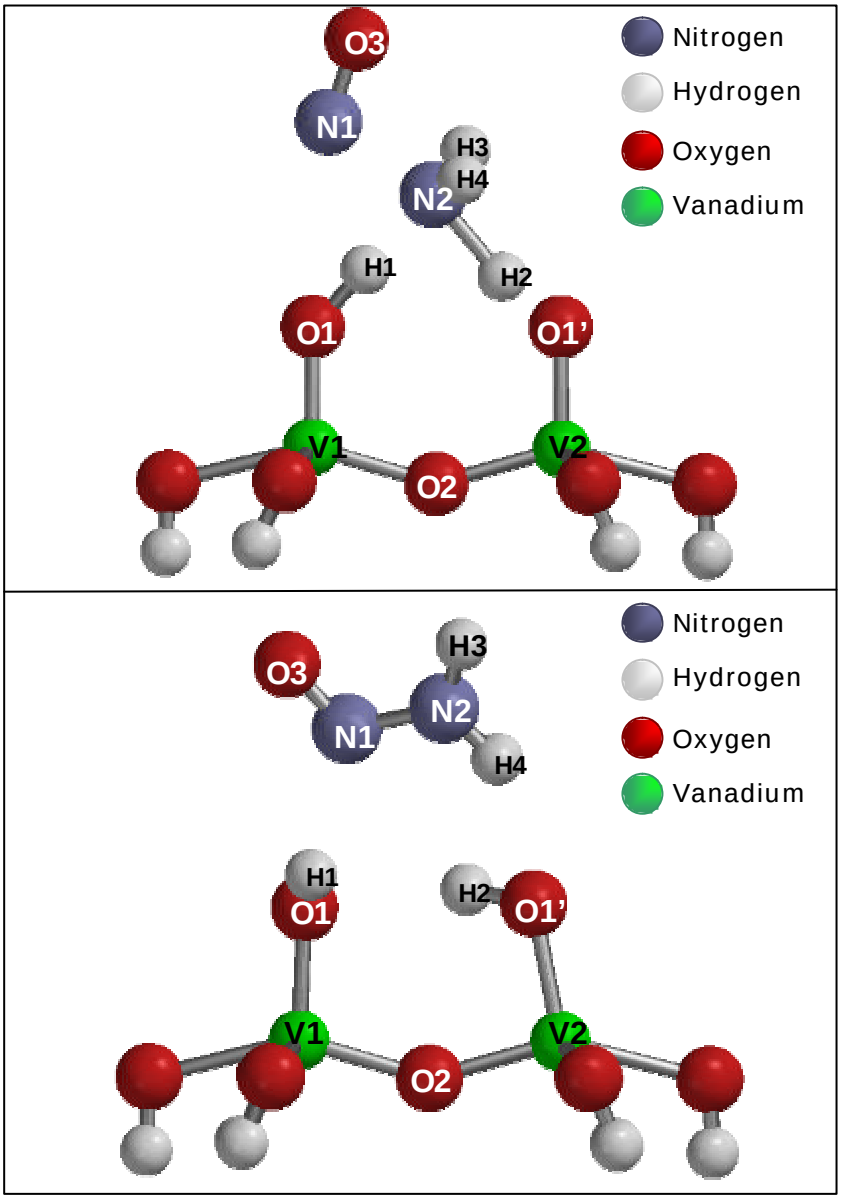

Figure 4.14. Approximate transition state and optimized geometry structures for the interaction of gas phase NO with preadsorbed NH_4, formation of NH_2NO (nitrosamide) species; (a) approximate transition state, (b) optimized geometry.

With the release of nitrosamide species from the catalytic surface, an additional hydroxyl group is formed. In the presence of oxygen, this H-atom on the catalyst surface can be reoxidized by O_2, or NO can also reoxidize these sites in the absence of oxygen.

Table 4.5. Bond distance and angle values for the approximate transition state and equilibrium geometry structures for the interaction of NO with the preadsorbed ammonia species.

	Approximate Transition State Structure	**Equilibrium Geometry Structure**
d(N1-N2), A	1.753	1.336
d(N1-O3), A	1.218	1.245
d(N2-H1), A	1.412	2.766
d(N2-H2), A	1.497	3.147
d(N2-H3), A	1.018	1.034
d(N2-H4), A	1.018	1.016
d(O1-H1), A	1.085	1.008
d(O1'-H2), A	1.085	0.975
d(V1-O1), A	1.655	1.732
d(V2-O1'), A	1.670	1.834
<(O1-V1-O2)	105.67	103.82
<(O1'-V2-O2)	105.20	94.62
<(V1-O2-V1')	148.17	148.17
<(V1-O1-H1)	136.83	118.53
<(V2-O1'-H2)	130.43	110.98

4.1.2.3. Third Step of SCR of NO by NH_3 over V_2O_5

The rest of the catalytic pathway of the SCR reaction of NO by NH_3 is completed by the gas phase decomposition of NH_2NO to reaction products N_2 and H_2O according to the following reaction:

$$NH_2NO \; ? \; H_2O + N_2 \qquad (4.2)$$

Before investigating the decomposition mechanism of NH_2NO into reaction products, the optimized structure for nitrosamide molecule was obtained. For this purpose NH_2NO molecule formed at the end of the NO interaction with preadsorbed ammonia species reaction is taken as the input geometry for the equilibrium geometry calculations. In Figure 4.15 the optimized geometry is given. All the bond distance and angle values as well as the vibration frequency data show very good agreement with the theoretical and experimental values reported in the literature. In Table 4.6, a comparison of these values with the literature is represented.

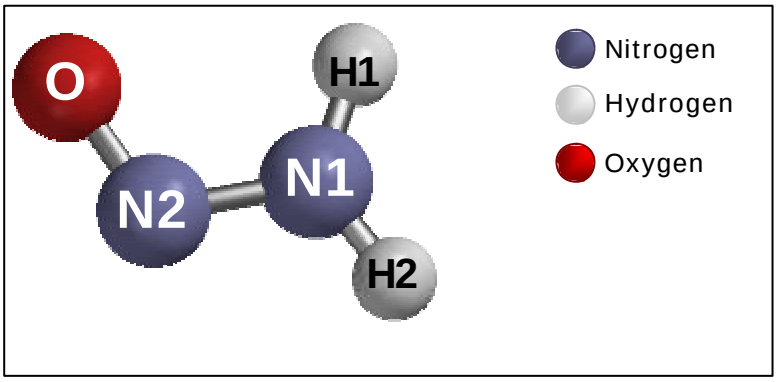

Figure 4.15. Optimized geometry for nitrosamide (NH_2NO) molecule

Table 4.6. Comparison of the calculated bond distance and vibration frequency data of NH_2NO with literature

Geometry	This Work B3LYP/6-31G**	Aschi et al. (1997) MP2(Full)/6-31G*	Duan et al. (1995) CASSCF/cc-pVDZ
d(N1-N2), A	1.336	1.341	1.375
d(N2-O), A	1.221	1.236	1.219
d(N1-H1), A	1.018	1.019	1.022
d(N1-H2), A	1.008	1.010	1.005
<(N1-N2-O)	113.66	113.0	113.4
<(H1-N1-N2)	119.34	117.9	114.7
<(H2-N1-N2)	117.37	115.9	113.4

Frequency, cm^{-1}	This Work, Calculated	Crowley et al. (1990), Experimental
NH_2 scissors	1523	1521
NNH deform.	1177	1207

In order to yield the reaction products N_2 and water, NH_2NO molecule must undergo a series of H atom migrations and some isomerization reactions. Therefore, as the first step of the gas phase nitrosamide decomposition reaction, hydrogen migration from N1 atom to O atom was investigated. For this purpose a coordinate driving calculation was performed by selecting the distance between O and H1 atoms as reaction coordinate. Energy profile obtained by means of this calculation, where the relative energy is calculated with respect to gas phase total energy of NH_2NO molecule, is illustrated in Figure 4.16.

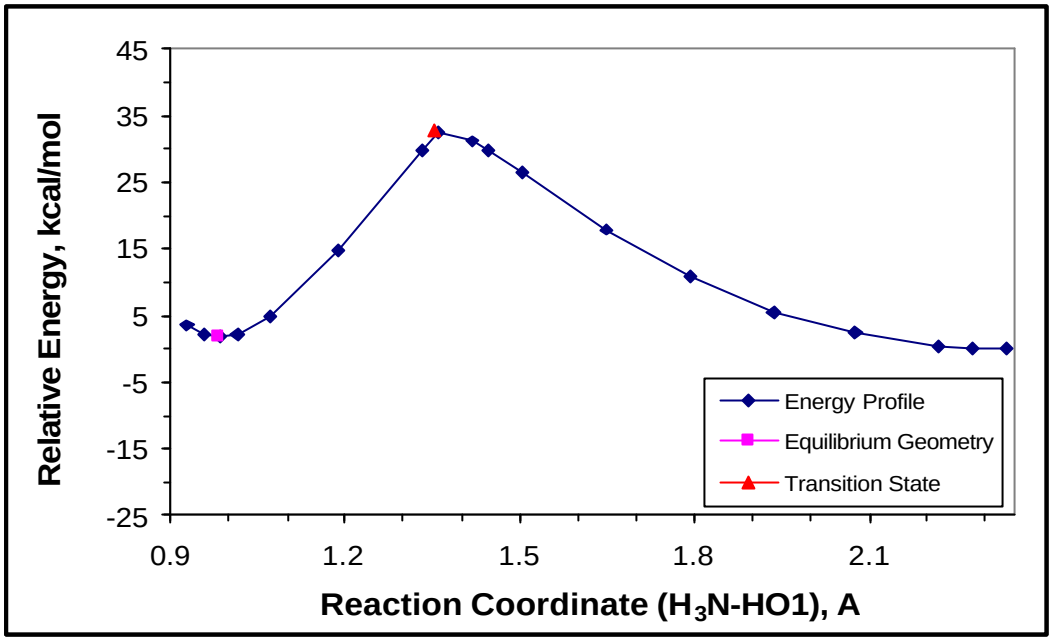

Figure 4.16. Energy profile for the coordinate driving calculation carried out for the first H migration reaction of NH_2NO decomposition reaction.

The relative energy difference of equilibrium geometry was calculated as 1.7kcal/mol corresponding to a slightly endothermic reaction and that for the transition state geometry was obtained as 33.0kcal/mol. These values are very close to what has been calculated in the literature. A comparison with literature is given in Table 4.12.

Transition state geometry and the optimized geometry structures are given in Figure 4.17. Moreover, structural parameters of these geometries are reported in Table 4.7.

Here it should be noted that in the calculated vibration frequency set of the transition state structure, there is only one imaginary vibration (i1498.97), representing the migration of H atom from N1 to O atoms.

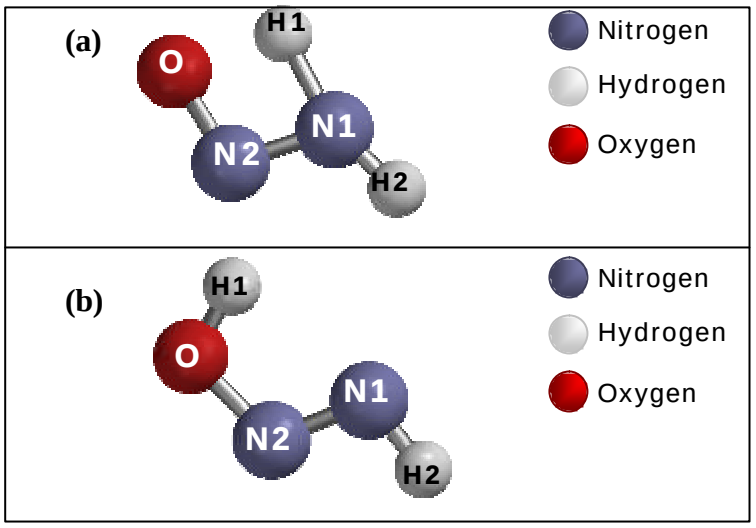

Figure 4.17. Transition state and equilibrium geometry structures for the first step of NH_2NO decomposition; (a) transition state, (b) equilibrium geometry

Table 4.7. Bond distance and angle values for the transition state and equilibrium geometry structures for the first H migration reaction of NH_2NO decomposition reaction.

	Transition State Structure		**Equilibrium Geometry Structure**	
	This Work	Duan et al. (1995)[a]	This Work	Duan et al. (1995)[a]
d(O-H1), A	1.352	1.359	0.984	0.983
d(N1-N2), A	1.275	1.287	1.239	1.255
d(O-N2), A	1.288	1.292	1.364	1.373
d(H1-N1), A	1.300	1.311	2.097	-
d(N1-H2), A	1.021	1.005	1.028	1.040
<(H1-O-N2)	78.25	78.1	105.72	104.5
<(O-N2-N1)	102.90	103.4	111.59	111.4
<(N2-N1-H1)	80.69	-	62.78	-
<(N2-N1-H2)	117.63	117.8	105.73	104.2

[a] Geometries were obtained at CASSCF (12-in-11)/cc-pVDZ level

Second step of the NH_2NO decomposition reaction is the isomerization reaction of hydrogen atom (H1) bonded to oxygen atom. H1 atom in the optimized geometry obtained at the end of first step has a trans conformation with respect to N1N2 bond and a cis conformation with respect to ON2 bond. This structure must isomerize to opposite case in order to let H2 atom migration to O atom for the next steps.

For this purpose, isomerization of the H1 atom about ON2 bond was investigated by means of the coordinate driving calculation for which the dihedral angle between the plane formed by N1-N2-O atoms and H1 atom was selected as the reaction coordinate. During the calculation the reaction coordinate was increased from 0° to 180° step by step.

Energy profile obtained by this calculation is given in Figure 4.18, where relative energy was calculated with respect to gas phase total energy of NH_2NO molecule. The relative energy difference for the equilibrium geometry and transition state structures were calculated as 1.5kcal/mol and 11.4kcal/mol, respectively. These values are again in a good agreement with what has been reported in literature.

The transition state structure with only one imaginary vibration frequency (i465.67cm^{-1}) and the equilibrium geometry are illustrated in Figure 4.19. Bond distances and angles of these structures were compared with theoretical literature in Table 4.8.

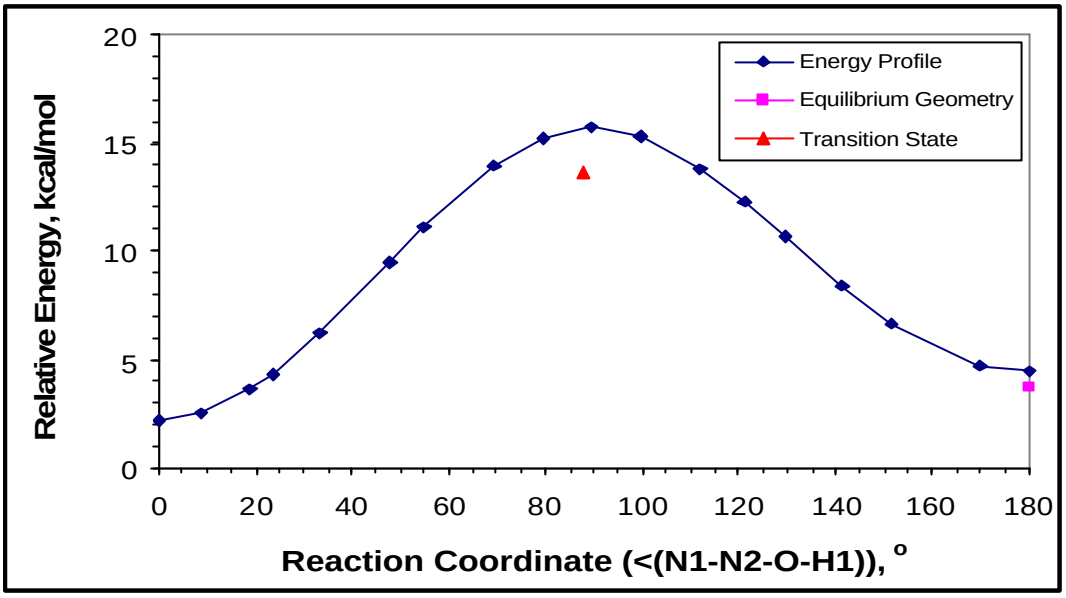

Figure 4.18. Energy profile for the second step of NH_2NO decomposition, where reaction coordinate is the dihedral angle between N1-N2-O-H1.

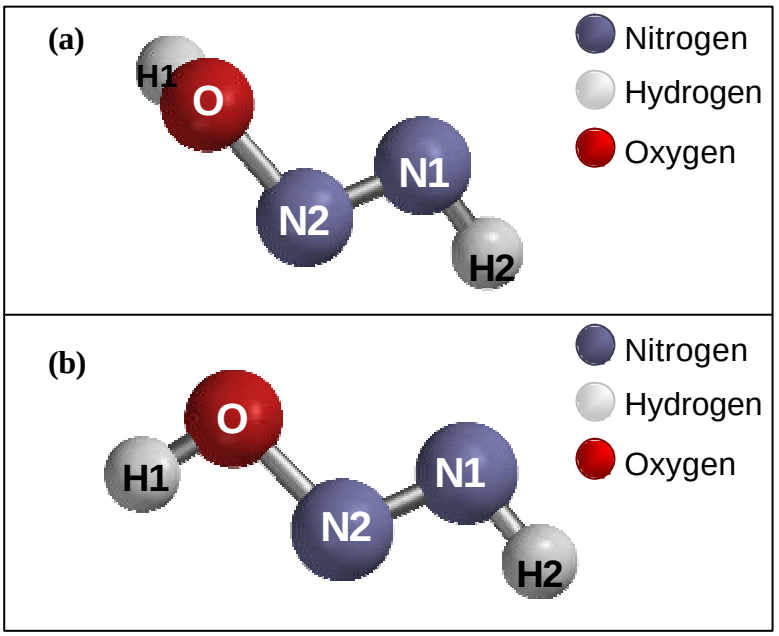

Figure 4.19. Transition state and equilibrium geometry structures for the second step of NH_2NO decomposition; (a) transition state, (b) equilibrium geometry

Table 4.8. Bond distance and angle values for transition state and equilibrium geometry structures of the 2nd step of NH_2NO decomposition reaction.

	Transition State Structure		**Equilibrium Geometry Structure**	
	This Work	Duan et al. (1995)[a]	This Work	Duan et al. (1995)[a]
d(O-H1), A	0.971	0.975	0.969	0.973
d(N1-N2), A	1.228	1.244	1.234	1.252
d(O-N2), A	1.440	1.454	1.394	1.395
<(H1-O-N2)	103.92	101.9	102.17	101.4
<(O-N2-N1)	109.15	108.8	108.99	108.9
<(N1-N2-O-H1) [b]	87.96	88.0	180	180

[a] Geometries were obtained at CASSCF (12-in-11)/cc-pVDZ level
[b] Dihedral angle between the plane of N2-N1-O and H1 atom

After isomerization of H1 atom about ON2 bond from cis to trans conformation, another isomerization reaction was considered for the third step of the NH_2NO decomposition reaction. In this step, H2 atom isomerizes from trans conformation to cis conformation about N1N2 bond. Therefore, for the coordinate driving calculation, the angle between N2, N1 and H2 atoms was selected as the reaction coordinate and it was increased from 106° to 286° step by step during the calculation. From the results of this coordinate driving calculation, energy profile reported in Figure 4.20 was obtained for which the relative energy was defined as the difference between calculated total system energy and the total gas phase energy of NH_2NO molecule. Transition state and equilibrium geometry structures are given in Figure 4.21 and their bond distance and angle values are compared in Table 4.9.

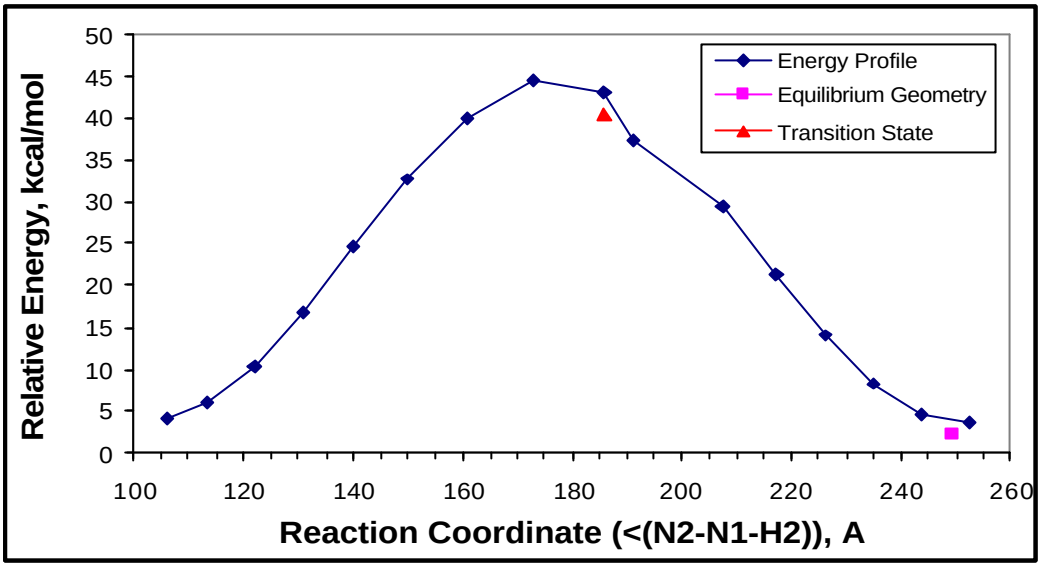

Figure 4.20. Energy profile for the third step of NH_2NO decomposition.

Relative energy differences for both the equilibrium geometry and the transition state structures agree well with the literature values. These values were calculated as -1.77 kcal/mol and 36.47 kcal/mol, respectively. Comparison of these values as well as those for the other steps of NH_2NO decomposition reaction with literature is given in Table 4.12.

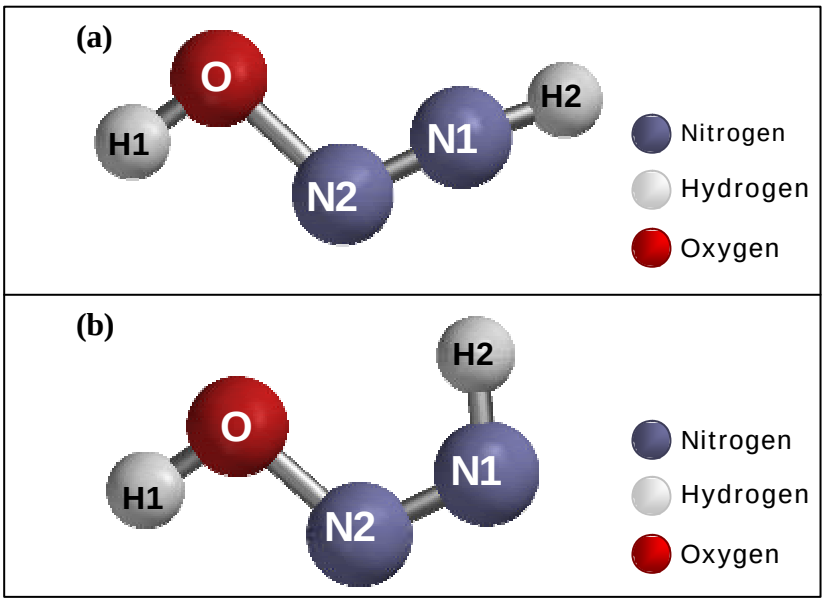

Figure 4.21. Transition state and equilibrium geometry structures for the third step of NH_2NO decomposition; (a) transition state, (b) equilibrium geometry

Table 4.9. Bond distance and angle values for transition state and equilibrium geometry structures of the 3rd step of NH_2NO decomposition reaction.

	Transition State Structure		**Equilibrium Geometry Structure**	
	This Work	Duan et al. (1995)[a]	This Work	Duan et al. (1995)[a]
d(N1-H2), A	0.994	0.985	1.040	1.050
d(N1-N2), A	1.184	1.193	1.224	1.246
d(O-N2), A	1.528	1.554	1.419	1.409
<(N2-N1-H2)	185.74	174.7	249.29	251.5
<(O-N2-N1)	111.07	110.9	112.42	111.8

[a] Geometries were obtained at CASSCF (12-in-11)/cc-pVDZ level

In order to obtain N_2 and H_2O molecules at the end of the gas phase NH_2NO decomposition reaction, an additional coordinate driving calculation, starting from the final geometry of the third step, was carried out. Reaction coordinate was selected as the distance between H2 and O atoms for this calculation. Energy profile obtained at the end of this calculation is given in Figure 4.22. By considering the relative energy differences of transition state and equilibrium geometry structures, it was concluded that an activation energy of 28.74 kcal/mol is needed for the formation of N_2 and H_2O products with a heat of formation energy of -62.4 kcal/mol corresponding to a highly exothermic reaction. As in previous steps, these values agree well with the literature (see Table 4.12). Transition state and equilibrium geometry structures are illustrated in Figure 4.23 and in Table 4.10, bond distances and angles for these geometries can be seen.

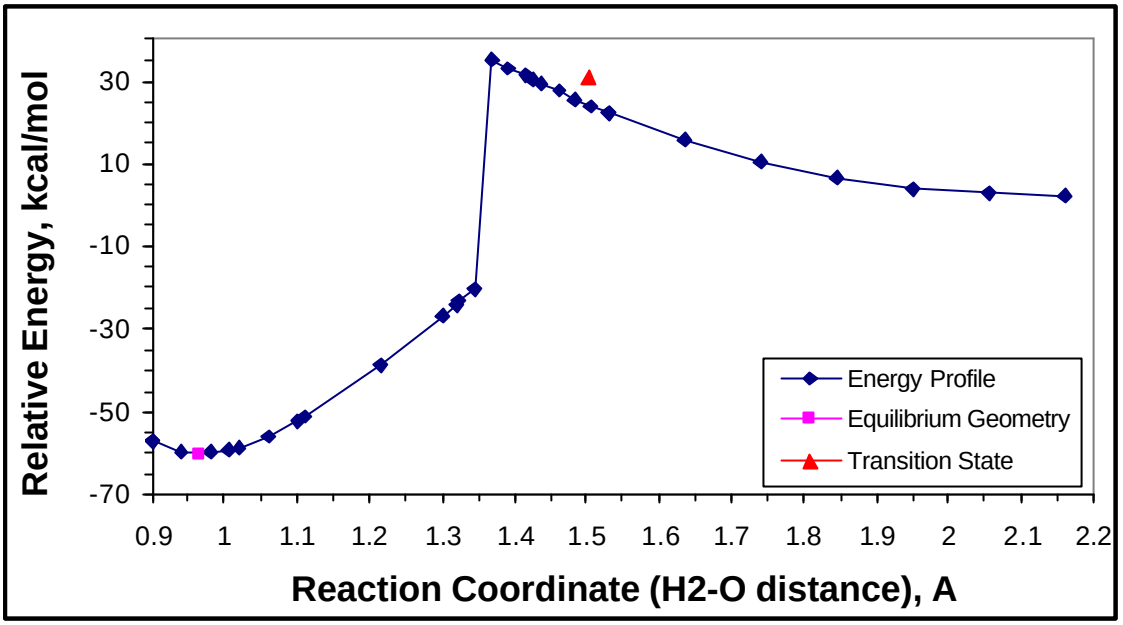

Figure 4.22. Energy profile for the last step of NH_2NO decomposition reaction

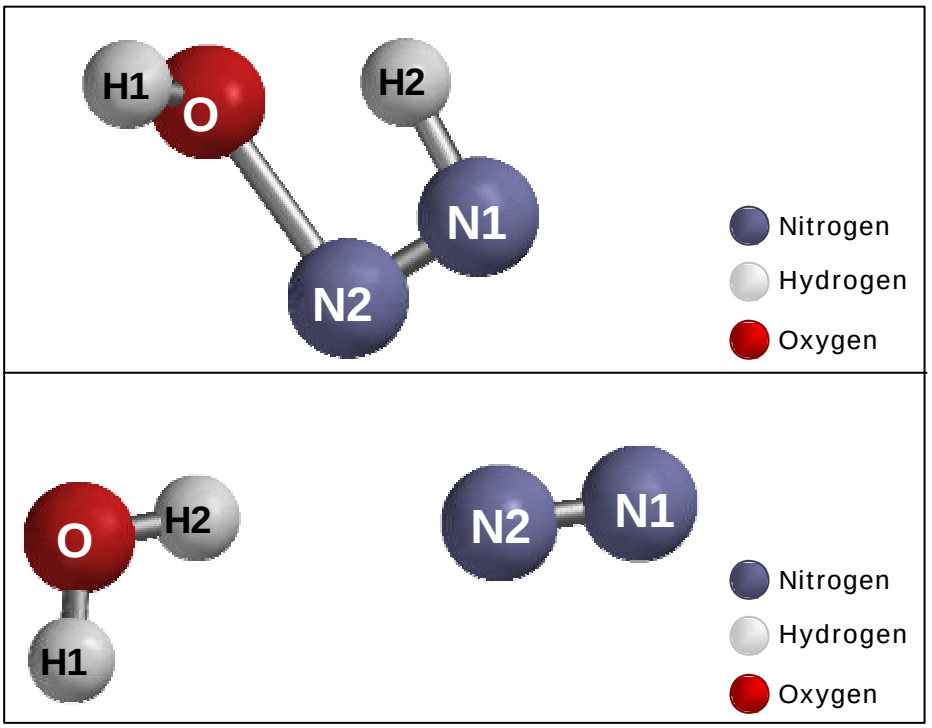

Figure 4.23. Transition state and equilibrium geometry structures for the last step of NH_2NO decomposition; (a) transition state, (b) equilibrium geometry

Table 4.10. Bond distance and angle values for transition state and equilibrium geometry structures of the last step of NH_2NO decomposition reaction.

	Transition State Structure		**Equilibrium Geometry Structure**	
	This Work	Duan et al. (1995)[a]	This Work	Duan et al. (1995)[a]
d(N1-H2), A	1.165	1.140	2.388	-
d(N1-N2), A	1.165	1.170	1.105	1.115
d(O-N2), A	1.839	1.924	3.333	-
d(O-H1), A	0.974	0.983	0.965	0.971
d(O-H2), A	1.501	1.613	0.965	-
<(O-N2-N1)	92.63	88.8	171.16	-
<(H1-O-H2)	33.03	-	103.68	101.0

[a] Geometries were obtained at the CASSCF (12-in-11)/cc-pVDZ level

Vibration frequencies were also calculated for transition state and equilibrium geometry structures. As it is the case for other transition state structures obtained in previous steps, the transition state structure of this step has only one imaginary vibration frequency (i1436.64cm^{-1}) representing the migration of H2 atom from N1 atom to O atom. In Table 4.11, vibration frequencies calculated for the equilibrium geometry is compared with the experimentally observed frequencies of N_2 and H_2O molecules, which are the reaction products of the SCR reaction of NO by NH_3. Comparison of the calculated values of bond distances and angles in the final geometry with the experimental values can also be seen in Table 4.11.

Table 4.11. Comparison of the calculated bond distance and vibration frequency data of the reaction products with experimentally obtained ones.

Geometry		
N_2	**This Work, B3LYP/6-31G****	**Stewart et al. (1990), Experimental**
d(N-N), A	1.105	1.094
H_2O	**This Work, B3LYP/6-31G****	**Stewart et al. (1990), Experimental**
d(O-H), A	0.965	0.957
<(H-O-H)	103.68	104.5
Frequency, cm^{-1}		
N_2	**This Work, B3LYP/6-31G****	**Huber et al. (1979) , Experimental**
Stretching, N-N	2367.0	2359
H_2O	**This Work, B3LYP/6-31G****	**Stephens et al. (1990), Experimental**
Stretching (sym.), O-H	3658.4	3657
Bending, O-H	1604.9	1595
Stretching (asym.), N-H	3762.8	3756

In order to summarize the energetics of the gas phase decomposition reaction of NH_2NO into N_2 and H_2O, a global energy profile was plotted by combining relative energy differences of transition and equilibrium geometries of steps 1, 2, 3 and 4 of NH_2NO gas phase decomposition reaction. The global energy profile is represented in Figure 4.24, where the relative energy is calculated w.r.t. gas phase total energy of NH_2NO.

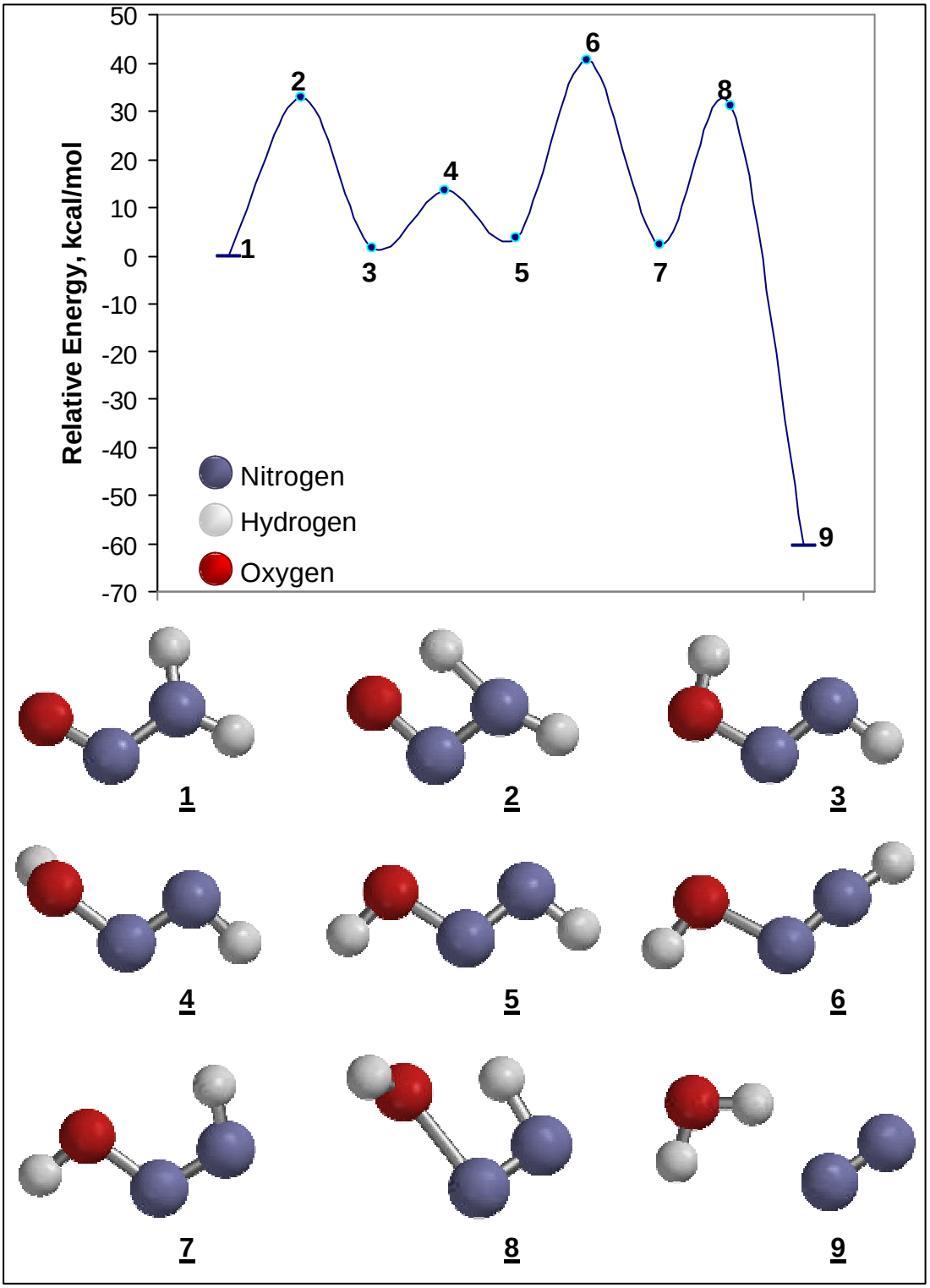

Figure 4.24. Global energy profile for the gas phase NH_2NO decomposition reaction.

Table 4.12. Relative energies of the geometries given in Figure 4.24, with respect to gas phase total energy of NH_2NO molecule (geometry 1).

	Relative Energies of the Geometries		
	This Work [a]	Gilardoni et al. (1997) [b]	Duan et al. (1995) [c]
Geometry 1	0.00	0.00	0.00
Geometry 2	32.98	32.30	35.14
Geometry 3	1.70	2.85	-1.36
Geometry 4	13.62	12.54	9.37
Geometry 5	3.68	3.67	1.10
Geometry 6	40.53	35.66	44.49
Geometry 7	2.28	3.03	0.44
Geometry 8	31.02	24.20	34.42
Geometry 9	-60.12	-62.47	-72.77

[a] Calculated at B3LYP/6-31G** level
[b] Calculated at B3LYP/6-311++G** level
[c] Calculated CASSCF (12-in-11)/cc-pVDZ level

CHAPTER 5

CONCLUSIONS

The catalytic pathway for the selective catalytic reduction reaction of NO by NH_3 reaction on V_2O_5 surface was simulated by means of the density functional theory calculations carried out at B3LYP/6-31G** level.

As an initiation reaction, ammonia activation mode over vanadium pentoxide catalytic surface was investigated. For this purpose, coordinate driving calculations were performed for two different possible reactions, namely, Brønsted acidic and Lewis acidic ammonia adsorptions. The results of these calculations showed that ammonia is hardly adsorbed on Lewis acidic V=O site, while it is easily adsorbed over Brønsted acidic V-OH site through a nonactivated process. Therefore, it is concluded that the SCR reaction is initiated more favorably by the ammonia activation on Brønsted acidic V-OH site, on which it adsorbed as NH_4^+ ion.

Vibration frequencies calculated for the optimized geometry of the Brønsted acidic adsorption reaction agree well with what has been observed experimentally in literature. Moreover, the relative energy difference calculated for the optimized geometry is also close to the experimentally obtained

desorption activation energy of ammonia on V_2O_5 surface. In addition to these, the relative energy difference of the transition state obtained for this reaction (-17.1kcal/mol) proves that ammonia activation over Brønsted acidic V-OH site is a nonactivated process. This is also in agreement with what has been suggested in experimental literature.

As the second step of the SCR reaction, NO interaction with the preadsorbed NH_4^+ species was investigated. By means of the coordinate driving calculations, it is observed that this interaction leads to the formation of NH_2NO (nitrosamide) molecule, which is released from the catalytic surface at the end of the interaction.

The rest of the reaction was completed by the calculations carried out for the gas phase decomposition reaction of NH_2NO species. Accordingly, gas phase decomposition of NH_2NO starts with hydrogen atom migration from N to O atom, and the species undergoes two series isomerization reactions. The reaction is then ended with a second hydrogen atom migration reaction which leads to the formation of H_2O and N_2 reaction products. All the transition state and equilibrium geometry structures obtained for the elementary steps of the gas phase decomposition reaction of NH_2NO show again a good agreement with the literature. Moreover, vibration frequency data for the final structure as well as the bond distance and angle values fit excellently with the experimentally observed values of the N_2 and H_2O molecules.

This study showed that theoretical quantum chemical calculations can be used as a reliable tool in the field of heterogeneous catalysis. They can provide valuable information about the nature of the active sites involved in the catalytic

reactions. In addition to this, they can help experimental researchers make predictions before running the actual expensive surface science experiments so that they can be better prepared for making observations. In the future, this tool will become more and more powerful with rapidly developing computer technology.

REFERENCES

1. Agar, D.W. and Ruppel, W., "Extended Reactor Concept for Dynamic $DeNO_x$ design," *Chem. Eng. Sci.* 43, 8 (1988).

2. Akbulut, B., MSc. Dissertation, METU, Ankara (2000).

3. Andzelm, J., Wimmer, E., "Density Functional Gaussian-type-orbital Approach to Molecular Geometries, Vibrations, and Reaction Energies", *J. Chem. Phys.* 96, 2, 1280 (1992).

4. Anstrom, M., Topsøe, N-Y., Dumesic, J.A., "Theoretical Insight into the Nature of Ammonia Adsorption on Vanadia-based Catalysts for SCR Reaction", *Catalysis Letters*, 78, 1-4, 281 (2002).

5. Anstrom, M., Topsøe, N-Y., Dumesic, J.A., "Density Functional Theory Studies of Mechanistic Aspects of the SCR Reaction on Vanadium Oxide Catalysts", *J. Catalysis*, 213, 115 (2003).

6. Aschi, M., Grandinetti, F., "Gaseous protonated nitrosamide. A G2 theoretical study on the structure, stability, and interconversion of $(H_2N\text{-}NO)H^+$ isomers", *Chemical Physics Letters*, 267, 98 (1997).

7. Becke, A. D., *Phys. Rev., B.*, 38, 3098 (1988).

8. Becke, A. D., Roussel, M. R. *Phys. Rev., A.*, 39, 3761, (1989).

9. Busca, G., Lietti, L., Ramis, G., Berti, F., "Chemical and Mechanistic Aspects of the Selective Catalytic Reduction of NOx by Ammonia over Oxide Catalysts: A review", *Appl. Catalysis B: Environmental*, 18, 1 (1998).

10. Campbell, L.M., Stone, D.K., Shareef, G.S., "Sourcebook: NO_x Control Technology Data", EPA Report NO. EPA600/S2-91/029., Washington, D.C., (Aug. 1991).

11. Chakrabarti, A., Hermann, K., Druzinic, R., Witko, M., Wagner, F., Petersen, M., “Geometric and Electronic Structure of Vanadium Pentoxide: A Density Functional Bulk and Surface Study”, *Physical Review B*, 59, 16 (1999).

12. Cho, M. and D.P. Hannaym. Foster Wheeler Energy Corp.; S. Kahn, Bechtel Corp.; S.R. Taylor, U.S. Generating Co.; "Operating Experience of a Selective Catalytic Reduction System for Flue Gas Denitrification in a Coal-fired Cogeneration Plant" (1995).

13. Cho, S.M. Foster Wheeler Energy Corp., and Dubow, S.Z., Bechtel Corp., "Design of a Selective Catalytic Reduction System for NO_x Abatement in a Coal-fired Cogeneration Plant," presented at the Annual Meeting of the American Power Conference (1992).

14. Clark, T., “A Handbook of Computational Chemistry”, *John Wiley & Sons*, New York (1985).

15. Duan, X., Page, M., “Theoretical Characterization of Structures and Vibrational Frequencies for Intermediates and Transtion States in the Reaction of NH_2 with NO”, *J. of Mol. Str. (Theochem),* 333, 233 (1995).

16. Dumesic, J.A., Topsøe, N-Y., Topsøe, H., Chen, Y., Slabiak, T., ”Kinetics of Selective Catalytic Reduction of Nitric Oxide by Ammonia over Vanadia/Titania”, *J. Catalysis*, 163, 409 (1996).

17. Eddinger, James A., "Status of EPA Regulatory Development Program for Revised NO_x: New Source Performance Standards for Utility and Non-utility Units- Performance and Costs of Control Options”

18. Farrauto, R. J., Heck, R. M., Speronnelo, B. K., *C & EN*, 34–44 (Sept. 7, 1992).

19. Finley, J. W., Stephens, P.J., “Density functional theory calculations of molecular structures and harmonic vibrational frequencies using hybrid density functionals”, *J. of Mol. Str. (Theochem)*, 357, 225 (1995).

20. Flagan, R.C., Seinfeld, J. H., ”Fundamentals of Air Pollution Engineering”, *Prentice Hall Inc.*, New Jersey (1988).

21. Foster Wheeler Energy Corp., “Logan (Keystone) Instruction Manual for Boiler, Auxiliaries and SCR" (1994).

22. Gilardoni, F., Weber, J., Baiker, A., “Density Functional Investigation of the Mechanism of the Selective Catalytic Reduction of NO by NH_3 over Vanadium Oxide Model Clusters”, *Inter. J. Quan. Chem.*, 61, 683 (1997).

23. Gilardoni, F., Weber, J., Baiker, A., “Mechanism of the Vanadium Oxide-Catalyzed Selective Catalytic Reduction of NO by NH3. A Quantum Chemical Modeling”, *J. Phys. Chem. A*, 101, 6069 (1997).

24. Haber, J., Witko, M., Tokarz, R., ”Vanadium Pentaoxide I. Structures and Properties”, *Applied Catalysis A: General*, 157, 3 (1997).

25. Haber, J., Witko, M., Tokarz, R., ”Vanadium Pentaoxide II.Quantum Chemical Modeling”, *Applied Catalysis A: General*, 157, 23 (1997).

26. Harrison, J. A., Maclagan, R.G.A.R., Whyte, A.R.,”The Structure and Vibrational Frequencies of NH_2NO”, *Chem. Phys. Letters*, 130, 1-2, 98 (1986).

27. Heck, R.M., Farrauto, R.J., “Catalytic Air Pollution Control, Commercial Technology”, *Van Nostrand Reinhold*, New York, (1995).

28. Hehre, W., Radom, L., Schleyer, P. Pople, J., “Ab initio Molecular Orbital Theory“, *John Wiley & Sons*, New York (1986).

29. Hehre, W., Burke, L. D., Shusterman, A. J., “A Spartan Tutorial”, *Wavefunction, Inc.*, Irvine CA (1993).

30. Hehre, W., Yu, J., “A Guide to Molecular Mechanics and Molecular Orbital Calculations in SPARTAN”, *Wavefunction, Inc.*, Irvine CA (1997).

31. Hehre, W., Yu, J., Klunzinger, P. E., “A Guide to Density Fuctional Calculations in SPARTAN”, *Wavefunction, Inc.*, Irvine CA (1997).

32. Hermann, K., Witko, M., Druzinic, “Electronic Properties, Structures and Adsorption at Vanadium Oxide: Density Functional Theory Studies”, *Faraday Discuss.*, 114, 53 (1999).

33. Hermann, K., Witko, M., Druzinic, R., Chakrabarti, A., Tepper, B., Elsner, M., Gorschlüter, A., Kuhlenbeck, H., Freund, H.J., ”Properties and Identification of Oxygen Sites at the V_2O_5 (010) Surface: Theoretical Cluster Studies and Photoemission Experiments”, *J. Elect. Spec. And Relat. Phen.*, 98-99, 245 (1999).

34. Huber, K.P.; Herzberg, G., “Molecular Spectra and Molecular Structure. IV. Constants of Diatomic Molecules”, *Van Nostrand Reinhold Co.*, New York, (1979).

35. Inomata, M., Miyamoto, A., Murakami, Y., “Mechanism of the Reaction of NO and NH_3 on Vanadium Oxide Catalyst in the Presence of Oxygen under the Dilute Gas Condition”, *J. Catalysis*, 62, 140 (1980).

36. Inomata, M., Miyamoto, A., Murakami, Y., ”Determination of the Number of V=O Species on the Surface of Vanadium Oxide Catalysts. 2. V_2O_5/TiO_2 Catalysts”, *J. Phys. Chem.*, 85, 2372 (1981).

37. Janssen, F.J.J.G., van den Kerkhof, F.M.G., Bosch, H., Ross, J.R.H., “Mechanism of the Reaction of Nitric Oxide, Ammonia, and Oxygen Over Vanadia Catalysts. 1. The Role of Oxygen Studied by way of Isotopic Transients Under Dilute Conditions”, *J. Phys. Chem.*, 91, 5921 (1987).

38. Janssen, F.J.J.G., van den Kerkhof, F.M.G. “Mechanism of the Reaciton of Nitric Oxide, Ammonia, and Oxygen Over Vanadia Catalysts. 2. Isotopic Transient Studies with Oxygen-18 and Nitrogen-15”, *J. Phys. Chem.*, 91, 6633 (1987).

39. Jensen, F., “Introduction to Computational Chemistry”, *John Wiley & Sons*, New York (1998).

40. Kohn, W., Sham, L. J., *Phys. Rev.*, 140, A1133 (1965).

41. Lee, C., Yang, W., Parr, R. G. *Phys. Rev., B.*, 37, 785, (1988).

42. Levine, I., “Pysical Chemistry”, 3rd Edition, *McGraw-Hill*, New York (1988).

43. Lietti, L., Ramis, G., Berti, F., Toledo, G., Robba, D., Busca, G., Forzatti, P., “Chemical, Structural and Mechanistic Aspects on NOx SCR over Commercial and Model Oxide Catalysts”, *Catalysis Today*, 42, 101 (1998).

44. Michalak, A., Witko, M., Hermann, K., ”Density Functional Cluster Studies on the (010) Surface of Vanadium Pentoxide”, *Surface Science*, 375, 385 (1997).

45. Ming, W. W., “Vibrational Frequency Prediction Using Density Functional Theory”, *Chemical Physics Letters*, 256, 4-5, 391 (1996).

46. Miyamoto, A., Inomata, M., Yamazaki, Y., Murakami, Y., “Mechanism of the Reaction Between No and NH_3 on V_2O_5 in the Presence of Oxygen”, *J. Catalysis*, 57, 526 (1979).

47. Ozkan, U.S., Cai, Y., Kumthekar, M.W., ”Investigation of the Mechanism of Ammonia Oxidation and Oxygen Exchange Over Vanadia Catalysts Using N-15 and O-18 Tracer Studies”, *J. Catalysis*, 149, 375 (1994).

48. Ozkan, U.S., Cai, Y., Kumthekar, M.W., “Investigation of the Reaction Pathways in Selective Catalytic Reduction of NO with NH_3 over V_2O_5 Catalysts: Isotopc Labelling Studies Using $^{18}O_2$, $^{15}NH_3$, ^{15}NO, and $^{15}N^{18}O^{1}$”, *J. Catalysis*, 149, 390 (1994).

49. Ozturk, S., Onal, I., Senkan, S., “Partial Oxidation of Methane on the SiO_2 Surface – A Quantum Chemical Study”, *Ind. Eng. Chem. Res.,* 29, 250, (2000).

50. Ozturk, S., PhD. Dissertation, METU, Ankara (1998).

51. Perdew, J. P., Wang, Y., *Phys. Rew. B.*, 33, 8800, (1986).

52. Perdew, J. P., *Phys. Rev., B.*, 33, 8822, (1986); 34, 7406, (1986).

53. Perdew, J. P., Wang, Y., *Phys. Rew. B.*, 45, 13244, (1992).

54. Pople, J. A., Gill, P. M. W., Handy, N. C., *Int. J. Quantum Chem.* 56, 303 (1995).

55. Pople J. A., Beveridge, D.L., “Approximate Molecular Orbital Theory”, McGraw-Hill, New-York (1970).

56. Ramis, G., Yi, L., Busca, G., Turco, M., Kotur, E., Willey, R.J., ”Adsorption, Activation and Oxidation of Ammonia over SCR Catalysts”, *J. Catalysis*, 157, 523 (1995).

57. Ramis, G., Yi, L., Busca, G., “Ammonia Activation Over Catalysts for the Selective Catalytic Reduction of NO_x and the Selective Catalytic Oxidation of NH_3. An FT-IR study”, *Catalysis Today*, 28, 373 (1996).

58. Ramirez R., Casal, B., Utrera, L., Ruis-Hitzky, E., “Oxygen Reactivity in Vanadium Pentoxide: Electronic Structure and Infrared Spectroscopy Studies” *J. Phys. Chem.*, 94, 8960 (1990).

59. Rummenhohl, V., STEAG Aktiengesellschaft; and J. Cochran, Black & Veatch. "Relating the German DENOX Experience to U.S. Power Plants: Lessons Learned from more than 30,000 MW of DENOX Retrofits," presented to the ASME JPG Conference, 94-JPGC-PWR-52 (1994).

60. Shareef, G.S., Stone, D.K., Ferry, K.R., Johnson, K.L., Locke, K.S. "Selective Catalytic Reduction NO_x Control for Small Natural Gas-fired Prime Movers," paper 92-136.06, presented at *85th Annual AWMA Meeting & Exhibition,* Kansas City, Mo., June 21–26 (1992).

61. Shimanouchi, T., "Tables of Molecular Vibrational Frequencies Consolidated Volume I"**,** *National Bureau of Standards*, 1-160 (1972).

62. Slater, J.C., *Phys. Rev.* 36, 57 (1930).

63. Slater, J.C., *Phys. Rev.* 81, 385, (1951).

64. Spartan'02 Windows, "Tutorial and User's Guide", *Wavefunction, Inc.*, Irvine CA (2001).

65. Speronello, B.K., Chen, J.M., Heck, R.M., "Family of Versatile Catalyst Technologies for NO_x and CO Removal in Co-generation," paper 92-109.06, presented at *85th Annual AWMA Meeting & Exhibition,* Kansas City, Mo., June 21–26 (1992).

66. Srnak, T.Z., Dumesic, J.A., Clausen, B.S., Törnqvist, E., Topsøe, N-Y.,"Temperature-Programmed Desorption/Reaction and *in Situ* Spectroscopic Studies of Vanadia/Titania for Catalytic Reduction of Nitric Oxide", *J. Catalysis* 135, 246 (1992).

67. Stephens, P. J., Jalkanen, K. J., Amos, R.D., Lazzeretti, P., Zanasi, R., "Ab Initio Calculations of Atomic Polar and Atomic Axial Tensors for HF, H_2O, NH_3, and CH_4.", *J. Phys. Chem.* 94, 1811 (1990).

68. Stewart, J.J.P., "MOPAC: A Semiempirical Molecular Orbital Program", *J. Computer-Aided Molec. Design,* **4**, 1-105 (1990).

69. Takagi, M., Kawai, T., Soma, M., Onishi, T., Tamaru, K., "Mechanism of Catalytic Reduction between NO and NH_3 on V_2O_5 in the Presence of Oxygen", *J. Phys. Chem.*, 80, 4, 430 (1976).

70. Topsøe Nan-Yu, "Characterization of the Nature of Surface Sites on Vanadia-Titania Catalysts by FTIR, *J. Catalysis*, 128, 499 (1991).

71. Topsøe, N-Y., Anstrom, M., Dumesic, J.A., “Raman, FTIR and Theoretical Evidence for Dynamic Structural Rearrangements of Vanadia/Titania DeNOx Catalysts”, *Catalysis Letters*, 76, 1-2, 11 (2001).

72. Topsøe, N-Y., Topsøe, H., Dumesic, J.A.,”Vanadia/Titania Catalysts for Selective Catalytic Reduction (SCR) of Nitric Oxide by Ammonia; I. Combined Temperature Programmed *in situ* FTIR and On-Line Mass Spectroscopy Studies”, *J Catalysis*, 151, 226 (1995).

73. Topsøe, N-Y., Topsøe, H., Dumesic, J.A.,”Vanadia/Titania Catalysts for Selective Catalytic Reduction (SCR) of Nitric Oxide by Ammonia; II.Studies of Active Sites and Formulation of Catalytic Cycles”, *J Catalysis*, 151, 241 (1995).

74. Uzman, N., MSc. Dissertation, METU, Ankara (2000).

75. Wagner, P.A., Kelly, J.G., "Permitting and Startup Experience with the first SCR Installed in the USA on a Pulverized Coal Boiler", U.S. Generating Co., Presented at the Electrical Generation Association Environmental Conference, (1994).

76. Weidinger, G.F., U.S. Generating Co., "Getting to Know low-NO_x Burners and SCR", ICAC Forum '94, (1994).

77. Witko, M., Hermann, K., Tokarz, R., “Adsorption and Reactions at the (010) V_2O_5 surface: Cluster model studies”, *Catalysis Today*, 50, 553 (1999).

78. Wyckoff, R.W.G., “Crystal Structures”, 2nd Edition, Volume 2, *John Wiley & Sons*, New York (1963).

79. Xuefeng, Z., Wheeless, C.J.M., Ruifeng, L., “Density Functional Theory Study of Vibrational Spectra. 1.Performnace of Several Density Functional Methods in Predicting Vibrational Frequencyies”, *Vibrational Spectroscopy*, 12, 1, 53 (1996).

80. Zeldovich, Y.B., Sadovnikov, P.Y., Frank-Kamenetskii, D.A., “Oxidation of Nitrogen in Combustion” *M. Shelf, Trans.,* Acedemy of Sciences of USSR, Institute of Chemical Physics, Moscow-Leningrad (1947).

81. Ziegler, T., “Approximate Density Functional Theory as a Practical Tool in Molecular Energetics and Dynamics”, *Chemical Review*, 91, 5, 651 (1990).

APPENDICES

A. Sample Calculations

In this part, a sample coordinate driving calculation is illustrated. For this purpose the last step of the NH_2NO decomposition reaction was selected.

Performing Coordinate Driving Calculation:

In order to perform coordinate driving calculation, first of all a reaction coordinate must be determined. In the case of the last step of the gas phase decomposition reaction of NH_2NO, reaction coordinate is the distance between oxygen atom and H atom which is bonded to nitrogen atom. After having determining the reaction coordinate, a constraint is applied to the distance between these atoms. In Figure A1 the constraint is represented.

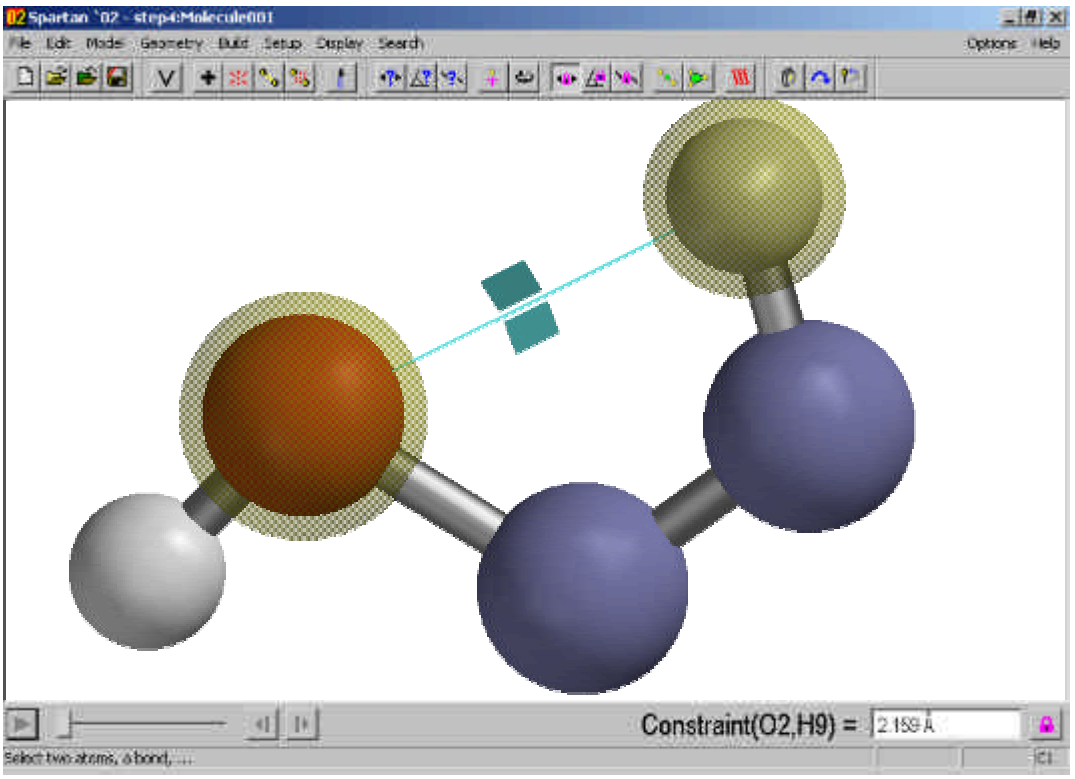

Figure A1. Representation of the constraint applied between O and H atom, which is the reaction coordinate of the last step of NH_2NO decomposition.

Then from the "Properties" menu under the "Display" bar, the initial and final values of the reaction coordinate as well as the number of steps are entered by clicking on the "Dynamic" option. In Figure A2, the property window is illustrated. In this case the reaction coordinate is decreased from 2.16A to 0.9A by 13 steps.

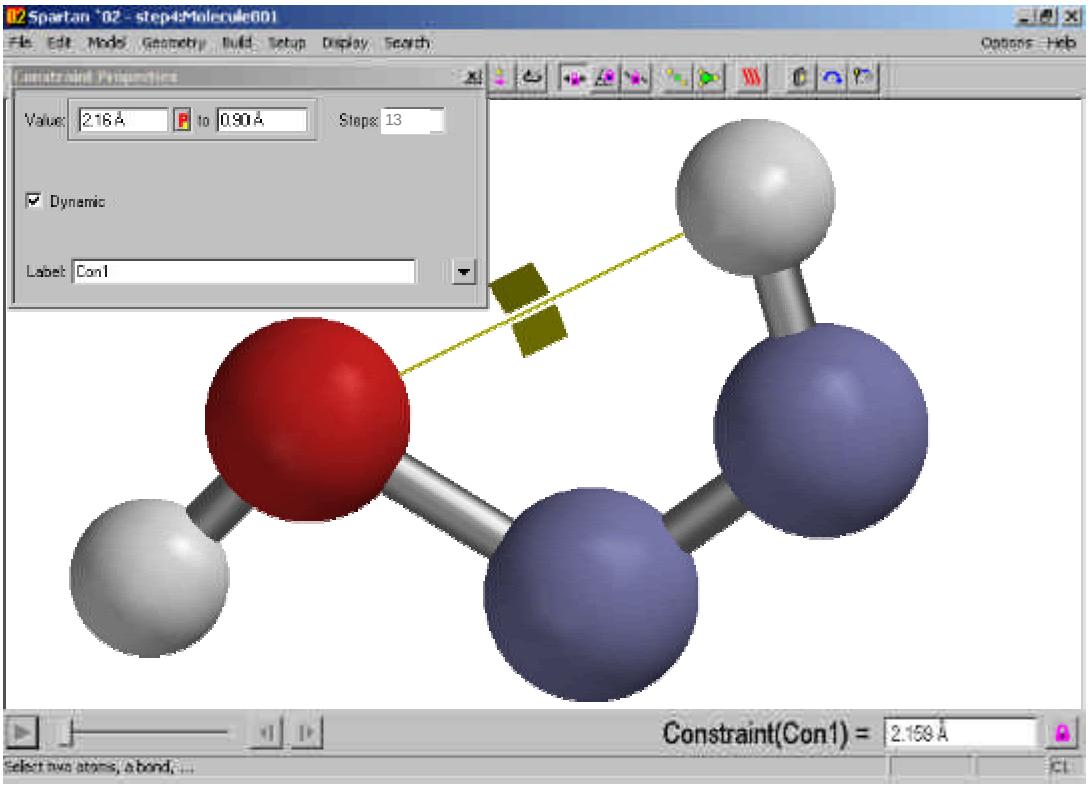

Figure A2. Constraint "Property" window, initial and final values of the constraint and the number of steps are entered.

In order to submit the coordinate driving calculation, "Calculations" menu under the "Setup" bar must be opened. On the "Calculations" menu "Energy Profile" should be selected for the coordinate driving calculations. Also, type of the quantum chemical method and the basis set as well as the charge and spin multiplicity options should be specified according to the reaction. Moreover, in the "Options" bar keywords, that specify the convergence criteria, could be entered. While the default values were used for the single point energy calculations, the following keywords were used for all of the coordinate driving calculations.

Options:

SCF_CONVERGENCE=4

GEOMETRYCYCLE=1000

GRADIENTTOLERANCE=1.E-3

DISTANCETOLERANCE=1.E-2

SCFCYCLE=10000

The “Calculations” menu is illustrated in Figure A3. After having entered all the necessary options, the coordinate driving calculation can be submitted by pressing on the “Submit” button.

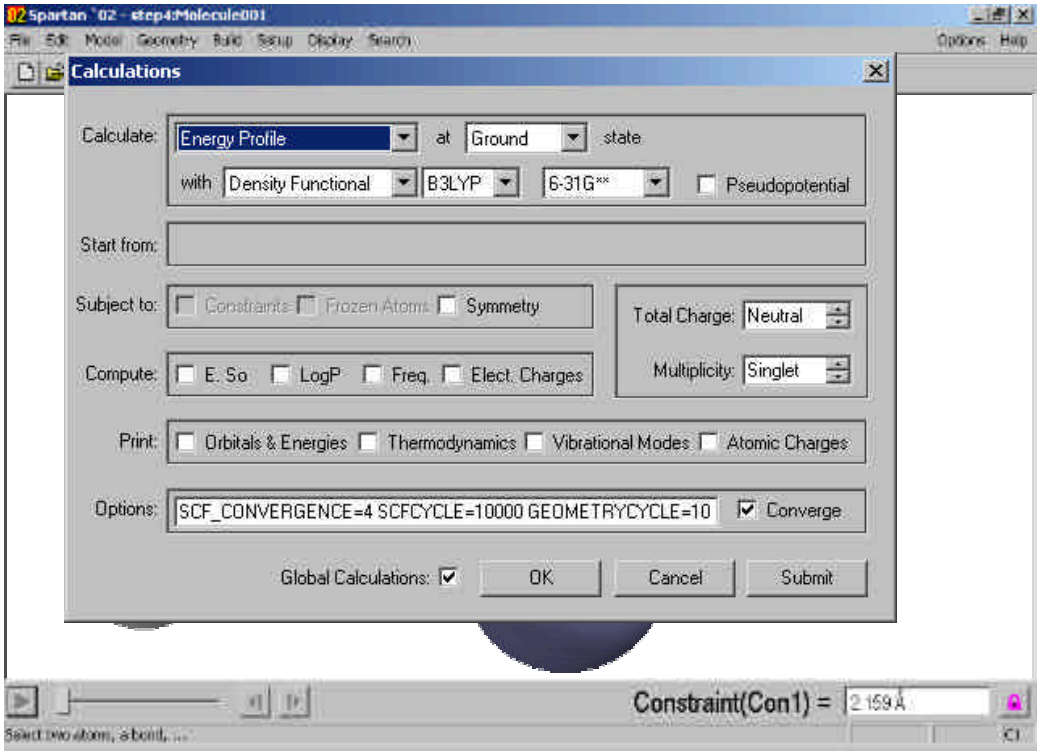

Figure A3. “Calculations” menu.

At the end of the computation, results are written in a separate file, namely “inputfilename.Profile1”. Thus, in order to reach the results of the calculation this file must be opened. When this file is opened, the geometries at each step can be animated continuously by pressing on the play button located

at the left bottom corner of the screen. The energy profile can also be obtained from the “Plot” menu under “Display” bar. However, before doing so, energies of the geometries and the reaction coordinate values at each step must be entered to the “Spreadsheet”, which is located under the “Display” bar. In Figure A4, a spreadsheet on which all the energies and O-H bond distance values at each step of the calculation were entered is represented.

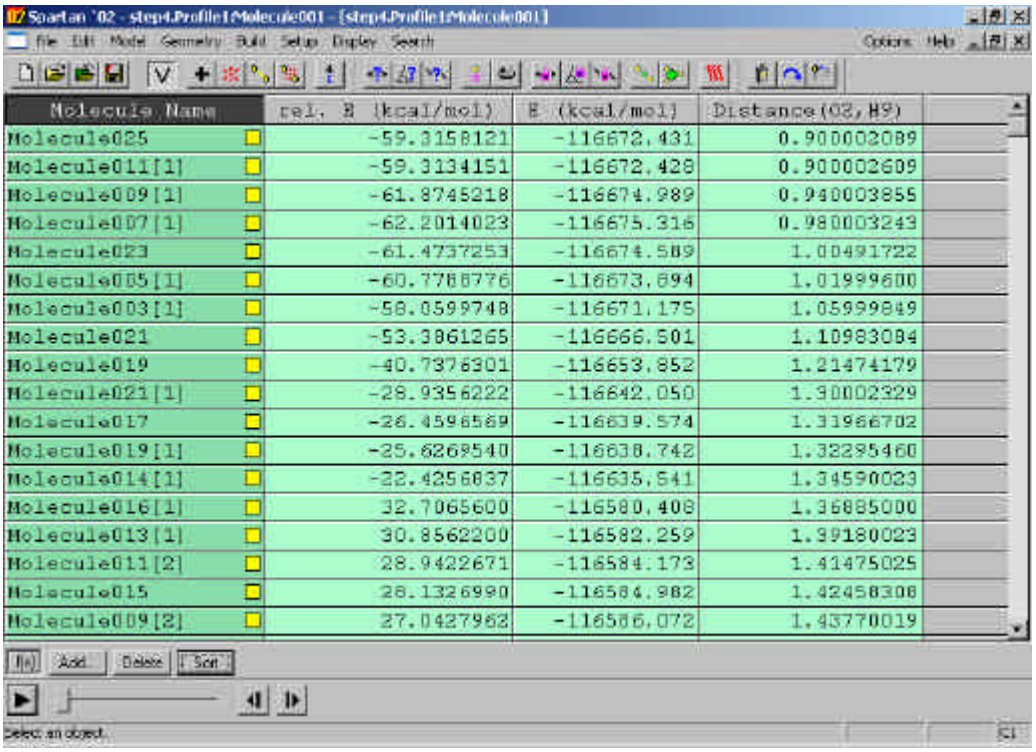

Molecule Name	rel. E (kcal/mol)	E (kcal/mol)	Distance(O2,H9)
Molecule025	-59.3158121	-116672.431	0.900002089
Molecule011[1]	-59.3134151	-116672.428	0.900002609
Molecule009[1]	-61.8745218	-116674.989	0.940003855
Molecule007[1]	-62.2014023	-116675.316	0.980003243
Molecule023	-61.4737253	-116674.589	1.00491722
Molecule005[1]	-60.7788776	-116673.894	1.01999600
Molecule003[1]	-58.0599748	-116671.175	1.05999849
Molecule021	-53.3861265	-116666.501	1.10983084
Molecule019	-40.7376301	-116653.852	1.21474179
Molecule021[1]	-28.9356222	-116642.050	1.30002329
Molecule017	-26.4596569	-116639.574	1.31986702
Molecule019[1]	-25.6269540	-116638.742	1.32295460
Molecule014[1]	-22.4256837	-116635.541	1.34590023
Molecule016[1]	32.7065600	-116580.408	1.36885000
Molecule013[1]	30.8562200	-116582.259	1.39180023
Molecule011[2]	28.9422671	-116584.173	1.41475025
Molecule015	28.1326990	-116584.982	1.42458308
Molecule009[2]	27.0427963	-116586.072	1.43770019

Figure A4. “Spreadsheet” menu and entries on it.

After having entered all the necessary values to the “Spreadsheet”, a plot of energy vs reaction coordinate can be drawn. For this purpose, “Plots” menu under the “Display” bar should be opened and x and y axis of the graph should be specified. For this case, x axis was selected as the reaction coordinate (O-H distance) and y axis was selected as the energy. When “Ok” button is pressed under “Plots” menu, the graph appears on the screen. “Plots” menu and the energy vs. reaction coordinate graph are illustrated in Figure A5 and Figure A6, respectively.

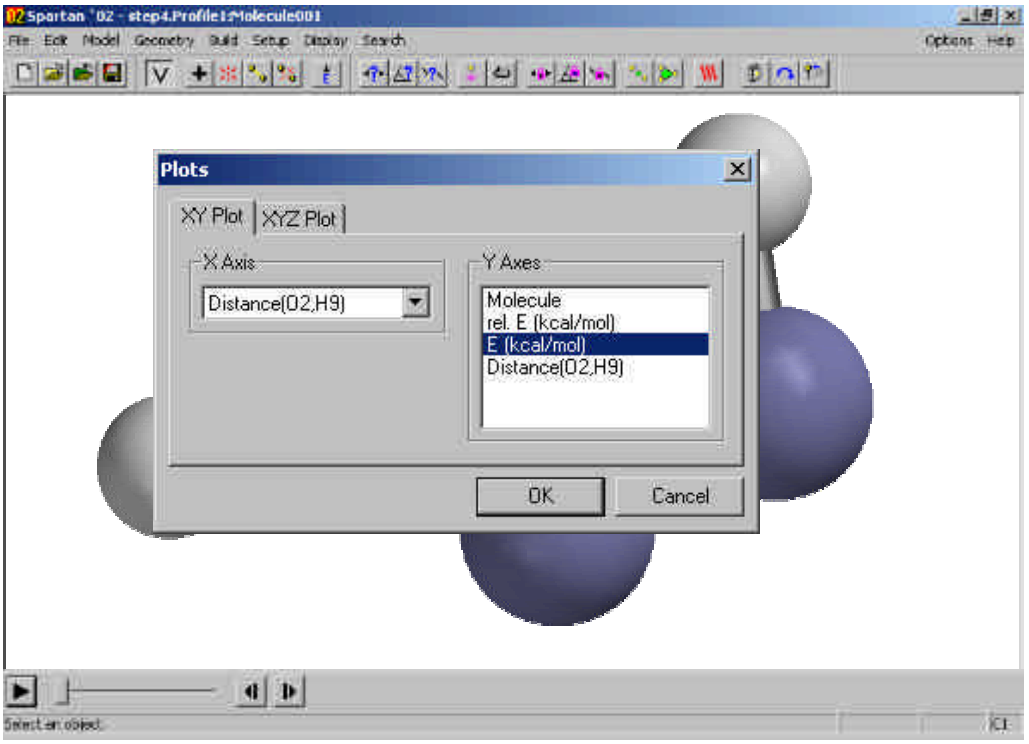

Figure A5. "Plots" Menu.

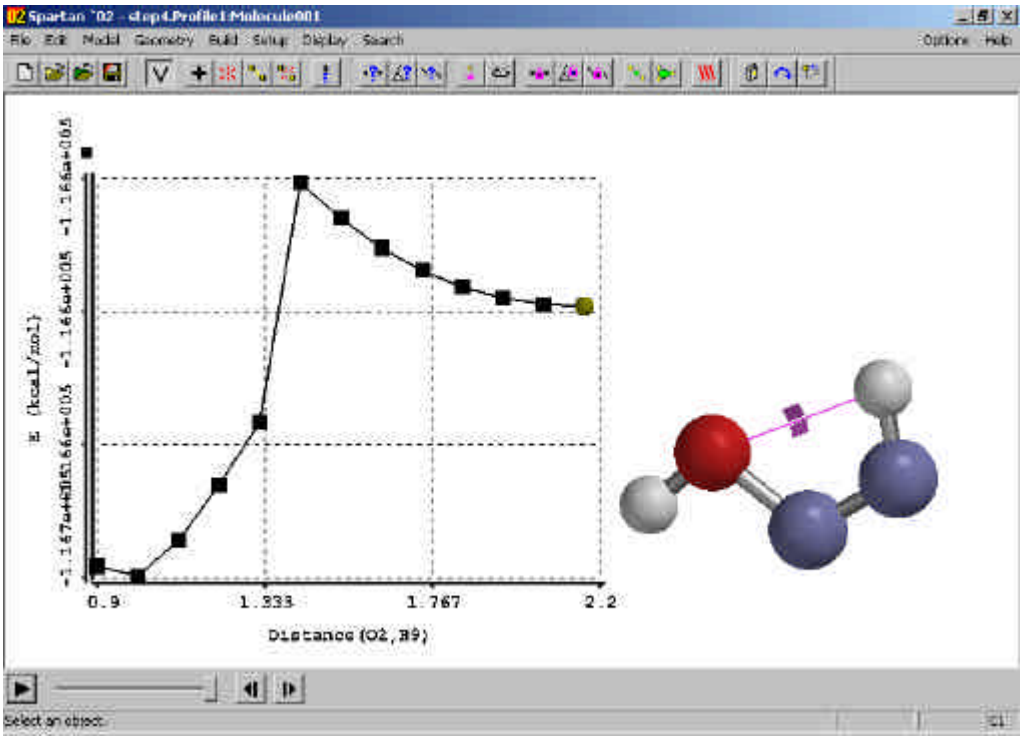

Figure A6. Energy vs. reaction coordinate graph obtained by coordinate driving calculation.

In order to achieve a successful transition state geometry calculation, a good input geometry must be given to the program. The geometry with the maximum energy on the energy profile is the best choice for this. Besides, for equilibrium geometry calculation the geometry with minimum energy on the energy profile would be a good input geometry. For these geometries, transition state geometry and equilibrium geometry calculations could be carried out by selecting proper job types from the "Calculations" menu, which is shown in Figure A2. To calculate the vibration frequencies for these geometries, single point energy calculations should be performed by checking "Freq." box in the "Calculate" menu. At the end of the calculations, vibration frequencies can be seen from the "Vibrations" menu under "Display" bar (for transition state geometries there should be only one imaginary frequency). In Figure A7 "Vibrations" menu can be seen.

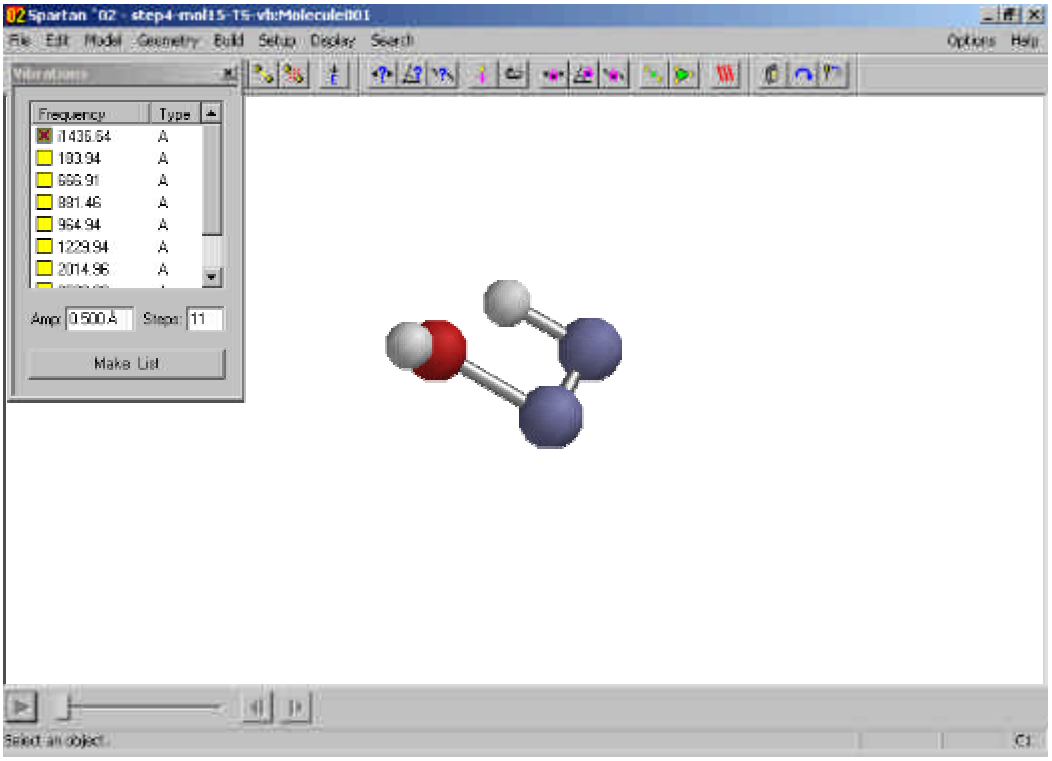

Figure A7. "Vibrations" Menu

B. Sample Input and Output Files

In this part, text versions of the input and output files of SPARTAN'02 are represented.

Table B1. Input file for a sample calculation.

```
C DYNCON OPT B3LYP 6-31G** CONSTRAIN PARTIAL
C CONVERGE NOSYMTRY SCF_CONVERGENCE=4 SCFCYCLE=2000
C GEOMETRYCYCLE=150 GRADIENTTOLERANCE=1.E-3
 DISTANCETOLERANCE=1.E-2
Molecule001
-1 1
 8   3.060421777  -0.781736306   1.135092615
 8   3.060332650   2.782250148   1.128112991
 8  -1.106937605  -0.781921862   1.093558871
23  -0.731469871   0.999180263   0.630252322
23   2.694104150   0.999332789   0.664393106
 8  -0.541520365   0.995586668  -0.952523955
 8  -2.699052537   1.000045011   1.096942427
 8   4.651994336   1.000372324   1.170206206
 8  -1.107026732   2.782064593   1.086579248
 8   0.976449109   1.000212949   1.135760699
 1  -1.489749453   2.698284324   1.962993791
 1  -2.751888859   1.002509711   2.055483251
 1  -1.489612166  -0.693862511   1.969574851
 1   3.431234473  -0.665508731   2.012923670
 1   4.672437087   1.002401936   2.129985471
 1   3.431166030   2.669708472   2.006415468
 8   2.451477607   0.995841150  -1.050267077
 1   1.487640368   0.995239073  -1.275483954
 1   0.747511773   0.971528336  -5.005577438
 7   0.370979721   0.990155094  -4.059912648
 1  -0.230003275   1.810814407  -4.018163807
 1  -0.252376278   0.187887974  -3.995105208
ENDCART
ATOMLABELS
"O8"
"O18"
"O37"
"V15"
"V16"
"O41"
"O45"
"O46"
"O47"
"O49″
"H7"
"H12"
"H21"
"H25"
"H44"
"H48"
"O1"
```

Table B1. *(cont.)*

```
"H2"
"H0"
"N1"
"H1"
"H3"
ENDATOMLABELS
FROZEN
    1    2    3    4    5    7    8    9   10   11   12   13
   14   15   16
ENDFROZEN
HESSIAN
    0    0    0    0    0    9    0    0    0    0   13   13
   13   13   13   13    8   13   13    5   13   13
    3    4    1
    7    4    1
    9    4    1
    4   10    1
   10    5    1
    1    5    1
    5    2    1
    5    8    1
    4    6    2
    9   11    1
    7   12    1
    3   13    1
    1   14    1
    8   15    1
    2   16    1
   17   18    1
    5   17    1
   19   20    1
   20   21    1
   20   22    1
ENDHESS
CONSTRAINT
    4   10    5   20   0.000000     0.00
ENDCON
DYNCON
   18   20    0    0   3.000000     0.00   0.900000   31
ENDDYNCON
BEGINPROPIN
ENDPROPIN
```

There are two different output files of SPARTAN'02, one is "normal" and the other is "verbose". Samples for these files are given in Table B2 and Table B3 respectively. Since, verbose files contain too many pages (about thousands of pages), only a part of them is illustrated here.

Table B2. Normal Output file for a sample calculation.

```
Spartan '02 Mechanics Program:  (PC/x86)           Release  115B


  Reason for exit: Successful completion
  Mechanics CPU Time : 000:00:00.2
  Mechanics Wall Time: 000:00:00.2
Spartan '02 Quantum Mechanics Program:  (PC/x86)   Release  115B

Job type: Geometry optimization.
Method: UB3LYP
Basis set: 6-31G**
Number of shells: 92
Number of basis functions: 288

SCF model:
 An unrestricted hybrid HF-DFT SCF calculation will be
 performed using Pulay DIIS extrapolation


Optimization:
         Step      Energy          Max Grad.      Max Dist.
            1   -2755.8463949       0.015364       0.210134   9
            2   -2755.8447286       0.018216       0.197959   8
            3   -2755.8430634       0.014538       0.104240   7
            4   -2755.8411629       0.023807       0.134407   6
            5   -2755.8397675       0.026459       0.153528   5
            6   -2755.8389447       0.027121       0.151838   4
            7   -2755.8386918       0.031299       0.074552   3
            8   -2755.8381156       0.031511       0.146396   2
            9   -2755.8440295       0.016909       0.136027   2
           10   -2755.8457856       0.016578       0.170500   1
           11   -2755.8473368       0.019603       0.077008   1
           12   -2755.8489114       0.015528       0.150501
           13   -2755.8498465       0.014155       0.133805
           14   -2755.8519132       0.011429       0.146333
           15   -2755.8533607       0.008442       0.146367
           16   -2755.8549094       0.009163       0.137168
           17   -2755.8555898       0.005379       0.145312
           18   -2755.8558767       0.007962       0.067406
           19   -2755.8559881       0.004477       0.037841
           20   -2755.8560916       0.003685       0.044725
           21   -2755.8561786       0.003726       0.099712
           22   -2755.8562935       0.005589       0.059155
           23   -2755.8563421       0.007222       0.060353
```

Table B2. *(cont.)*

```
          24   -2755.8564602       0.003328       0.083070
          25   -2755.8565812       0.003297       0.050127
          26   -2755.8567009       0.003516       0.070409
          27   -2755.8568940       0.003047       0.126727
          28   -2755.8570712       0.003503       0.038392
          29   -2755.8572578       0.002607       0.126562
          30   -2755.8574571       0.008942       0.043755
          31   -2755.8576251       0.007336       0.071777
          32   -2755.8577117       0.002316       0.051054
          33   -2755.8578114       0.001886       0.051989
          34   -2755.8578639       0.003457       0.013053
          35   -2755.8578350       0.001649       0.053876
          36   -2755.8578517       0.002237       0.019639
          37   -2755.8579468       0.001538       0.028846
          38   -2755.8579575       0.001388       0.031003
          39   -2755.8579729       0.001682       0.061921
          40   -2755.8580228       0.002414       0.036300
          41   -2755.8580534       0.001695       0.073246
          42   -2755.8580522       0.001345       0.045657
          43   -2755.8580712       0.001251       0.016370
          44   -2755.8580911       0.001228       0.030924
          45   -2755.8581209       0.002641       0.011061
          46   -2755.8581050       0.001093       0.021305
          47   -2755.8581332       0.001128       0.063024
          48   -2755.8581646       0.001907       0.022981
          49   -2755.8581295       0.000764       0.022370
          50   -2755.8581675       0.000867       0.014607
          51   -2755.8581456       0.000825       0.018714
          52   -2755.8581692       0.000760       0.011850
          53   -2755.8581854       0.000625       0.163366
          54   -2755.8581280       0.005857       0.067169
          55   -2755.8581009       0.007283       0.090314
          56   -2755.8581814       0.002309       0.104023
          57   -2755.8582284       0.001629       0.072681
          58   -2755.8581839       0.003993       0.053976
          59   -2755.8582176       0.002236       0.012295
          60   -2755.8582427       0.000979       0.013394
          61   -2755.8582467       0.000651       0.013355
          62   -2755.8582273       0.000656       0.011592
          63   -2755.8582168       0.000725       0.010463
          64   -2755.8582606       0.000592       0.026195
          65   -2755.8582205       0.001009       0.006517
          66   -2755.8582880       0.000759       0.027937
          67   -2755.8582237       0.000622       0.022770
          68   -2755.8582820       0.001059       0.013652
          69   -2755.8582617       0.000882       0.013588
          70   -2755.8582467       0.000955       0.005562
  Reason for exit: Successful completion
  Quantum Mechanics Program CPU Time : 023:29:28.4
  Quantum Mechanics Program Wall Time: 007:55:31.5

  Spartan '02 Properties Program:  (PC/x86)           Release  115B
  Reason for exit: Successful completion
  Properties Program CPU Time : 000:00:02.6
  Properties Program Wall Time: 000:00:02.7
```

Table B 3. Verbose Output file for a sample calculation.

```
                Spartan '02
              build 115B (Dec 19 2001)

 Wavefunction Developers:
    B.J. Deppmeier, A.J. Driessen, T.S. Hehre, W.J. Hehre,
    J.A. Johnson, P.E. Klunzinger, J.M. Leonard, I.N. Pham
    W.J. Pietro, Jianguo Yu

 Q-Chem Developers:
   J. Kong, C.A. White, A.I. Krylov, C.D. Sherrill,
   R.D. Adamson, T.R. Furlani, M.S. Lee, A.M. Lee,
   S.R. Gwaltney, T.R. Adams, C. Ochsenfeld, A.T.B. Gilbert,
   G.S. Kedziora,  V.A. Rassolov, D. R. Maurice, N. Nair,
   Y. Shao, N.A. Besley, P.E. Maslen, J.P. Dombroski,
   H. Dachsel, W.M. Zhang, P.P. Korambath, J. Baker,
   E.F. C. Byrd, T. Van Voorhis, M. Oumi, S. Hirata,
   C.P. Hsu, N. Ishikawa, J. Florian, A. Warshel,
   B.G. Johnson, P.M.W. Gill, M. Head-Gordon, J.A. Pople

 Wavefunction Inc.           Sales:   sales@wavefun.com
 Irvine CA                   Support: support@wavefun.com
                             Web:     www.wavefun.com


Copyright © 1995 - 2001
-----------------------------------------------------


 Windows PC (Intel x86)
              Spartan 'O2 Quantum Mechanics Module

====================================================================
==
User input:
====================================================================
==
$comment
Molecule001
$end
$molecule
 -1 2
    8     -1.421035117      1.579984835      2.677693781
    8     -1.476318019      1.522526952     -0.885372242
    8      1.666439062     -1.219258262      2.674930466
   23      1.675276727     -0.655533204      0.883277527
   23     -0.862630441      1.645447673      0.885548987
    8      2.841547904      0.579529458      0.824499221
    8      2.802878457     -2.334081472       0.89285036
    8     -2.643296348      2.603665697      0.897724843
    8       1.61115595     -1.276716115     -0.888135557
    8       0.07832284      0.133172636      0.895336437
    1      1.298605866     -2.178319838     -0.783239505
    1      2.190954561      -3.07346994      0.913679217
```

Table B3. *(cont.)*

```
    1      1.351226912     -2.123550977      2.608029787
    1     -2.291092668      1.185500041      2.583028109
    1     -3.309847896      1.913133904      0.919052551
    1     -2.342853896      1.131723252      -0.75132707
    8      0.215341799      2.820966886      0.844429326
    1      1.852380229       3.34179299       0.87666785
    1      3.288439911      3.323750121     -0.006276805
    7      2.863989232      3.584270556      0.882468521
    1      3.127288847      1.262763349      1.524416645
    1      3.006555396      4.575297709      1.061395986
    7      3.656202658      2.669922011      2.203250118
    8      4.820468034      2.987481737      2.266071445
$end
$rem
JOBTYPE    OPT
TIDY_SYM   TRUE
EXCHANGE          B3LYP
CORRELATION       none  (built-in)
FAST_XC           TRUE
VARTHRESH         2
BASIS             6-31G**
VARTHRESH         0
FAST_XC           FALSE
SMALL_PROD_XCMAT  10
SYMMETRY          FALSE
SCF_CONVERGENCE   4
MAX_SCF_CYCLES    10000
GEOM_OPT_MAX_CYCLES     1000
GEOM_OPT_TOL_GRADIENT    1000
GEOM_OPT_TOL_DISPLACEMENT     10000
UNRESTRICTED      TRUE (setting default UHF)
SYMMETRY          FALSE
USE_SP_DERIV      2GEOM_OPT_HESSIAN      READ
EXTERNAL_HESSIAN      TRUE
GUI                GUI_SPARTAN
TERSE_OUTPUT       TRUE
$end
$opt
CONSTRAINT
tors   4  10   5  20 0.000000
ENDCONSTRAINT
FIXED
1   XYZ
2   XYZ
3   XYZ
4   XYZ
5   XYZ
7   XYZ
8   XYZ
9   XYZ
10   XYZ
11   XYZ
12   XYZ
13   XYZ
14   XYZ
```

Table B3. *(cont.)*

```
15   XYZ
16   XYZ
ENDFIXED
$end
=================================================================
==
Processing $rem in C:\PROGRAM
FILES\WAVEFUNCTION\SPARTAN02V101\auxdir\preferences.
   (Site specific preferences.)
  ... THRESH             9
  ... SCF_CONVERGENCE    7
  ... SMALL_PROD_XCMAT   9
  ... GUI              GUI_SPARTAN
  ... TERSE_OUTPUT     TRUE
Processing $rem in system registry
  ... MEMORY       131072000  #  1000 MB
  ... CD_MAX_DISK  685768704  #  38000 MB
Processing $rem in the input.
  ... JOBTYPE    OPT
  ... TIDY_SYM   TRUE
  ... EXCHANGE          B3LYP
  ... CORRELATION       none  (built-in)
  ... FAST_XC           TRUE
  ... VARTHRESH         2
  ... BASIS             6-31G**
  ... VARTHRESH         0
  ... FAST_XC           FALSE
  ... SMALL_PROD_XCMAT  10
  ... SYMMETRY          FALSE
  ... SCF_CONVERGENCE   4
  ... MAX_SCF_CYCLES    10000
  ... GEOM_OPT_MAX_CYCLES     1000
  ... GEOM_OPT_TOL_GRADIENT    1000
  ... GEOM_OPT_TOL_DISPLACEMENT     10000
  ... UNRESTRICTED      TRUE (setting default UHF)
  ... SYMMETRY          FALSE
  ... USE_SP_DERIV      2
  ... GEOM_OPT_HESSIAN      READ
  ... EXTERNAL_HESSIAN      TRUE
  ... GUI                GUI_SPARTAN
  ... TERSE_OUTPUT       TRUE

#####################################################
#  Entering fldman.exe on Wed Jul 16 10:14:03 2003  #
#####################################################

 ----------------------------------------------------
       Standard Nuclear Orientation (Angstroms)
    I     Atom         X            Y            Z
 ----------------------------------------------------

    1      O      -2.292919     0.543192     1.860084
    2      O      -2.657549     0.294587    -1.676445
    3      O       0.933547    -2.090516     1.712563
    4      V       0.753614    -1.622639    -0.097575
```

Table B3. *(cont.)*

```
    5      V      -1.898545     0.542271     0.023688
    6      O       1.839583    -0.334321    -0.321028
    7      O       1.969472    -3.238391    -0.109353
    8      O      -3.721880     1.407359     0.150868
    9      O       0.568918    -2.339121    -1.823966
   10      O      -0.877570    -0.917203     0.021017
   11      H       0.317510    -3.248732    -1.647953
   12      H       1.403893    -4.006003     0.002327
   13      H       0.664558    -3.012033     1.718054
   14      H      -3.144591     0.100221     1.863648
   15      H      -4.344468     0.685700     0.265638
   16      H      -3.485841    -0.132434    -1.445871
   17      O      -0.895528     1.767620    -0.171343
   18      H       0.706444     2.372559    -0.312505
   19      H       2.058198     2.381390    -1.319912
   20      N       1.699567     2.666482    -0.409965
   21      H       2.147159     0.398712     0.316466
   22      H       1.801850     3.671584    -0.292565
   23      N       2.654402     1.865041     0.876147
   24      O       3.800176     2.244676     0.817979
 ----------------------------------------------------
 Molecular Point Group                C1    NOp =  1
 Largest Abelian Subgroup             C1    NOp =  1
 Nuclear Repulsion Energy =  1706.8310793978 hartrees
 There are       76 alpha and       75 beta electrons
 Requested basis set is 6-31G(d,p)
 There are 92 shells and 288 basis functions

#####################################################
#  Entering gesman.exe on Wed Jul 16 10:14:04 2003  #
#####################################################

 Smallest overlap matrix eigenvalue = 3.62E-003
 Multipole matrices computed through 2nd order

#####################################################
#  Entering scfman.exe on Wed Jul 16 10:14:05 2003  #
#####################################################

 Exchange:     0.2000 Hartree-Fock + 0.0800 Slater + 0.7200 Becke
 Correlation:  0.8100 LYP + 0.1900 VWN1RPA
 An unrestricted hybrid HF-DFT SCF calculation will be
 performed using Pulay DIIS extrapolation
 Exchange:     0.2000 Hartree-Fock + 0.0800 Slater + 0.7200 Becke
 Correlation:  0.8100 LYP + 0.1900 VWN1RPA
 SCF converges when DIIS error is below 1.0E-004
 Creating differential electron density of 4.38 Mb
 Warning!  Inaccurate integrated density:
   Number of electrons =   151
   Numerical integral  =   150.0011
   Relative error      =    -0.66 %
 ---------------------------------------
  Cycle       Energy         DIIS Error
 ---------------------------------------
    1   -2756.1155273542     4.62E-002
```

Table B3. *(cont.)*

```
    2   -2753.6880079440     1.54E-002
 Using incremental e-density
    3   -2707.6985501896     6.77E-002
    4   -2750.8426508361     2.58E-002
    5   -2730.8857251206     4.26E-002
    6   -2754.9755239602     1.10E-002
    7   -2752.3956298567     2.08E-002
    8   -2755.5525828101     6.51E-003
    9   -2755.7270739298     3.74E-003
   10   -2755.8257522373     1.68E-003
   11   -2755.8324071542     1.30E-003
   12   -2755.8459262115     2.25E-004
   13   -2755.8462117355     1.53E-004
   14   -2755.8463948859     5.69E-005  Convergence criterion met
 ---------------------------------------
 <S^2> = 0.7533
 SCF time:  CPU 608.78 s  wall 611922.00 s


#######################################################
#  Entering anlman.exe on Wed Jul 16 10:24:18 2003  #
#######################################################

 Analysis of SCF Wavefunction


#######################################################
#  Entering drvman.exe on Wed Jul 16 10:24:18 2003  #
#######################################################

 Calculating analytic gradient of the SCF energy

Spartan '02 Fast HF Program:  (PC/x86)             Release  115B
  Job run on machine :                DFT
  Calculation started: Wed Jul 16 10:24:20 2003

  JOBNAME.TEMP

  Run type: Molecular gradient (no SCF)
  Model: UHF/ABASIS
  Number of shells:  92
    34 S shells
    10 P shells
    32 SP shells
    16 6D shells
  Number of basis functions: 288
  Number of electrons:       151
  Number of heavy atoms:      14
  Number of hydrogens:        10
  Use of molecular symmetry disabled
  Molecular charge:  -1
  Spin multiplicity:  2
  Memory model: direct   32.2 Mb

  Point Group = C1  Order =  1 Nsymop =  1
```

Table B3. *(cont.)*

```
  This system has   0 degrees of freedom

                  Cartesian gradient (a.u.)
    Atom          X            Y            Z
    ----   ------------ ------------ ------------

    O   1   -0.2299215   -0.1129346   -0.0625239
    O   2   -0.2107916   -0.0998698    0.1231819
    O   3   -0.0726983   -0.2495894   -0.0582982
    V   4    0.0159098    0.0498212   -0.0093275
    V   5    0.0900397    0.0481598   -0.0131342
    O   6   -0.0041233    0.0810984    0.1520447
    O   7   -0.1761835   -0.1669194    0.0295512
    O   8   -0.1197815   -0.2086721    0.0270189
    O   9   -0.0555946   -0.2371055    0.1065106
    O  10    0.0266570    0.0521279   -0.0069310
    H  11    0.0716028    0.2585499   -0.0352694
    H  12    0.1409429    0.2152007   -0.0292505
    H  13    0.0737418    0.2601963   -0.0164115
    H  14    0.2360425    0.1216439   -0.0147198
    H  15    0.1757171    0.1820823   -0.0308658
    H  16    0.2322791    0.1191533   -0.0503793
    O  17   -0.0994877   -0.1276999    0.0203919
    H  18    0.1824249    0.0545435   -0.0201516
    H  19   -0.0849982    0.0705058    0.2097932
    N  20   -0.0918654    0.1082564   -0.1616520
    H  21   -0.0674645   -0.1600417   -0.1254810
    H  22   -0.0251018   -0.2339094   -0.0314802
    N  23    0.3979032    0.1106471   -0.0291304
    O  24   -0.4052490   -0.1352446    0.0265138

  E(HF)  =   -2755.8463949 a.u.
  Reason for exit: Successful completion
  Fast HF Program CPU Time : 000:02:45.5
  Fast HF Program Wall Time: 000:02:45.8
  Gradient of SCF Energy
             1            2            3            4            5
6
    1  -0.0256231  -0.0263851   0.0227250  -0.0215973   0.0372174  -
0.0002257
    2   0.0162344   0.0155557  -0.0243036   0.0096628  -0.0578335  -
0.0002793
    3   0.0073750  -0.0038784   0.0159995   0.0028582   0.0003070  -
0.0000377
             7            8            9           10           11
12
     1   0.0065657  -0.0004740   0.0190094  -0.0283085  -0.0055266
0.0007141
     2  -0.0037859  -0.0013236  -0.0257138   0.0423332   0.0101613
0.0121996
    3  -0.0004191   0.0001498  -0.0166283  -0.0009431   0.0071499  -
0.0010705
            13           14           15           16           17
18
```

Table B3. *(cont.)*

```
    1  -0.0076076   0.0090412   0.0102406   0.0103749   0.0002750  -
0.0002294
     2   0.0093596  -0.0038154    0.0042823  -0.0028819   0.0001824
0.0000126
    3  -0.0072066  -0.0073788  -0.0013668   0.0058129  -0.0002686  -
0.0000441
            19           20           21           22           23
24
    1   0.0000629   0.0111395  -0.0000036  -0.0000877  -0.0105079  -
0.0004798
    2  -0.0001000  -0.0090799   0.0000221   0.0002973   0.0093988  -
0.0002191
    3  -0.0004129   0.0148345  -0.0000641   0.0001450  -0.0149307  -
0.0000793

 Max gradient component =      5.783E-002
 RMS gradient           =      1.412E-002
 Gradient time:  CPU 211.28 s  wall 211625.00 s

#######################################################
#  Entering optman.exe on Wed Jul 16 10:27:49 2003  #
#######################################################

**WARNING** Cannot use Internal Coordinates with Fixed Atoms
  Cartesian Optimization Enforced

 Cartesian Hessian read from HESS file


** CONSTRAINED OPTIMIZATION IN CARTESIAN COORDINATES **
   Searching for a Minimum

Optimization Cycle:   1

                        Coordinates (Angstroms)
     ATOM               X           Y           Z
    1  O          -2.292918    0.543192    1.860084
    2  O          -2.657548    0.294587   -1.676444
    3  O           0.933547   -2.090515    1.712562
    4  V           0.753613   -1.622639   -0.097575
    5  V          -1.898544    0.542271    0.023688
    6  O           1.839582   -0.334321   -0.321028
    7  O           1.969471   -3.238389   -0.109353
    8  O          -3.721878    1.407358    0.150868
    9  O           0.568917   -2.339119   -1.823965
   10  O          -0.877570   -0.917203    0.021017
   11  H           0.317510   -3.248731   -1.647953
   12  H           1.403893   -4.006001    0.002327
   13  H           0.664557   -3.012032    1.718053
   14  H          -3.144589    0.100221    1.863647
   15  H          -4.344466    0.685700    0.265638
   16  H          -3.485840   -0.132434   -1.445870
   17  O          -0.895528    1.767619   -0.171343
   18  H           0.706444    2.372557   -0.312505
   19  H           2.058197    2.381389   -1.319911
```

Table B3. *(cont.)*

```
   20  N           1.699566    2.666480   -0.409964
   21  H           2.147158    0.398712    0.316466
   22  H           1.801850    3.671582   -0.292565
   23  N           2.654401    1.865041    0.876147
   24  O           3.800174    2.244674    0.817978
   Point Group: c1    Number of degrees of freedom:  66


   Energy is  -2755.846394886

            Atoms with "Fixed" Coordinates
                Atom    Coordinates
                  1        X  Y  Z
                  2        X  Y  Z
                  3        X  Y  Z
                  4        X  Y  Z
                  5        X  Y  Z
                  7        X  Y  Z
                  8        X  Y  Z
                  9        X  Y  Z
                 10        X  Y  Z
                 11        X  Y  Z
                 12        X  Y  Z
                 13        X  Y  Z
                 14        X  Y  Z
                 15        X  Y  Z
                 16        X  Y  Z

              Constraints and their Current Values
                                          Value     Constraint
   Dihedral:        4  10   5  20        -1.176        0.000
  cartesian optimization with constraints (P)

   Using Penalty Function Algorithm


 27 Hessian modes will be used to form the next step
  Hessian Eigenvalues:
    -0.158472    -0.099426    -0.081222    -0.050829    -0.038033    -
0.025338
    -0.017211     -0.013981     -0.005138      0.002757      0.016782
0.036378
       0.060416     0.104690     0.247466     0.383610     0.435650
0.526515
       0.563883     0.753370     0.954861     1.534612     2.788339
3.162199
     3.507595    5.069598   17.080207
**WARNING** Hessian does not have the Desired Local Structure

 Minimum Search - Taking Simple RFO Step
 Searching for Lamda that Minimizes Along All modes
 Value Taken    Lamda =  -0.15847943
 Calculated Step too Large.  Step scaled by  0.002075
 Step Taken.  Stepsize is  0.300000
```

Table B3. *(cont.)*

```
                              Maximum     Tolerance    Cnvgd?
         Gradient            0.015364      0.001000      NO
         Displacement        0.210134      0.010000      NO
         Energy change      *********      0.000001      NO

 ----------------------------------------------------
       Standard Nuclear Orientation (Angstroms)
    I     Atom         X            Y            Z
 ----------------------------------------------------
    1      O      -2.295072     0.544037     1.859255
    2      O      -2.659702     0.295432    -1.677274
    3      O       0.931394    -2.089671     1.711734
    4      V       0.751460    -1.621794    -0.098404
    5      V      -1.900699     0.543116     0.022859
    6      O       1.950781    -0.419770    -0.274147
    7      O       1.967318    -3.237546    -0.110182
    8      O      -3.724033     1.408204     0.150039
    9      O       0.566764    -2.338276    -1.824795
   10      O      -0.879723    -0.916358     0.020188
   11      H       0.315357    -3.247887    -1.648783
   12      H       1.401740    -4.005158     0.001498
   13      H       0.662404    -3.011188     1.717225
   14      H      -3.146744     0.101066     1.862819
   15      H      -4.346622     0.686545     0.264809
   16      H      -3.487995    -0.131589    -1.446700
   17      O      -0.903811     1.770123    -0.169102
   18      H       0.698008     2.371942    -0.309616
   19      H       2.054462     2.389719    -1.319213
   20      N       1.676728     2.687319    -0.418785
   21      H       2.120118     0.419318     0.306880
   22      H       1.803607     3.683332    -0.295990
   23      N       2.647696     1.873470     0.859022
   24      O       3.796563     2.245612     0.816662
 ----------------------------------------------------
 Molecular Point Group                 C1    NOp =  1
 Largest Abelian Subgroup              C1    NOp =  1
 Nuclear Repulsion Energy =  1704.4659605499 hartrees
 There are       76 alpha and       75 beta electrons

#####################################################
#  Entering fldman.exe on Wed Jul 16 10:27:50 2003  #
#####################################################

 Requested basis set is 6-31G(d,p)
 There are 92 shells and 288 basis functions
 Applying Cartesian multipole field
    Component          Value
    ---------          -----
     (1,0,0)       1.00000E-010
     (0,1,0)       2.00000E-010
     (0,0,1)       -3.00000E-010

#####################################################
#  Entering gesman.exe on Wed Jul 16 10:27:50 2003  #
#####################################################
```

Table B3. *(cont.)*

```
 Smallest overlap matrix eigenvalue = 3.63E-003
 Multipole matrices computed through 2nd order

#######################################################
#  Entering scfman.exe on Wed Jul 16 10:27:51 2003  #
#######################################################
                                   .
                                   .
                                   .
                                   .
                                   .
                                   .
                                   .
An unrestricted hybrid HF-DFT SCF calculation will be
 performed using Pulay DIIS extrapolation
 Exchange:     0.2000 Hartree-Fock + 0.0800 Slater + 0.7200 Becke
 Correlation:  0.8100 LYP + 0.1900 VWN1RPA
 SCF converges when DIIS error is below 1.0E-004
 Creating differential electron density of 4.38 Mb
 ---------------------------------------
  Cycle       Energy         DIIS Error
 ---------------------------------------
    1   -2755.8585017646     8.21E-005
    2   -2755.8577585381     2.67E-004
 Using incremental e-density
    3   -2755.8582467069     8.04E-005  Convergence criterion met
 ---------------------------------------
 <S^2> = 0.7529
 SCF time:  CPU 134.16 s  wall 134922.00 s


#######################################################
#  Entering anlman.exe on Wed Jul 16 18:04:34 2003  #
#######################################################

 Analysis of SCF Wavefunction


#######################################################
#  Entering drvman.exe on Wed Jul 16 18:04:34 2003  #
#######################################################

 Calculating analytic gradient of the SCF energy

Spartan      '02      Fast      HF      Program:            (PC/x86)
Release  115B
  Job run on machine :                DFT
  Calculation started: Wed Jul 16 18:05:23 2003

  JOBNAME.TEMP

  Run type: Molecular gradient (no SCF)
  Model: UHF/ABASIS
  Number of shells:  92
    34 S shells
```

Table B3. *(cont.)*

```
    10 P shells
    32 SP shells
    16 6D shells
  Number of basis functions: 288
  Number of electrons:       151
  Number of heavy atoms:      14
  Number of hydrogens:        10
  Use of molecular symmetry disabled
  Molecular charge:  -1
  Spin multiplicity:  2
  Memory model: direct   32.2 Mb

  Point Group = C1  Order =  1 Nsymop =  1
  This system has   0 degrees of freedom
                 Cartesian gradient (a.u.)
    Atom         X            Y            Z
    ----   ------------ ------------ ------------

    O   1   -0.2299266   -0.1124421   -0.0628369
    O   2   -0.2108021   -0.0994865    0.1233381
    O   3   -0.0729532   -0.2504798   -0.0578550
    V   4    0.0166803    0.0444859   -0.0044689
    V   5    0.1009043    0.0519859   -0.0131548
    O   6   -0.0608871    0.1250314    0.1743787
    O   7   -0.1763760   -0.1679803    0.0297014
    O   8   -0.1198442   -0.2089070    0.0270081
    O   9   -0.0564639   -0.2377425    0.1060394
    O  10    0.0230775    0.0540876   -0.0073376
    H  11    0.0716492    0.2592777   -0.0351410
    H  12    0.1411830    0.2155724   -0.0292207
    H  13    0.0739156    0.2606981   -0.0167169
    H  14    0.2357312    0.1214723   -0.0145667
    H  15    0.1757843    0.1821505   -0.0308723
    H  16    0.2320487    0.1189926   -0.0504758
    O  17   -0.1125943   -0.1329318    0.0201488
    H  18    0.2055655    0.0406280   -0.0179238
    H  19   -0.0665035    0.0828755    0.2078696
    N  20   -0.1269612    0.0938614   -0.1798004
    H  21   -0.0110857   -0.2030737   -0.1525805
    H  22   -0.0249201   -0.2311812   -0.0007323
    N  23    0.5322624    0.0665454    0.0786149
    O  24   -0.5394840   -0.0734397   -0.0934154

  E(HF)  =   -2755.8582467 a.u.
  Reason for exit: Successful completion
  Fast HF Program CPU Time : 000:02:41.0
  Fast HF Program Wall Time: 000:02:41.2
 Gradient of SCF Energy
             1            2            3            4            5
6
    1  -0.0256483  -0.0265065   0.0226566  -0.0128336   0.0417733  -
0.0000455
    2   0.0165480   0.0157035  -0.0241180   0.0072827  -0.0624366  -
0.0001635
```

Table B3. *(cont.)*

```
    3   0.0061409  -0.0029923   0.0160755   0.0038444   0.0001625  -
0.0000540
              7            8            9           10           11
12
     1   0.0077001  -0.0003524    0.0183686  -0.0408692  -0.0057629
0.0001956
    2  -0.0047981  -0.0026153  -0.0268246   0.0519811   0.0104622
0.0124191
    3  -0.0006629   0.0001632  -0.0181344  -0.0007776   0.0074236  -
0.0009232
           13           14           15           16           17
18
    1  -0.0073371   0.0089781   0.0100493   0.0103628  -0.0002330  -
0.0001488
    2   0.0094439  -0.0037204   0.0046009  -0.0028454  -0.0003115  -
0.0000201
    3  -0.0074054  -0.0072138  -0.0013190   0.0056377   0.0000374
0.0000278
            19           20           21           22           23
24
    1  -0.0000195   0.0000020  -0.0000261  -0.0000354   0.0000462  -
0.0000347
    2  -0.0000073   0.0009531  -0.0007472  -0.0002207   0.0001039  -
0.0000579
    3   0.0001214  -0.0002182   0.0001106  -0.0000218   0.0000120  -
0.0000037
 Max gradient component =      6.244E-002
 RMS gradient           =      1.490E-002
 Gradient time:  CPU 252.38 s  wall 252735.00 s

#####################################################
#  Entering optman.exe on Wed Jul 16 18:08:46 2003  #
#####################################################


 Cartesian Hessian Update
 Hessian Updated using BFGS Update


** CONSTRAINED OPTIMIZATION IN CARTESIAN COORDINATES **
   Searching for a Minimum

   Optimization Cycle:  70

                        Coordinates (Angstroms)
     ATOM               X           Y           Z
    1  O          -2.294006    0.535065    1.802379
    2  O          -2.658635    0.286460   -1.734149
    3  O           0.932459   -2.098642    1.654857
    4  V           0.752526   -1.630766   -0.155280
    5  V          -1.899632    0.534144   -0.034017
    6  O           1.838468   -0.312640   -0.353296
    7  O           1.968383   -3.246516   -0.167058
    8  O          -3.722966    1.399231    0.093163
    9  O           0.567830   -2.347247   -1.881670
```

Table B3. *(cont.)*

```
  10  O          -0.878657   -0.925330   -0.036688
  11  H           0.316422   -3.256858   -1.705658
  12  H           1.402805   -4.014128   -0.055378
  13  H           0.663470   -3.020159    1.660348
  14  H          -3.145677    0.092094    1.805942
  15  H          -4.345554    0.677573    0.207933
  16  H          -3.486927   -0.140561   -1.503575
  17  O          -0.886785    1.738798   -0.219982
  18  H           0.840338    2.565308   -0.457766
  19  H           2.127059    2.430326   -1.466406
  20  N           1.836226    2.780383   -0.557378
  21  H           1.853230    0.455405    0.261152
  22  H           1.943864    3.790496   -0.561187
  23  N           2.568166    1.775791    1.608716
  24  O           3.707595    1.931773    1.794997
  Point Group: c1    Number of degrees of freedom:  66


  Energy is  -2755.858246707

           Atoms with "Fixed" Coordinates
               Atom    Coordinates
                 1        X  Y  Z
                 2        X  Y  Z
                 3        X  Y  Z
                 4        X  Y  Z
                 5        X  Y  Z
                 6        X  Y  Z
                 7        X  Y  Z
                 8        X  Y  Z
                 9        X  Y  Z
                10        X  Y  Z
                11        X  Y  Z
                12        X  Y  Z
                13        X  Y  Z
                14        X  Y  Z
                15        X  Y  Z
                16        X  Y  Z
            Constraints and their Current Values
                                        Value     Constraint
  Dihedral:        4  10   5  20       -0.256        0.000
 cartesian optimization with constraints (P)

  Using Penalty Function Algorithm


 27 Hessian modes will be used to form the next step
  Hessian Eigenvalues:
      0.002257     0.004610     0.007396     0.007620     0.009412
0.017631
     0.019603     0.033915     0.041619     0.050494     0.065281
0.108973
      0.131492     0.144412     0.164758     0.202087     0.220887
0.413457
```

Table B3. *(cont.)*

```
      0.481193     0.649627     0.727080     1.203087     1.774711
2.752023
     4.091413    4.518052   14.481468

Minimum Search - Taking Simple RFO Step
 Searching for Lamda that Minimizes Along All modes
 Value Taken    Lamda =  -0.00000185
 Step Taken.  Stepsize is  0.013847

                            Maximum     Tolerance    Cnvgd?
         Gradient           0.000955      0.001000     YES
         Displacement       0.005562      0.010000     YES
         Energy change      0.000015      0.000001      NO


#######################################################
#  Entering anlman.exe on Wed Jul 16 18:08:47 2003  #
#######################################################

 Analysis of SCF Wavefunction


 Total job wall time:  2.8e+007 s
```